ABSTRACT

Title of Document: QUANTITATIVE HERMETICITY ASSESSMENT OF PACKAGES WITH MICRO TO NANO-LITER CAVITIES

Arindam Goswami, Doctor of Philosophy, 2008

Directed By: Professor Bongtae Han, Mechanical Engineering

Hermeticity is a measure of the "leak-proof ness" of packages with internal cavities and is critical for ensuring proper operation of the devices/circuits enclosed in them. The most widely used hermeticity detection technique in the industry is the helium fine leak test. The exiting conduction based governing equation is examined to investigate the *volume dependant* limits of the test when applied to metal sealed MEMS packages. The results clearly indicate that the test has limited applicability for small internal volumes (10^{-6} cc – 10^{-3} cc). The limited applicability of the guidelines specified in Method 1014.11 of the MIL-STD-883F document for hermeticity characterization is also characterized.

To cope with these limitations, a regression analysis based procedure is developed and implemented to extract the true leak rate from the apparent leak data. While the apparent leak rate obtained directly from the He mass spectrometer changes with the test parameters, the true leak rate remains constant and this can be used as a metric to evaluate a package seal.

The hermeticity of polymer sealed MEMS packages is also studied. Unlike metal sealed packages, gas transport in polymer sealed packages occurs via diffusion. A gas diffusion based model is proposed to study the hermetic behavior of these packages. An effective numerical scheme is developed to implement this model and simulate the change in cavity pressure as gas flows into or out of the cavity through the polymeric seal. An optical interferometry based leak test is developed to experimentally measure this change in cavity pressure. The experimental data is used to verify the validity of the proposed numerical scheme and the assumption of adiabatic boundary conditions made in the numerical model. An inverse method is presented to determine the two diffusion properties, diffusivity and solubility, of the polymeric seal by using the experimental data iteratively with the numerical data. The proposed method offers unique advantages over the routinely practiced/existing gas diffusion property measurement techniques.

QUANTITATIVE HERMETICITY ASSESSMENT OF PACKAGES WITH
MICRO AND NANO LITER CAVITIES

By

Arindam Goswami

Dissertation submitted to the Faculty of the Graduate School of the
University of Maryland, College Park, in partial fulfillment
of the requirements for the degree of

Doctor of Philosophy
2008

Advisory Committee:
Professor Bongtae Han, Chair
Professor Peter Sandborn
Professor Patrick McCluskey
Professor Teng Li
Professor Kyu Yong Choi

Dedication

To the two strongest and most loving people I know: my mother, whose sacrifices

made all of this possible, and my dad who gave me the most valuable lessons in the

short time that he had.

Acknowledgements

When I was growing up my sister used to tell me that I was adopted. I know that that is not true, so for starters I thank my parents without whom I would not have been here – literally. My sister – who I love immensely, is an amazing woman and were it not for her and Amit's constant badgering and nagging to finish up and visit them soon, this thesis would have taken much longer. So thanks are due to them and also their three year old daughter Aarya who has been growing up so fast that I had to blaze through the last few months so I could see her before she grew up any more. For their unwavering encouragement and love, I'd also like to thank my extended family which, unaware of the time wasting potential of the internet, thinks I must have been working on something super cool since it took me such a long time in grad school.

I gratefully acknowledge the guidance of my advisor, Dr. Han. This project and actually this effort would not have been possible without him. He taught me a lot of things – too many to list here but the biggest of them is how to *think*. I will remember that all my life. Thanks are due to my committee members who were always forthcoming with advice and accommodating as my schedule for the defense kept changing. Dr. Jang, thank you for the incredible help – you were a God-sent. I learnt a lot from you and your humble manner. I'd also like to acknowledge Dr. Ham's contribution for running so many experiments and offering such valuable insights.

I spent a lot of time in College Park and made so many friends – the ones I met in school, the CRC, Rotaract, at the house parties, the hikes and of course the

neighbors and the room-mates. You are all awesome and I wish I could acknowledge you all individually but I really need to submit this thing in the next hour or so. Not to mention that my wrists are weary from having typed out 150 odd pages and you guys will never read this anyway.

Onto my lab-mates: I have to thank SM, CW, Dr. Yoon and Yuri (for showing me the ropes), John (for showing me that machining was cool), Austin (for showing me that PBJ, day after day, is still awesome), Chris (for showing me that work always gets done, so its best to spend time thinking about the other important things), Alan (for all the chats about beer and books), Nathan (for the stock tips and the zillion chats about all things funny), Laura (for drawing those figures, for the brownies, for the chats and for keeping me entertained with celebrity gossip), Yong (for *that* USB key), Hongbo (for the funniest observations about everything under the sun), Michelle (for all the chats and for bringing those deli sandwiches and candy from time to time – its hard to do all this on an empty stomach), Haejin and Bongmin (for all the jokes – yeah right!, right?). On a more serious note, I think only we know the bond that we all have. Thanks guys, for always believing in me.

Dodo, I am sure of only one thing, but for what its worth that one thing is that you have always wanted the best for me. I'll always thank you for that. Thank you also for introducing me to Zips – laundry does not have to be a priority anymore. Last, and the most important, I thank Jenna. JJ, thanks for being the most awesome girl ever. I'll always love you for having *always* been there.

Table of Contents

List of Tables

List of Figures

Chapter 1: Introduction

1.1 Motivation

In electronics packaging, the role of the package is to protect the packaged device and to provide electrical and mechanical connections between the packaged device and the outside world. Hermeticity of the package is a measure of its "leak-proof ness" and thereby its ability to maintain an acceptable level of stable and sometimes inert ambience for the packaged device [2].

Hermeticity of these package impacts device reliability and hence lifetime expectation. Poor hermeticity can lead to ingress of contaminants, ambient gases and moisture thereby affecting the thermo-mechanical properties of packaging materials and potentially causing corrosion of metals in electronic packaging [3]. Absorbed moisture inside the package can also change the electric properties of the materials that the devices are made of [4]. In the case of MEMS, there are several instances of devices that exhibit excellent device characteristics per se, but are sensitive to environmental factors such as humidity and small particles [5]. Performance metrics such as the quality (Q) factor have been demonstrated to be sensitive to ambient pressure and hence hermetic quality of the package [6]. The problems are exacerbated for package volumes less than 1 µl [6] which are typical in current packages and are therefore the focus of this dissertation.

As a consequence of the salient points outlined above, hermeticity characterization is expected to play a significant role as newer package architectures and materials emerge and packaging paradigms change. Therefore, it is imperative that the

hermeticity phenomenon be understood at a fundamental level and appropriate tests may be designed to *quantitatively* characterize the same. This serves as the motivation for this dissertation.

1.2 Literature review

Hermeticity is assessed by measuring the rate of leakage of a specified fluid under specified conditions into the package. The spectrum of leak rates is divided into two regimes [2]:

a) Gross leaks (leakage rates more than 10^{-4} atm-cc/s)

b) Fine leaks (leakage rates less than 10^{-4} atm-cc/s)

Testing is done using a combination of gross leak tests and fine leak tests. The leak rates of the packages that are the focus of this thesis are in the fine leak regime. Following is a brief summary of the commonly employed tests to measure leak rates in this regime. Some of these tests are discussed in detail in subsequent chapters.

1.2.1 Helium fine leak test

Fine leaks have traditionally been measured using the helium fine leak test. The conceptual idea of the He fine leak test is to "bomb" the specimen with helium, i.e., subject it to pressurized helium for a period of time and then transfer it to a helium mass spectrometer to measure the rate at which the helium that was previously bombed in leaks out. This test and its procedure have been described in Method 1014.11 of the MIL-STD-883F document [7]. However, as discussed in Chapter 2, for the small volumes ($< 10^{-3}$ cc) that are typical of current and the next-generation

packages, the applicability of the helium fine leak test is limited and these limitations have not been characterized.

In addition, the helium fine leak test has by and large been used only for qualitative comparisons. There is no standardized procedure to extract a quantitative figure of merit of the package, independent of test conditions, from the helium fine leak test data. Further, data from the helium fine leak test does not lend itself to correlation with data from accelerated tests such as the 85°C/85% RH test which employ mixed gas environments as opposed to a single gas. This is a drawback of the helium leak test since these accelerated tests are a popular method of qualifying the reliability of packages.

In essence, the helium fine leak test in its present form is not capable of hermeticity evaluation of current and next-generation packages with cavity volumes on the micro- to nano-liter scale. This dissertation addresses some of these existing limitations.

1.2.2 Optical hermeticity tests

Optical methods have been developed to measure leak rates [8, 9]. The basic principle of the optical method is to pressurize the package at a known invariant pressure thereby deforming the cap. If the specimen is non-hermetic the pressurizing fluid leaks in and changes the pressure inside the cavity. Since the external pressure is held constant the pressure differential changes continuously as the fluid leaks in. This restores the cap it to its original undeformed state over a period of time. By using an optical technique to measure the deformation as a function of time, the *rate* at which the fluid leaks in can be calculated by using a calibration function relating cap

deformation to applied pressure differential. This technique and a novel application of the same are discussed in Chapter 5 and Chapter 6.

1.2.3 Accelerated tests

In these tests the package is subjected to high temperature and/or high humidity environments, thermal shock tests for extended periods of time [10]. The stress conditions for these tests are typically derived from JEDEC standards. Examples of these tests are included in Table 1-1.

Table 1-1 Examples of reliability tests [10].

Test	Condition
Wet High Temperature Storage	85°C/85%RH
Temperature cycle	JESD22-A104-B Condition G
Thermal Shock	JESD22-A106-A Condition C
High Temperature Storage Life	JESD22-A103-A

Package failure is decided based on a package dependant reliability criterion. This may include degradation of the bond, amount change in some performance metric of the packaged device etc. in a pre-decided amount of time. It should be noted that these tests do not *quantify* hermeticity. In addition, they are not physics of failure based tests. Therefore, it is not possible to make a direct correlation between these pass/fail tests and actual failures in the field.

In light of the motivation behind this work and the current state of the art vis-à-vis hermeticity testing, the following objectives were sought to be accomplished in this dissertation.

1.3 Objectives of the thesis

a) Develop a physical understanding of gas transport phenomenon underlying leakage through different types of sealing materials (metals and polymers) in order to model hermetic behavior of packages. This will enable a better understanding of the currently used hermeticity tests as well as aid the development of new ones.

b) Characterize the limits of the helium fine leak test by developing a physical understanding of the limitations of the test and quantitatively evaluate the same.

c) Develop a standardized procedure to analyze helium fine leak test data and to extract a hermeticity metric for the package from it that will be independent of the test conditions and package cavity volume. As mentioned above, the helium fine leak test has hitherto been used in a qualitative manner which makes the inferences drawn from the test dependant on these parameters. A metric which is independent of this constraint will enable a meaningful comparison between packages.

d) Characterize MIL spec guidelines for the helium fine leak test. Even in the domain of leak rates/package volumes in which the helium fine leak test can be used, the MIL spec guidelines for the test are such that when applied to packages with low volumes that are the focus of this dissertation, they may produce erroneous results. One of the objectives of this thesis is to develop a rigorous analytical framework to understand the circumstances in which this may happen and to therefore enable a more judicious use of these guidelines.

The following chapters present the details involved in accomplishing the above mentioned objectives. A brief overview of the organization of the dissertation is presented in the next section.

1.4 Organization of Dissertation

This first chapter introduces the reader to the motivation behind the current work and the objectives sought to be accomplished by it.

Chapter 2 discusses the helium fine leak test which is used widely in the industry to characterize hermeticity. A mathematical framework is developed to model this test in terms of the test conditions and package parameters. The sources of measurement uncertainty are characterized and the developed framework is used to describe, as a function of cavity volume, the practical and theoretical ranges of leak rates that can be measured by the Helium fine leak test. The concept of "true" leak rate as a hermeticity metric independent of test conditions/package volume is introduced and a regression analysis procedure to extract this metric from the helium fine leak test is outlined in this chapter. The motivation for and the underlying principle of the optical leak test are also discussed briefly. This chapter has been published as a research paper in the IEEE Transactions on Advanced Packaging.

Chapter 3 reviews the MIL spec based helium fine leak test (Test Condition A_1 and Test Condition A_2) guidelines for their applicability to packages with sub-micro liter cavity volumes. The validity of the criteria defined in the test guidelines is investigated using existing gas conduction models. The results show that the when the cavity volume is smaller than 10^{-2} cc, existing criteria are valid *only* over a limited domain of true leak rates and the size of this limited application domain shrinks as

volume gets smaller. This chapter concludes with a calculation of valid application

domain as a function of cavity volume. This chapter has been accepted for

publication as a research paper and is in the presses of Microelectronics Reliability.

While Chapters 2 and 3 establish the physical limits of the test and the

relevant guidelines, Chapter 4 addresses in detail the requirement and procedure for

quantitative analysis of the helium lea test data within these established limits. This

chapter examines the gas transport equations that govern "gas conduction" based gas

flow in the different stages of the helium fine leak test. A theoretical analysis of the

contribution of viscous and molecular modes to the total flow is presented. This

analysis provides the justification for a molecular flow based equation to be used for

the regression analysis outlined in Chapter 2. The experimental corroboration of the

proposed method and the successful implementation of the same to measure the true

leak rate of actual MEMS packages are reported in this chapter. This chapter is in the

presses of the IEEE Transactions on Advanced Packaging and will be published as a

research paper therein soon.

Chapter 5 and Chapter 6 focus on polymer sealed MEMS packages. The

motivation for this focus is two-fold. First, polymers are gaining widespread

acceptance as sealing materials for MEMS due to a host of advantages that they offer

and hence their hermetic characterization merits attention. Second, the "gas

conduction" based model discussed in Chapter 3 is not adequate to describe gas

transport through polymers, and thus a new approach is needed. In Chapter 5, a gas

diffusion based model is proposed to describe hermetic behavior of polymers when

used as sealing materials. A numerical scheme is developed to implement this gas

diffusion based model to simulate the change in cavity pressure when a polymer

sealed MEMS device is exposed to ambient gases. In Chapter 6, the optical leak test

is used to experimentally measure the same. Excellent agreement between the

numerical and experimental data corroborates the validity of the gas diffusion model

and provides a basis for experimentally measuring the properties which govern the

diffusion phenomenon.

Chapter 7 contains conclusions of the dissertation, a summary of the

contributions made by this study and a discussion of the direction in which this

present work can be extended

Chapter 2: On Ultra-Fine Leak Detection of Hermetic Wafer Level Packages[1]

ABSTRACT

Theoretical and practical ranges of leak rates measurable by the helium mass spectrometer are characterized. The effect of noise due to (a) background helium present in the spectrometer and (b) desorption of helium that attaches itself to the specimen surface during bombing is quantified experimentally. The results guide a framework to extract the true leak rate from the measured leak rate profile. An optical interferometry based hermeticity measurement technique for ultra-fine leaks is proposed. The setup to implement the technique is described and a preliminary experimental result is reported.

2.1 Introduction

Wafer level packaging has played a significant role in the successful commercialization of several MEMS devices. Hermeticity of these packages is one of the most important design/manufacturing parameters in determining the reliability of the devices they enclose. The small volumes make these packages susceptible to even very fine leaks. Therefore, detection of fine leaks in these packages is critical. Helium based fine leak testing has been used widely in the industry for fine leak detection and measurement. Because of the small internal volume of MEMS wafer

---

[1] This chapter has been published as a research paper in the *IEEE Transactions on Advanced Packaging* under the title "On ultra-fine leak detection of hermetic wafer level packages", by A. Goswami and B. Han.

level packages (typically less than 10^{-3} cc), however, the range of leakage rates that can be measured by the Helium fine leak tester is inherently limited.

The upper limit of the range of leak rates that can be measured has been discussed in previous studies [6, 11]. However, there also exists a lower limit and in many cases the leak rates that are to be measured can be below this lower limit. The primary aim of this paper is to (a) characterize the volume dependent range of measurable leak rates, and (b) lay the basis for developing a methodology, for cases in which the He fine leak tester can be used, to infer the true leak rate (L_a) of a specimen based on the measured leak rate measured by the fine leak test for subsequent use in a physics of failure based reliability prediction model.

This paper also proposes a new hermeticity detection technique for wafer level MEMS packages. This technique is based on an optical displacement measurement method which copes with the limitations of the He fine leak test. In this technique, the leak rate is calculated by subjecting the specimen to an invariant high pressure environment and measuring the time dependent surface deformation. The fundamental concepts of the technique are discussed and preliminary results are presented.

2.2 Helium Fine Leak Test

The conceptual idea of the He fine leak test is to "bomb" the specimen with He, i.e., subject it to helium pressurized at a value called the bombing pressure, P_b, for a period of time, t_b, and then transfer it to a He mass spectrometer where a vacuum is pulled to measure the rate at which He leaks out. The measured leak rate (R) is defined as the leak rate of a given package as measured under specified

conditions and employing a specified test medium [7]. This is the leak rate measured by the spectrometer. The measured leak rate is also referred to as *apparent leak rate*. It should be noted that in this arrangement there is a dwell time, t_{dwell}, between *completion* of bombing, i.e., when the specimen is taken out of the bombing chamber and the *start* of the measurement of the leak rate, during which some of the He escapes from the package.

The equivalent standard leak rate (L_a) of a package is defined as the leak rate when the high-pressure side is at 1 atmosphere (760 mm Hg absolute) and the low-pressure side is at a pressure of not greater than 1 mm Hg absolute (i.e., $\approx$ vacuum).

The equivalent standard leak rate is also referred to as the *true leak rate*. It is a characteristic of the package and is a function of the geometry of the leak opening. The measured leak rate, on the other hand, is a function of the test parameters (P_b, t_b, and t_{dwell}), the true leak rate (L_a) and the specimen volume (V).

The widely accepted relationship between the measured leak rate and the true leak rate [7, 11, 12] was derived originally by D. A. Howl and C. A. Mann with the assumption that all flow is molecular. In order to ensure the validity of this critical assumption, a supplementary analysis using the existing theoretical models [11, 13] was performed to quantify the effect of viscous conduction. The results clearly indicated that for the volumes and true leak rates considered in this paper, viscous conduction has virtually no effect on the results obtained with the assumption of pure molecular conduction.

A quantitative discussion about the results of the supplementary analysis is beyond the scope of this paper and the results will be reported in detail in a future

publication. For the remainder of the discussion this assumption of molecular flow will be implicit.

The assumption of molecular flow allows a simple conversion between the true leak rates when dealing with different fluids since, at a fixed temperature, the leak rates are inversely proportional to the square root of the molecular weight of the employed fluid medium. The Howl-Mann equation can be modified in terms of the true helium leak rate (L_a) as

$$R_i = \frac{L_a P_b}{P_\circ}(1 - e^{-L_a t_b / VP_\circ})e^{-L_a t_{dwell}/VP_\circ} \tag{1}$$

where $P_0 = 1$ atm and R_i is the measured leak rate at the instant the spectrometer is switched on.

As the specimen continues to leak inside the spectrometer, the measured leak rate decreases exponentially and is given by the following relationship:

$$R(t) = \frac{L_a P_b}{P_\circ}(1 - e^{-L_a t_b / VP_\circ})e^{-L_a t_{dwell}/VP_\circ}e^{-L_a t / VP_\circ} \tag{2}$$

where t is the lime elapsed since the spectrometer was started.

In an actual test, the lowest measured leak rate that a spectrometer can measure is R_{limit}, which is the measurement sensitivity of the spectrometer. This governs the minimum allowable value of R_i [6, 11]. If the true leak rate, L_a, is such that at the time of measurement the measured leak rate, R_i, is lower than R_{limit}, then the spectrometer will be unable to measure any leakage. For a given cavity volume, using this value for R_i and solving for L_a in Equation 1 yields two roots. These values correspond to the upper (L_{a_upper}) and lower (L_{a_lower}) limits of the true leak rate.

Physically, this means that if the true leak rate is outside of the range established by these limiting values, then the measured leak rate will be lower than the measurement sensitivity (R_{limit}) of the spectrometer and will not be detectable at the time of measurement in the spectrometer. If $L_a < L_{a\_lower}$, less helium is bombed into the specimen for a given bombing time and when the specimen is put in the spectrometer there is not enough helium coming out to be detected. On the other hand if $L_a > L_{a\_upper}$ then nearly all the helium bombed into the specimen leaks out during dwell time and hence there is not enough helium left to produce a detectable signal in the spectrometer [6, 11].

In all the analyses described below, R_{limit} was set = 10^{-10} atm-cc/s. This choice of spectrometer sensitivity reflects the capability of commonly used commercial He fine leak testers. Also, the bombing pressure, which commonly ranges from 3 atm to 10 atm, was set equal to the most representative value of 5 atm absolute.

2.2.1 Theoretical range of measurable true leak rates

The theoretical range of measurable true leak rates for the ideal case was investigated by setting the bombing time $t_b = \infty$ and the dwell time, $t_{dwell} = 0$ in Equation 1 for each cavity volume. This revealed that for the ideal case there is no upper limit but there is a lower limit that is independent of cavity volume. This is in accord with physical intuition since it is expected that in the absence of a dwell period, no He can leak out regardless of how high the true leak rate is.

In addition, under these ideal conditions, the total pressure inside all the packages, when they are loaded into the spectrometer, will be the same regardless of the true leak rate and the volume. Therefore, the initial measured leak rate, R_i, which

in the limiting case is equal to the spectrometer sensitivity, will be volume

independent. These results are plotted in Figure 2-1.
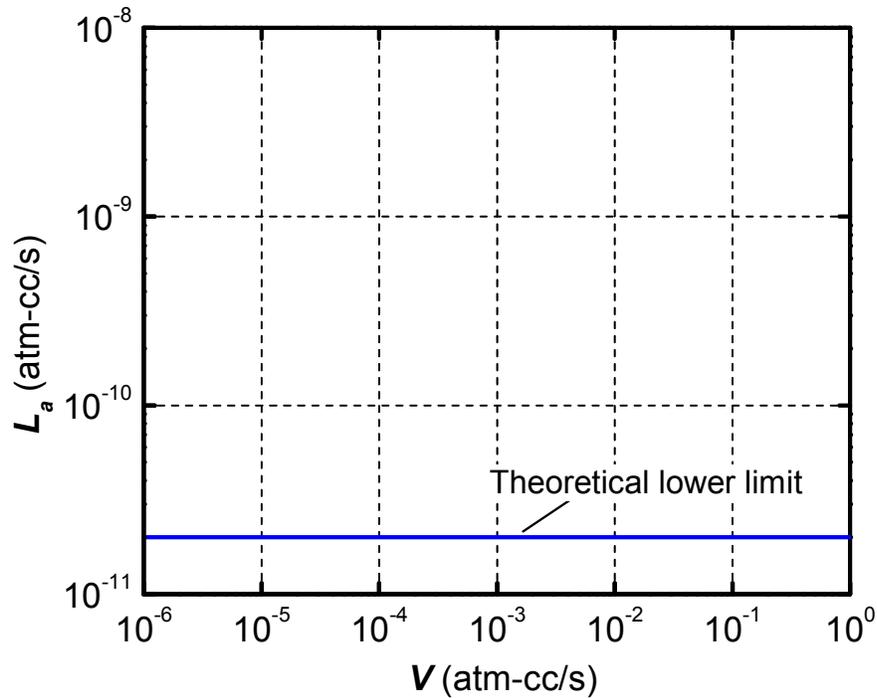
Figure 2-1 Lower limit of the fine leak test as a function of cavity volume for the

case of bombing pressure, P_b = 5 atm, spectrometer sensitivity, R_{limit} = 10^{-10} atm-

cc/s and *ideal* conditions of infinite bombing pressure and zero dwell time.

2.2.2 Practical range of measurable true leak rates

The limits using more practical values of t_b = 6 hours and dwell time, t_{dwell} =

10 minutes were also analyzed[2]. Figure 2-2 shows a plot (obtained using Equation 1)

of R_i as a function of L_a for a package with volume, V = 5 x 10^{-5} cc. Similar plots can

be found in the literature [8, 11].

---

[2] In the conference version of this paper [13] a value of t_{dwell} = 3 minutes was used. It was modified to
a more realistic value of 10 minutes in this paper as suggested by actual test operators. It should be
noted that the basic points illustrated remain the same.
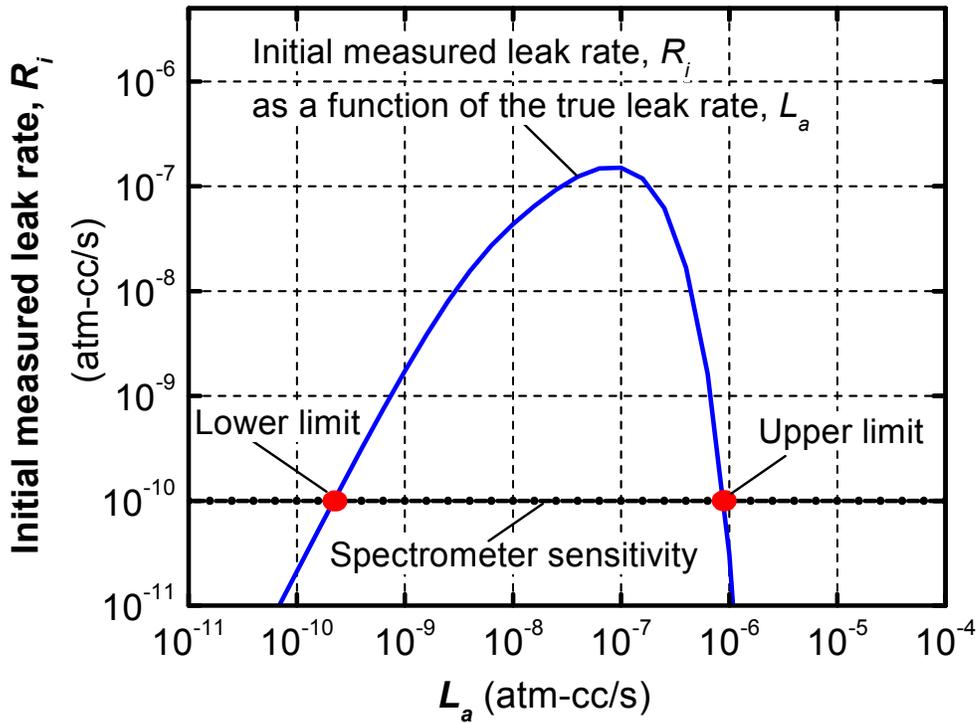
Figure 2-2 Initial measured leak rate, R_i, as a function of the true leak rate, L_a, for a cavity volume = 5 x 10^{-5} cc and test conditions: P_b = 5 atm, t_b = 6 hours and t_{dwell} = 10 minutes.

It is evident from Figure 2-2 that if the measured leak rate, R_i, has to be higher than the spectrometer sensitivity limit, R_{limit} = 10^{-10} atm-cc/s, i.e., for the spectrometer to be able to detect a signal, the true leak rate, L_a, has to be between the limits shown. For this particular case, L_{upper} and L_{lower} are equal to 8.9 x 10^{-7} atm-cc/s and 2.2 x 10^{-10} atm-cc/s, respectively. Leak rates higher than this upper limit or lower than the lower limit cannot be detected by the test.

In Figure 2-3 the practical upper and lower limits of the true leak rate are plotted as a function of cavity volume. It is evident that the upper limit becomes

lower as volumes decrease.   This poses a challenge in the hermeticity measurement

of small volume packages [6].
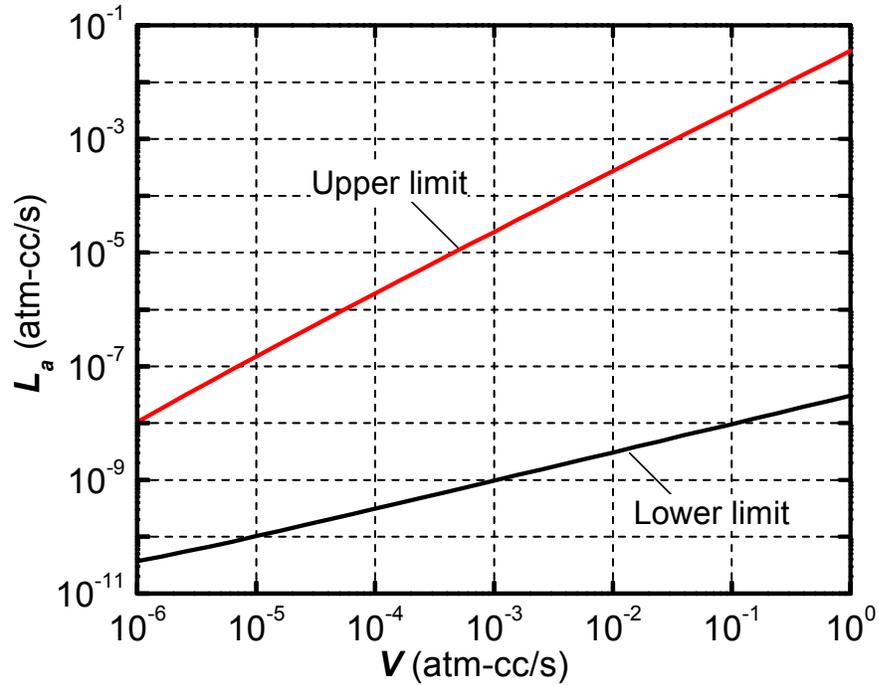
Figure 2-3 Dependence of upper and lower limits of the fine leak test on cavity volume for the case of P_b = 5 atm, t_b = 6 hours, t_{dwell} = 10 minutes and R_{limit} = 10^{-10} atm-cc/s.

In order to investigate the effect of test parameters on the volume dependent range of measurable true leak rates, test cases were simulated wherein the bombing pressure, bombing time and dwell time were varied independently with respect to the case depicted in Figure 2-3. More specifically, the bombing pressure was increased by two times (10 atm), the bombing time was increased by five times (30 hours) and the dwell time was decreased by a factor of 2 (5 minutes). These values were chosen

16

since they represent the far end of practically allowable values[3]. The results are

depicted in Figure 2-4.

Lower Limit (P_b = 5 atm, t_b = 6 hours, t_{dwell} =10 minutes)

Upper Limit (P_b = 5 atm, t_b = 6 hours, t_{dwell} =10 minutes)

☆ Lower Limit (P_b = 5 atm, $\boldsymbol{t_b}$ **= 30 hours**, t_{dwell} =10 minutes)

★ Upper Limit (P_b = 5 atm, $\boldsymbol{t_b}$ **= 30 hours**, t_{dwell} =10 minutes)

△ Lower Limit (P_b = 5 atm, t_b = 6 hours, $\boldsymbol{t_{dwell}}$ **= 5 minutes**)

▲ Upper Limit (P_b = 5 atm, t_b = 6 hours, $\boldsymbol{t_{dwell}}$ **= 5 minutes**)

□ Lower Limit ($\boldsymbol{P_b}$ **= 10 atm**, t_b = 6 hours, t_{dwell} =10 minutes)

■ Upper Limit ($\boldsymbol{P_b}$ **= 10 atm**, t_b = 6 hours, t_{dwell} =10 minutes)

Figure 2-4 Effect of test parameters on the practical limits of the helium fine leak

test.

It can be seen from these plots that changing the test parameters does not

significantly alter the volume dependent range of measurable true leak rates.

---

[3] For example, shortening the dwell time to below 5 minutes, although not impossible, is very difficult
to achieve in routine practice.

2.2.3 Sources of measurement uncertainty

There are sources of measurement uncertainties that can potentially influence the actual test results. The possible sources are discussed below.

Zero signal

Although practical values of test parameters were used to calculate the limits in Figure 2-3, the actual range of measurable true leak rates can be smaller due to a background noise. This noise is attributed to helium present in the ambient air that leaks into the spectrometer. We propose to call this signal the *zero signal*.

In order to quantify the zero signal, the leak tester was operated without any sample inside it. The signal obtained was, therefore, produced only by the background helium and the result is shown in Figure 2-5. The time interval between recording consecutive data points of the signal was 0.15 s. Only a few representative data points are plotted.

The practical implications of the zero signal are as follows: Even if the true leak rate is within the range plotted in Figure 2-3,

(a) It may be so high that the package is evacuated completely before the zero signal stabilizes, or

(b) It may be so low that the signal produced by the leakage from the specimen may not be much higher than the zero signal.
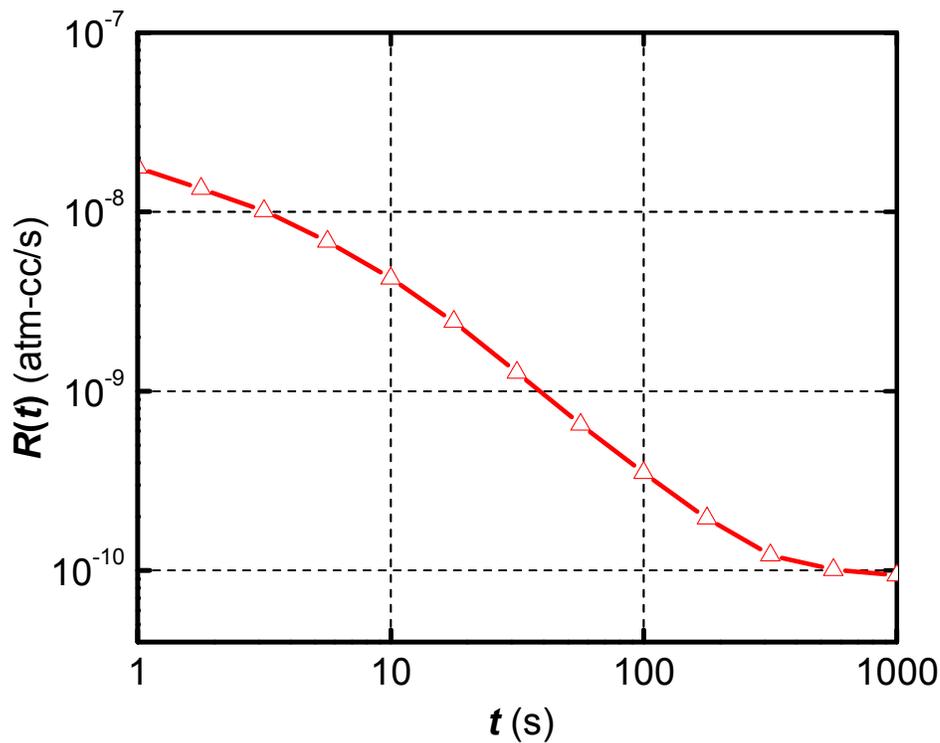
Figure 2-5 Zero signal due to helium present in the ambient air that leaks into the spectrometer.

Both of these cases are illustrated in Figure 2- 6 for a cavity volume, $V = 5$ x 10^{-5} cc. The practical upper and lower limits in the ideal case, i.e. without considering the zero signal, for a package with this volume were calculated and are 8.9 x 10^{-7} atm-cc/s and 2.2 x 10^{-10} atm-cc/s, respectively. In Figure 2-6, the measured leak rate profile (obtained using Equation 2) for these limiting values of the true leak rate have been superimposed on the zero signal data.

It can be seen that when $L_a = L_{a\_upper}$, the measured leak rate signal is evacuated before the zero signal stabilizes. On the other hand, when $L_a = L_{a\_lower}$, the

signal to noise ratio between the measured leak rate signal (signal) and the stabilized

value of the zero signal (noise) is poor.
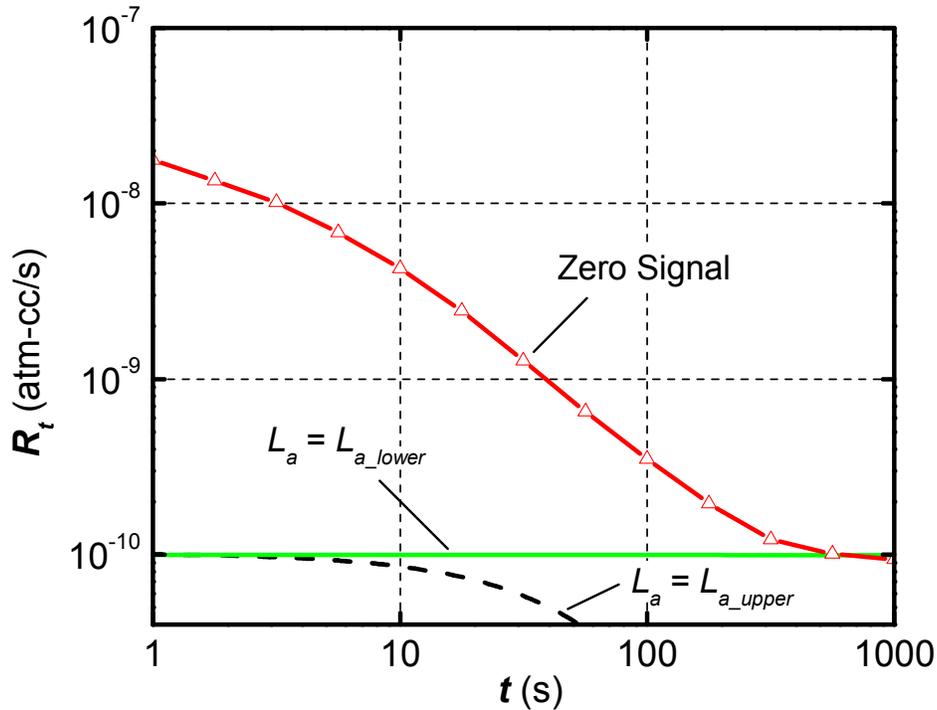
Figure 2-6 Measured leakage rate profiles of a package with $V = 5$ x 10^{-5} cc when

the true leak rates are at their limiting values (L_{a_upper} = 8.9 x 10^{-7} and L_{a_lower} =

2.2 x 10^{-10} atm-cc/s). Test parameters are; P_b = 5 atm, t_b = 6 hours and t_{dwell} = 10

minutes. The zero signal of Figure 2-5 is also shown.

Effect of desorption of helium from package surface

Helium particles can be adsorbed on the surface of the specimen during

bombing. When subjected to a vacuum in the spectrometer, they desorb and can be

detected in the spectrometer, too [11, 14]. For the devices being investigated, the

materials that are exposed to pressurized helium during bombing are gold and silicon.

The effect of this desorbed helium was quantified by conducting experiments on bare

silicon and gold wafers having a total surface area of 900 mm^2. This wafer was bombed with helium at 5 atm for 6 hours and transferred into the spectrometer after a dwell time of 10 minutes. The obtained signals are depicted in Figure 2-7.
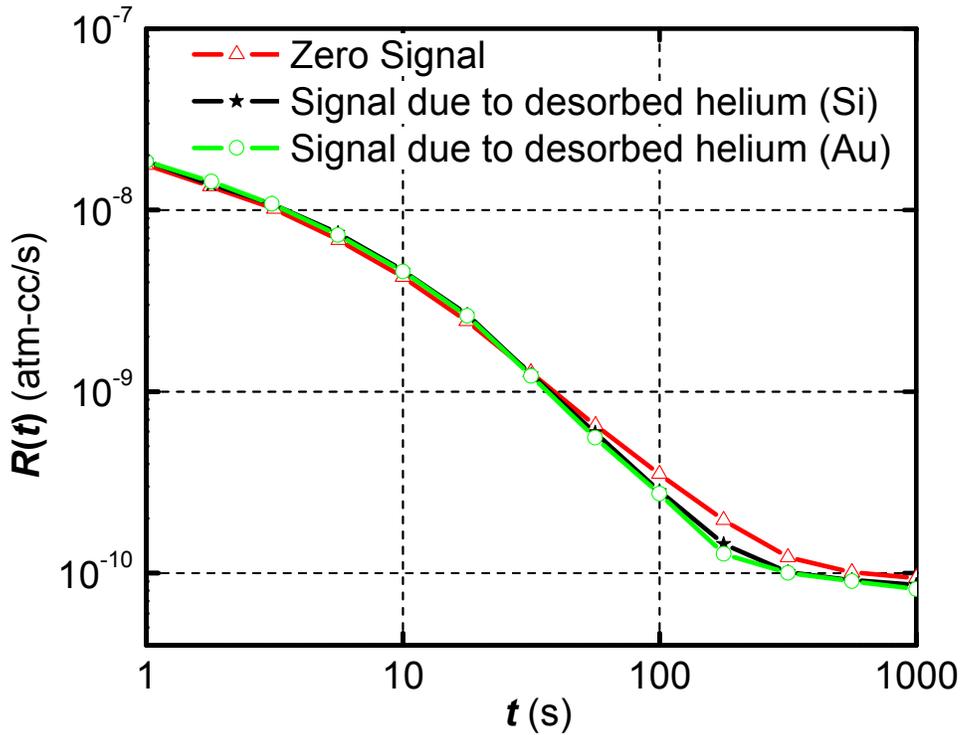
Figure 2-7 The signal due to desorption of helium adsorbed due to bombing.

The obtained signal is similar in magnitude and profile to the zero signal, which indicates that the effect of desorbed helium is negligible. It should be noted that the sample used for this experiment has an area of 900 mm^2. The surface area of a typical package which has a micro- to nano-liter cavity is usually less than 25 mm^2. Assuming a linear dependence on area, it is safe to say that the surface area signal will not influence measurements.

2.3 Extension of Hermeticity Measurement into the Quantitative Domain

The measured leak rate depends on the pressure differential. When there is leakage, the pressure differential changes with time and so does the measured leak rate. Therefore, the measured leak rate is time variant and is not of much use while estimating reliability. For reliability assessment the true leak rate should be used since it is the characteristic of a package and is independent of ambient conditions. In addition, correlating the true leak rates for two different gases is much more straightforward, which is important in practice since many wafer level packages are subjected to accelerated testing conditions in high temperature/humidity environments. Use of the true leak rate as a leakage metric facilitates meaningful correlation between how the package performs in the accelerated tests and how it does during actual operating conditions.

This motivates the development of new techniques to measure the true leak rate of packages and use it for a further quantitative analysis.

2.3.1 Inferring the true leak rate from the helium fine leak test

Hitherto only the initial measured leak rate has been used as a basis for characterization/comparison. However, the helium fine leak test contains more useful information, viz. the profile of the measured leak rate signal – i.e. the change of measured leak rate with time.

The true leak rate can be inferred from the measured leak rate by using the least squares method for regression analysis [15] of this measured leakage data.

Theoretically, the measured leak rate changes with time according to the following

relationship[4]:

$$R(t) = Ae^{-L_a t / VP_{\circ}} \tag{3}$$

where A and L_a are the parameters to be determined, V is the specimen volume, P_0 is

constant (1 atm) and t is the time elapsed since the end of dwell. Physically, A

represents the measured leak rate at the instant the helium leak tester is switched on

and L_a represents the true leak rate of the specimen. Therefore, in theory, in order to

calculate these two parameters two data points should suffice. However, due to

systematic and random noise in the system, a larger number of data points are

required. The error function, S, can be defined as:

$$S = \sum_{k=1}^{n} \left(Ae^{-L_a t_k / VP_{\circ}} - R(t_k) \right)^2 \tag{4}$$

where n is the number of data points, $R(t_k)$ and t_k are corresponding data points from

the measured leakage rate profile. The condition of least squares fit requires that:

$$\frac{\partial S}{\partial L_a} = 0 \tag{5}$$

$$\frac{\partial S}{\partial A} = 0 \tag{6}$$

Equations 5 and 6 are solved to yield the values for the parameters A and L_a.

The actual test data is shown in Figure 2-8, where the tested package has an

internal volume of 2.156 x 10^{-4} cc and the test parameters are: bombing pressure = 5

atm, bombing time = 6 hours, dwell time = 10 minutes. The regression technique

---

[4] This is a modified form of Equation 2 in which all the terms except for the last one have been

combined together.

discussed above was applied to this data to determine the true leak rate. The true leak rate of the package was determined to be 9.2 x 10^{-7} atm-cc/s and the corresponding value of A was 7.95 x 10^{-7} atm-cc/s. The measured leak rate profile for these values can be obtained by using Equation 3. This profile is also plotted in Figure 2-8. An extremely high coefficient of regression ($R^2 = 0.99$) was obtained for this fit and is evident in the plot, thereby validating the proposed approach.
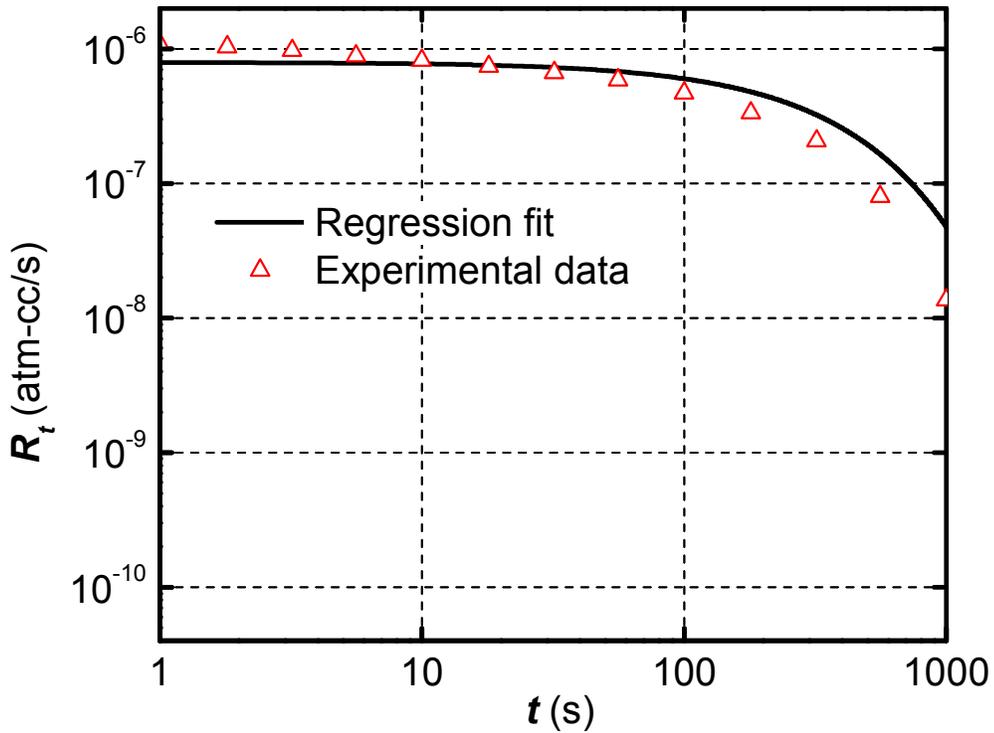
Figure 2-8 Application of the regression based technique to experimental data for the extraction of the true leak rate.

2.3.2 True leak rate from optical interferometry based hermeticity test

The limitations of the helium fine leak test have been established in the preceding sections. As package volumes become smaller, hermeticity requirements will become more stringent. This is because their small volumes will make them susceptible to

24

ultra-fine leaks.   Several studies have shown that the maximum acceptable leak rate for these packages is several orders of magnitude less than that for the larger volume packages [6, 13]. Therefore, an advanced technique to measure true leak rates smaller than the lower limit of the helium fine leak test is required.

Optical interferometry based hermeticity evaluation has been developed to extend hermeticity evaluation to the domain of true leak rates that cannot be measured by the helium fine leak test [8, 16]. Figure 2-9 illustrates the underlying concept. The specimen is placed in a pressure vessel, where it is subjected to a high pressure. For a non-hermetic specimen, the pressure differential (i.e., the difference between the applied external pressure and the cavity internal pressure) changes over a period of time, the change being proportional to the leak rate. Since the specimen deformation is proportional to the pressure differential (ΔP), the leak rate can be determined using an analytical relationship between the time dependent deformation and the true leak rate.
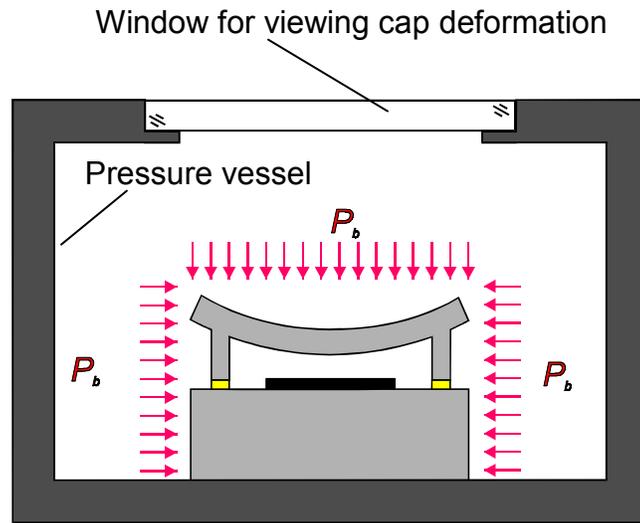
Specimen subjected to an invariant external pressure, P_b, at $t_1 = 0$
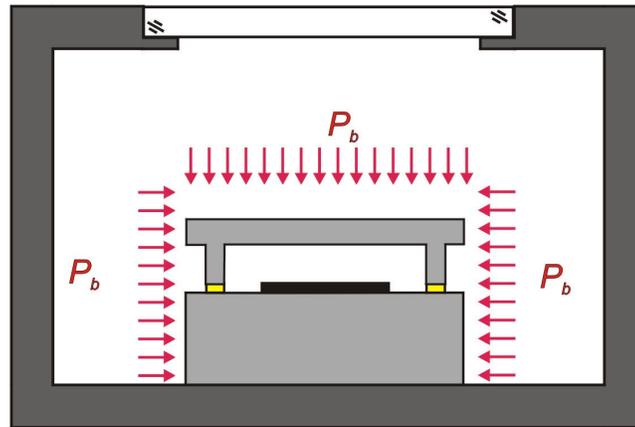
Non-hermetic specimen at $t_2 = \infty$

Figure 2-9 Schematic illustration of optical interferometry based scheme for hermeticity measurement.

When a package is subjected to external pressure, P_b, the pressure differential (ΔP) as a function of time (t) can be expressed as[5] [8]:

$$\Delta P_t = (P_b - p_i)e^{-L_a t / V P_o} \tag{7}$$

where p_i is the initial pressure in the package. The derivation of Equation 7 can be found in the Appendix. From Equation 7, one can have

$$L_a = \frac{V}{t_2 - t_1} ln\left(\frac{\Delta P_{t_1}}{\Delta P_{t_2}}\right) \tag{8}$$

where ΔP_{t_1} and ΔP_{t_2} are the pressure differential at time t_1 and t_2, respectively. In the proposed scheme, the measurand is the surface deformation, which is a function of the pressure differential, i.e. $W = f(\Delta P)$. Equation 8 can be rewritten as

$$L_a = ln\left(\frac{f^{-1}(W_{t_1})}{f^{-1}(W_{t_2})}\right)\left(\frac{V}{t_2 - t_1}\right) \tag{9}$$

where W_{t_1} and W_{t_2} are the surface deformation values at time t_1 and t_2, respectively. The relationship between the surface deformation and the pressure differential for a given specimen, $\Delta P = f^{-1}(W)$, can be obtained by a calibration process. Then, by measuring the deformation at two different times and relating these measurements to their corresponding pressure differential values, the true leak rate can be determined by using Equation 9.

A special case arises when the deformation is linearly proportional to the pressure differential, i.e. $W = k \cdot \Delta P$ where k is a constant. In this case, Equation 9 is reduced to a simplified form as:

---

[5] This is identical to Eq. 3 in the cited reference.

$$L_a = \ln\left(\frac{W_{t_1}}{W_{t_2}}\right)\left(\frac{V}{t_2 - t_1}\right) \tag{9'}$$

It is important to note that Equation 9' does not require *a calibration curve*, which makes the proposed method practical.

An important advantage of the technique is the control on dwell time which can be adjusted from 0 (measurement immediately after switching on the bombing pressure) to any arbitrary value less than the time to saturation (i.e., the point at which the pressure inside the cavity is equal to the bombing pressure).

Optical/Mechanical configuration

The test setup to implement the proposed concept is shown in Figure 2-11. The specimen is held inside a pressure vessel which is provided with a 12 mm thick window for the purpose of viewing. Both the vessel and the window are capable of withstanding pressures up to 50 atm. The pressure vessel is connected to a He cylinder through a pressure reducing regulator. A PC is used to provide a set point (i.e., desired pressure value) to a PID controller via a D/A converter. This controller controls the regulator to adjust the downstream pressure, i.e., the pressure in the vessel. This pressure is measured using a piezoresistive pressure sensor. The sensor is interfaced with a digital pressure indicator, which in turn is connected to the PC via an RS 232 interface. This completes a closed feedback loop to maintain a constant pressure during measurements.
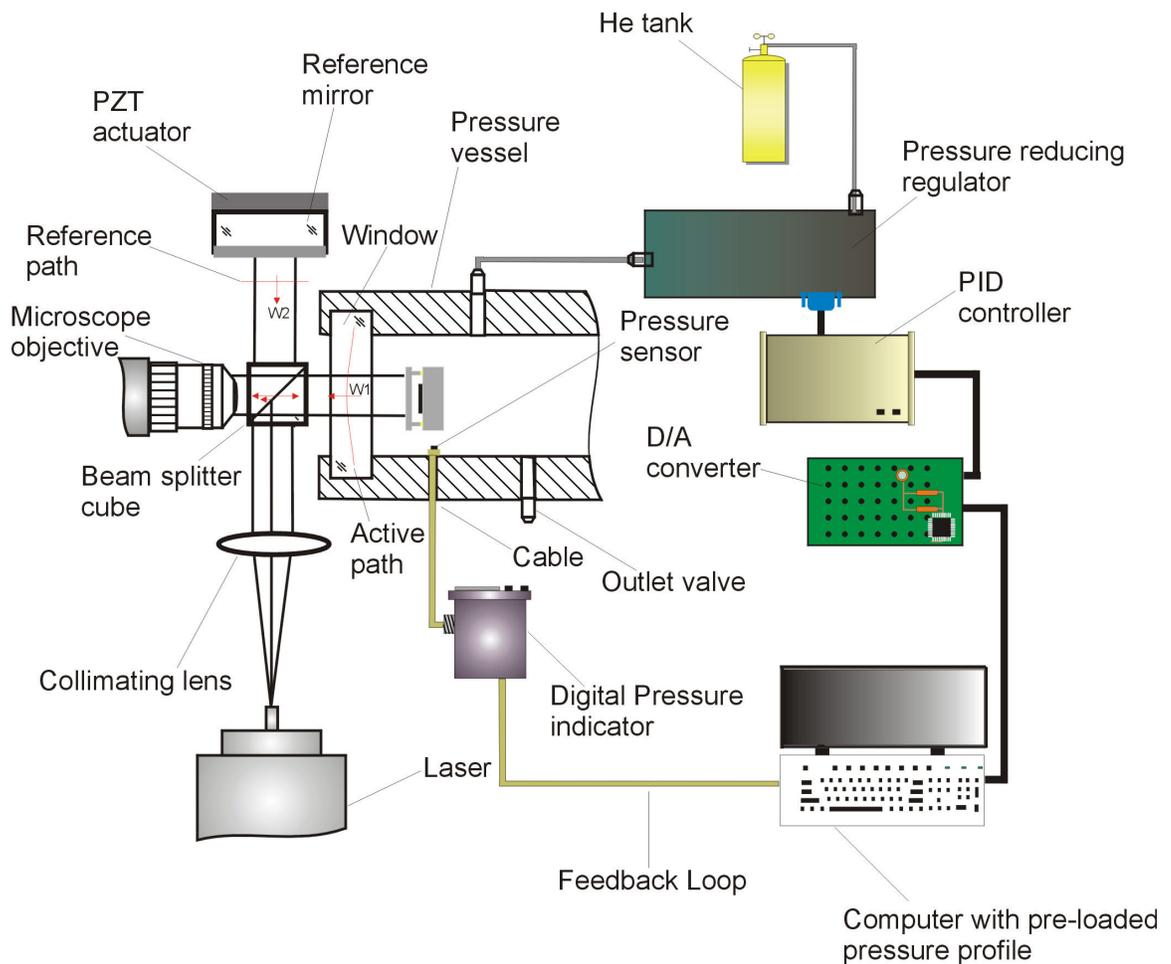
Figure 2-10 Top view of the optical/mechanical configuration of the test setup.

For extremely fine leaks, the pressure differential changes very slowly and hence, in a given time period, the change in cap deflection is small. The amount of cap deflection change can be increased by either waiting for a long time or by increasing the bombing pressure. In order to measure very fine leaks, within a practically allowable duration of time, the required displacement resolution would have to be on the order of a few tens of nanometers.

The required measurement resolution is achieved by employing a classical interferometric technique called *Twyman Green (T/G) interferometry* [17] together with well-known phase shifting technique. T/G interferometry measures surface contours (out-of-plane displacements) with sub-micron sensitivity and it can provide the desired resolution when it is combined with the phase shifting technique [18]. The technique is simple and it is ideally suited for the MEMS packages since the package surface provides a specular (mirror-like) surface, which is a critical requirement for the method. As illustrated in Figure 2-10, a collimated laser beam is split into two beams using a beam splitter – one of the beams is directed towards the specimen and the other towards the reference surface. The reflected wavefronts (which deform according to the surface that they reflect from) interfere to form an interferogram, which is captured using a camera. A piezoelectric actuator is attached to the reference mirror for phase shifting.

Preliminary experiment

The package used in the test is illustrated schematically in Figure 2-11(a). The package dimensions are 1 mm x 0.8 mm x 0.25 mm and the cap thickness is 30 μm. The cap and the substrate are made of silicon and a eutectic material is used for the peripheral seal between the two. The sealing was processed in an N_2 environment with an ambient pressure of 10^{-3} Torr at 400˚C. The tested package has a cavity with a height of ~ 10 μm and a volume of ~ 10^{-5} cc.

Cap deflection as a function of the pressure differential was determined using finite element analysis (FEA) and the result is plotted in Figure 2-11(b). The linear relationship between the applied pressure differential and the deflection is evident,

which confirms the validity of Equation 9' for leak rate calculations. Most specimens
have cap thicknesses larger than 30 μm and therefore will exhibit a linear relationship
between the applied pressure differential and the cap deflection. Therefore the
method can be used for a wide range of MEMS packages without a calibration curve.

(a)

(b)
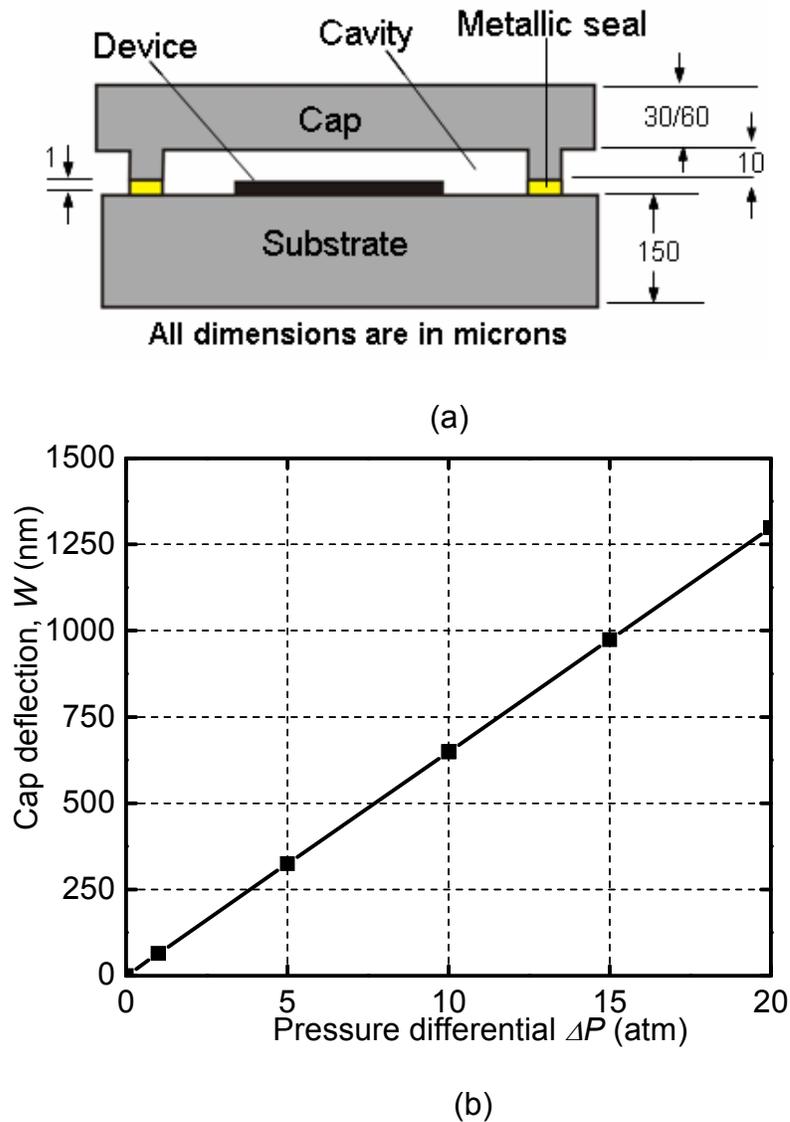
**Figure 2-11 (a) Schematic of the specimen and (b) cap deflection as a function of
the pressure differential for a cap thickness of 30 μm, obtained using finite
element analysis (FEA).**

The specimen was subjected to helium pressurized at 15 atm. The phase shifted images and the corresponding warpage pattern at time, $t_1 = 0$ and $t_2 = 45$ hours are shown in Figure 2-12. It is to be understood that the pressures employed in the experiment should be limited to the minimum values required to obtain discernible deformation change so as to ensure that there is no permanent damage to the seal.

At $t_1 = 0$: $W_{max} = W_A - W_B = 956$ nm

At $t_2 = 45$ hours: $W_{max} = W_A - W_B = 944$ nm
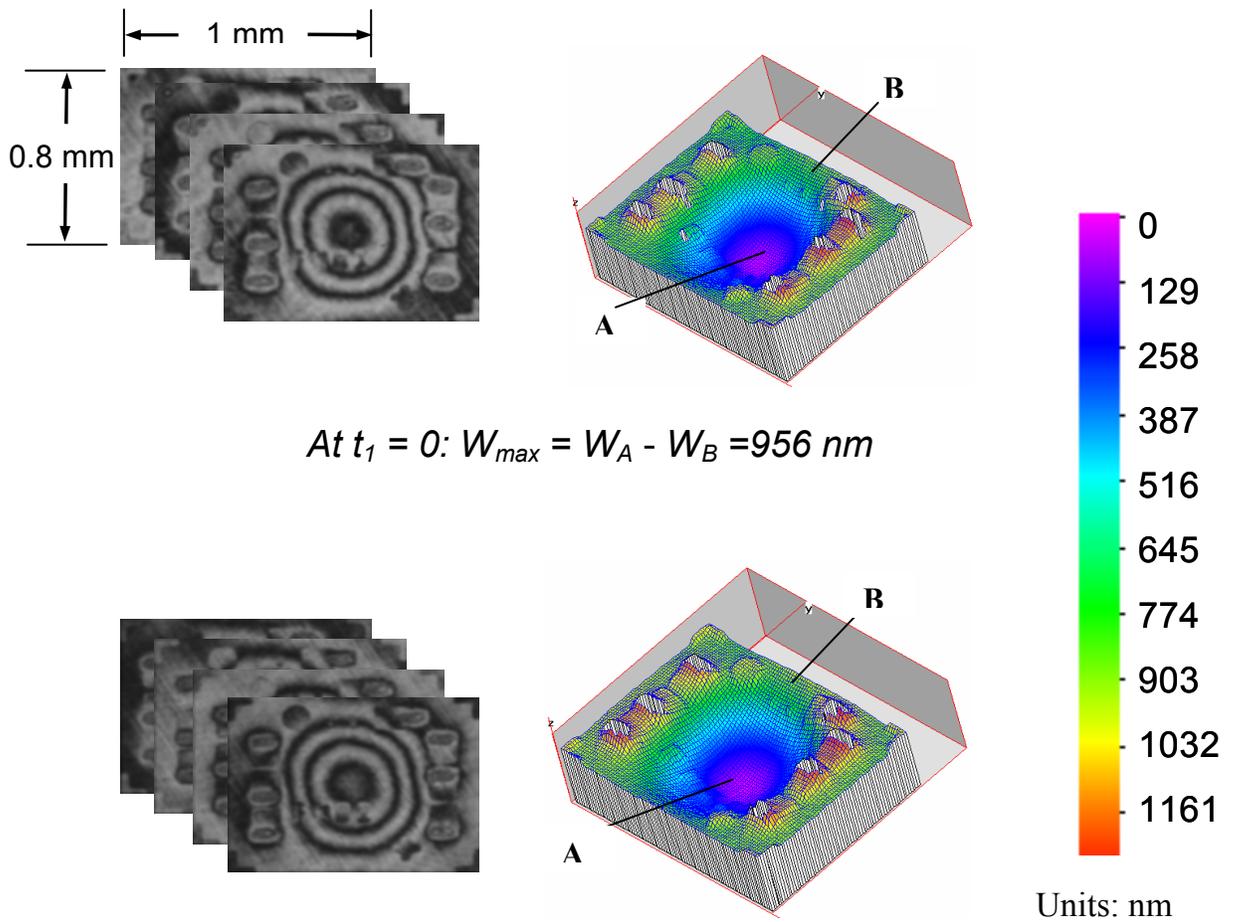
Figure 2-12 Deformation of a package with a cavity volume of 10^{-5} cc, subjected to a pressure of 15 atm.

The change in deformation at $t_2 = 45$ hours was only 12 nm. This change is smaller than the maximum displacement uncertainty of the measurement system (estimated to be as large as 30 nm). The true leak rate was calculated from Equation 9' using the maximum displacement uncertainty (30 nm). The value was 1.96×10^{-12} atm-cc/s. It is a clear indication that the package has leak rate much lower than the measurement limit of the helium fine leak test and a higher displacement resolution or a higher bombing pressure should be employed to measure the leak rates in this range.

2.4 Conclusion

The practical and theoretical ranges of leak rates that can be measured by the Helium fine leak test have been described as a function of cavity volume. This establishes the range of leak rates that the leak tester is *fundamentally capable* of measuring. It was demonstrated that changing the test parameters – within practically allowable limits - does not significantly alter the size of these ranges. Sources of measurement uncertainty were analyzed. These include the effect of helium present in the ambient air that leaks into the spectrometer (zero signal). Its effect was quantified experimentally. The zero signal contributed significantly to the net observed signal for approximately the first 2.5 minutes after starting the spectrometer. The effect of helium, adsorbed to the specimen surface during bombing, was also analyzed experimentally and it was shown to have a negligible impact on the observed signal.

Inferring the true leak rate was motivated by a need for quantitative hermeticity measurement and the potential for extending hermeticity measurement results into reliability analyses. A new procedure to extract the true leak rate by analyzing the *profile* of the measured leak rate data was discussed. An optical interferometry based hermeticity measurement technique was also presented as a tool to measure the leak rate beyond the practical limits of the helium fine leak test.

Appendix
Derivation of expression for pressure differential (ΔP_t) as a function of time (t) when a package with volume, V is subjected to external pressure, P_b.

The pressure differential ΔP is related to the measured leak rate, $R(t)$, by the following relationship:

$$R(t) = F(\Delta P) \tag{A-1}$$

where F is the conductance.

By definition, $R(t) = L_a$ when $\Delta P = 1$ atm.

$$\Rightarrow L_a = F(P_0) \text{ where } P_0 = 1 \text{ atm} \tag{A-2}$$

$$\Rightarrow F = \frac{L_a}{P_0} \tag{A-3}$$

Now, the equation for inflow of gas is:

$$\frac{dp}{dt} = \frac{F}{V}(P_b - p) \tag{A-4}$$

where p is the pressure inside the package.

Substituting the expression for F in Equation A-4, we get:

$$\frac{dp}{dt} = \frac{L_a}{VP_0}(P_b - p)` \tag{A-5}$$

By Integrating both sides, Equation A-5 yields

34

$$\Rightarrow \int_{p_i}^{p_t} \frac{dp}{(P_b - p)} = \int_0^t \frac{L_a}{V} dt \qquad \text{(A-6)}$$

$$\Rightarrow ln\left[\frac{P_b - p_i}{P_b - p_t}\right] = \frac{L_a t}{V} \qquad \text{(A-7)}$$

$$\Rightarrow ln\left[\frac{P_b - p_t}{P_b - p_i}\right] = -\frac{L_a t}{V} \qquad \text{(A-8)}$$

$$\Rightarrow \Delta P_t = (P_b - p_i)e^{-\frac{L_a t}{V}} \qquad \text{(A-9)}$$

where $\Delta P_t = P_b - p_t$.

Chapter 3: On the Applicability of MIL-Spec-Based Helium Fine Leak Test to Packages with Sub-micro liter Cavity Volumes[6]

ABSTRACT

The MIL-Spec-based helium fine leak test (test condition A_1 and test condition A_2) is reviewed for its applicability to the packages with sub-micro liter cavity volumes. The existing gas conduction models are utilized to investigate the validity of the criteria defined in the test guidelines in term of true leak rates. The application domains valid under the current guidelines are determined as a function of the internal cavity volume. The results show that only finite domain of true leak rates is valid when the volume is smaller than 10^{-2} cc and the invalid domain increases as the cavity volume decreases.

3.1 Introduction

Hermeticity of an electronic/MEMS package is a measure of its "leak-proof-ness" and the ability to maintain an acceptable level of stable and sometimes inert ambient for the packaged device. Poor hermeticity can lead to ingress of contaminants, ambient gases and moisture, thereby impacting device reliability.

---

[6] This chapter has been accepted for publication in *Microelectronics Reliability* under the title "On the applicability of mil-spec-based helium fine leak test to packages with sub-micro liter cavity volumes", by A. Goswami, B. Han and S. J. Ham.

Hermetic sealing is a critical requirement for maintaining a controlled internal environment for the packaged device.

The guidelines specified in Method 1014.11 of the MIL-STD-883F document [7] have been used widely in the industry for hermeticity qualification, typically for packages with cavity volumes larger than those of typical MEMS packages ($< 10^{-2}$ cc). The applicability of these guidelines has been discussed previously by Tao and Malshe [13]. Although the reference discussed the limited applicability of the Mil guidelines to smaller packages, it did not study the applicability of the Howl-Mann equation based Test Condition A_2 (the flexible method). It should be noted that the MIL-STD document specifies that "Flexible Method shall be used unless otherwise specified in the acquisition document, purchase order, or contract."[7].

The theoretical and practical limits that can be measured by the helium mass spectrometer have been characterized previously [16, 19]. This characterization is used in the present study to analyze the limitations of the MIL-STD guidelines for a helium mass spectrometer based hermeticity testing when they are applied to packages with small internal cavities ($< 10^{-2}$ cc).

3.2 Background

The MIL-STD specified fine leak detection techniques that are commonly used are:

a) The optical fine leak test (Test condition C_5)

b) The helium fine leak test (Test conditions A_1 and A_2)

3.2.1 Optical fine leak test (Test condition C5)

In the optical fine leak test [8, 16, 19] the specimen is placed in a pressure vessel, where it is subjected to an invariant pressure. For a non-hermetic specimen, the pressure differential (i.e., the difference between the applied external pressure and the cavity internal pressure) changes over a period of time. Since the specimen deformation is proportional to the pressure differential, the leak rate can be determined using an analytical relationship between the deformation and the true leak rate. The concept is illustrated schematically in Figure 3-1. It should be noted that the maximum value of the applied external pressure is less than or equal to the maximum pressure that the chamber and the specimen can withstand.
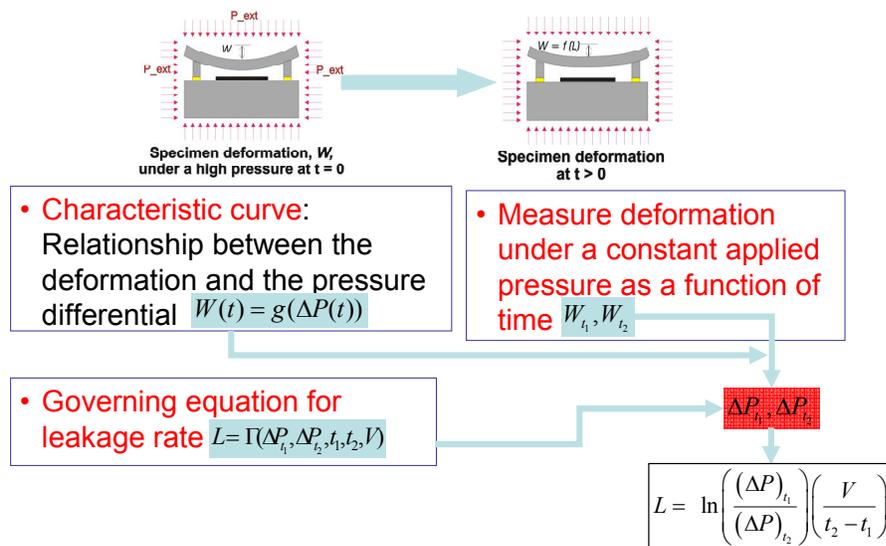
Figure 3-1 Deformation of a package with a cavity volume of 10^{-5} cc, subjected to a pressure of 15 atm.

Section 3.6.1 of the MIL-STD-883F document [7] specifies the following formula for calculating the maximum allowable thickness of the cap/lid of the specimen.

$$\frac{R^4}{ET^3} \geq A \tag{1}$$

where A is equal to 1 x 10^{-4} in the limiting case, R is the minimum width of free lid (inside braze or cavity dimension in inches), E is the modulus of elasticity of the lid material in psi and T is lid thickness in inches.

For a silicon lid (E = 150 GPa [12]) with the typical dimensions of 1 mm x 1 mm that can be seen in a Wafer Level Package (WLP) MEMS device, Eq. 1 yields a maximum allowable thickness of the cap/lid to be only 26.3 μm. According to the MIL-STD guidelines the optical fine leak test is inapplicable for a lid thickness greater than the value. In practice, most small volume packaged MEMS have a lid thickness on the order of a few hundred microns. Therefore, the optical fine leak test is not suitable for these packages, thereby motivating the use of the helium fine leak test.

3.2.2 Helium fine leak test (Test conditions A_1 and A_2)

Hermeticity Measurement with a Helium Mass Spectrometer

The definitions pertinent to this test are as follows [7]:

a)   Measured leak rate: The measured leak rate (R) is defined as the leak rate of a given package as measured under specified conditions and employing a specified test medium. The measured leak rate is expressed in units of atmosphere cubic centimeters per second (atm cc/s). The measured leak rate is also referred to as the *apparent leak rate*.

b)   Equivalent standard leak rate: The equivalent standard leak rate (L_a) of a package is defined as the leak rate when the high-pressure side is at 1 atm (760 mm Hg absolute) and the low-pressure side is at a pressure of less than 1 mm Hg absolute (i.e., ≈ vacuum). The equivalent standard leak

rate is also referred to as the *true leak rate*. It can be regarded as the leak rate *normalized* for a unit pressure differential.

The conceptual idea of the helium fine leak test is to "bomb" the specimen with helium, i.e., subject it to helium pressurized at a value called the bombing pressure, P_b, for a period of time, t_b, and then transfer it to a helium mass spectrometer to measure the rate at which helium leaks out. It is to be noted that in this arrangement there is a dwell time, t_{dwell}, between *completion* of bombing i.e., when the specimen is taken out of the bombing chamber and *start* of the measurement of the leak rate. During this time some of the helium escapes from the specimen. In the spectrometer, the specimen is subjected to a vacuum. The helium leaks out and produces a signal proportional to the rate at which it comes out. The leak rate measured by the spectrometer is the measured or apparent leak rate, R, as discussed above. The spectrometer is calibrated to indicate this apparent leak rate directly. Mathematically, the process can be described by the Howl-Mann equation [11], which has the following form:

$$R_i = \frac{L_a P_b}{P_0}\left(\frac{M_a}{M_{helium}}\right)^{\frac{1}{2}}\left\{1-e^{-\frac{L_a t_b}{V P_0}\left(\frac{M_a}{M_{helium}}\right)^{\frac{1}{2}}}\right\}e^{-\frac{L_a t_{dwell}}{V P_0}\left(\frac{M_a}{M_{helium}}\right)^{\frac{1}{2}}} \tag{2}$$

where $M_a = 28.7$ g and $M_{helium} = 4$ g are the molecular weight of air and helium, in grams, respectively; $P_0 = 1$ atm is the atmospheric pressure and R_i is the apparent leak rate at the instant the spectrometer is switched on.

The terms $\left\{ 1 - e^{-\frac{L_a t_b}{V P_0} \left(\frac{M_a}{M_{helium}} \right)^{\frac{1}{2}}} \right\}$ and $e^{-\frac{L_a t_{dwell}}{V P_0} \left(\frac{M_a}{M_{helium}} \right)^{\frac{1}{2}}}$ represent the exponential rise and

decay in the cavity pressure during the bombing time and the dwell period,

respectively [20]. As the specimen continues to leak inside the spectrometer, the

apparent leak rate decreases exponentially and is given by the following relationship:

$$R(t) = R_i \cdot e^{-\frac{L_a t}{V P_0} \left(\frac{M_a}{M_{helium}} \right)^{\frac{1}{2}}} \qquad (3)$$

where t is the lime elapsed since the spectrometer is turned on. It is obvious that the

apparent leak rate depends on package parameters (L_a, V) and the test conditions (P_b,

t_b, t_{dwell}). In addition, its value changes continuously during the test, i.e., it varies with

the passage of time, t.

Test Conditions A$_1$ and A$_2$

The MIL-STD document prescribes two methods for the test; viz. fixed (A$_1$) and

flexible (A$_2$) but advocates the use of the latter as the default choice. It should be

noted that neither one of these two methods "quantifies" the package leak rate.

Rather, they "qualify" it in that they establish that the leak rate is larger or smaller

than a specified reject limit.

    a) Fixed method: In the fixed method, the specimen is tested using the
appropriate conditions specified in Table 3-1. The time, t_b, is the time under
the bombing pressure and the time, t_{dwell}, is the maximum time that is allowed
after release of pressure before the device is tested in the spectrometer. The
package is deemed "good" if the apparent leak rate is lower than the reject
limit specified based on its internal cavity volume.

b) Flexible method: In the flexible method, the reject limit is first established in terms of the true air leak rate. This value of "L_a" is substituted in the Howl-Mann equation. The user can choose any values for the test parameters P_b, t_b and t_{dwell} (the method is called flexible for this reason). The only guideline is that the chosen parameters should produce a measurable signal in the spectrometer. The package is deemed "good" if the apparent leak rate is lower than the value calculated from the Howl-Mann equation using the reject limit as L_a. The document specifies certain rejection limits and states that these limits should be used unless otherwise specified [7]. These limits are summarized in Table 3-2. It should be noted that the "unless otherwise specified" clause specified above provides the user with the option to set up different reject criteria depending on the application.

Table 3-1: Specified conditions for the "fixed" method

Volume of package (V) in cm^3	Bombing condition			R_i Reject limit (atm cc/s He)
	P_b (Psia±2)	Minimum exposure time (t_b: hours)	Maximum dwell (t_{dwell}: hours)	
<0.05 >0.05 - <0.5 >0.5 - <1.0 >1.0 - <10.0 >10.0 - <20.0	75 75 45 45 45	2 4 2 5 10	1 1 1 1 1	5 x 10^{-8} 5 x 10^{-8} 1 x 10^{-7} 5 x 10^{-8} 5 x 10^{-8}

Table 3-2: Specified limits for the flexible method

Volume of package (V) in cm^3	L_a Reject limit (atm cc/s)
<0.01	5×10^{-8}
>0.01 - <0.4	1×10^{-7}
>0.4	1×10^{-6}

3.3 Mil-Spec Based Helium Fine Leak Test for Smaller Volumes

The leak behavior of packages when subjected to the helium fine leak test is investigated for different cavity volumes. The test parameters and the measurement sensitivity of the spectrometer used in the analysis include P_b = 5 atm, t_b = 6 hours, t_{dwell} = 10 minutes and R_{limit} = 10^{-10} atm-cc/s. These values are chosen to be consistent with the requirements of both the test conditions (A$_1$ and A$_2$). Leak rates larger than the detection domain of the gross leak test (10^{-4} atm-cc/s) are not considered since they are of no practical importance.

Equation 2 can be used to obtain a plot of R_i versus L_a for a given volume. The plots of R_i versus L_a for three different volumes (0.001 cc, 0.1 cc and 10 cc) are shown in Figure 3-2.
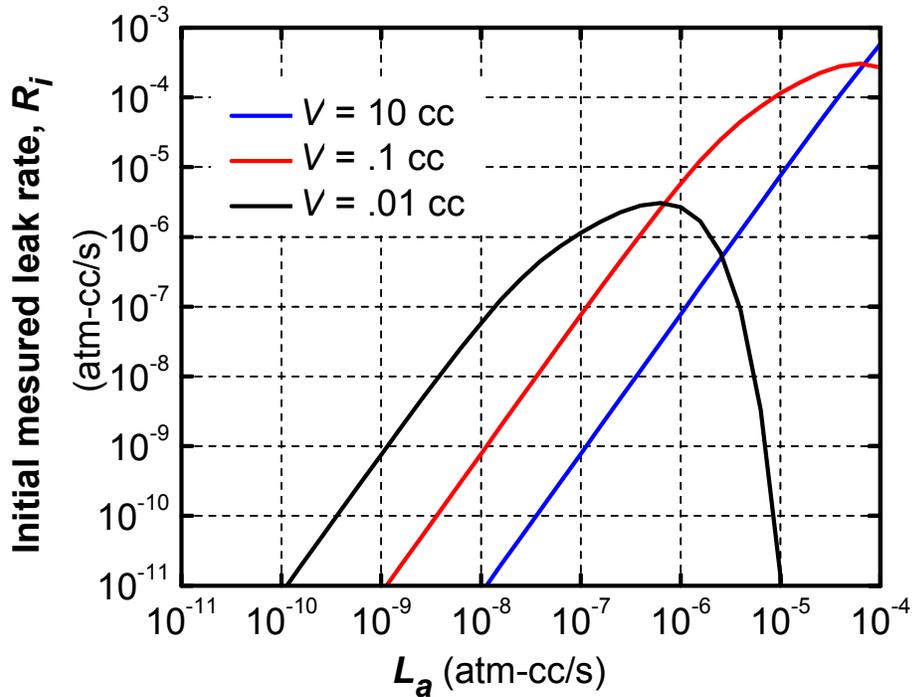
Figure 3-2 Initial apparent leak rate, R_i, as a function of the true leak rate, L_a, for cavity volumes of 0.1 cc, 0.001 cc and 10 cc. The test parameters are $P_b = 5$ atm, $t_b = 6$ hours and $t_{dwell} = 10$ minutes.

For the larger cavity volumes (0.1 cc and 10 cc), there exists one to one correspondence between R_i and L_a. As the cavity volume decreases, however, there are two value of L_a, which can produce the same R_i; i.e., the true leak rate cannot be defined uniquely from a measured apparent leak rate. This limits the applicability of the helium fine leak test for smaller volumes.

The following definitions will be used in the following sections to address the applicability of the method:

a) True Pass: Good packages that meet the passing criterion

b) True Fail: Bad packages that do not meet the passing criterion

c) False Pass: Bad packages that meet the passing criterion

d) False Fail: Good packages that do not meet the passing criterion

3.3.1 Measurable Limit (Inherent False Signal)

The spectrometer measurement limit is defined as the lowest apparent leak rate that the instrument can detect. Superposition of the spectrometer measurement limit, i.e. R_{limit}, on the plot of R_i versus L_a yields the range of measurable leak rates [16, 19]. This is schematically illustrated in Figure 3-3 where a plot (obtained using Eq. 2) of R_i as a function of L_a for a package with volume, $V = 5 \times 10^{-5}$ cc. Similar plots can be found in the literature [8, 16, 19].

It is evident from Figure 3-3 that the apparent leak rate, R_i, has to be higher than the measurement limit (R_{limit}) of the spectrometer to be able to detect a signal [16, 19]. If the true leak rate is outside of the range established by these limiting values, the measured leak rate will be lower than the measurement limit and will not be detectable at the time of measurement. For the packages with true leak rates higher than the upper limit (region shaded in grey), nearly all the helium bombed into the packages leaks out during the dwell time, while the amount of helium bombed into the package is not sufficient to produce a detectable helium signal for those with true leak rates lower than the lower limit (region shaded in green).
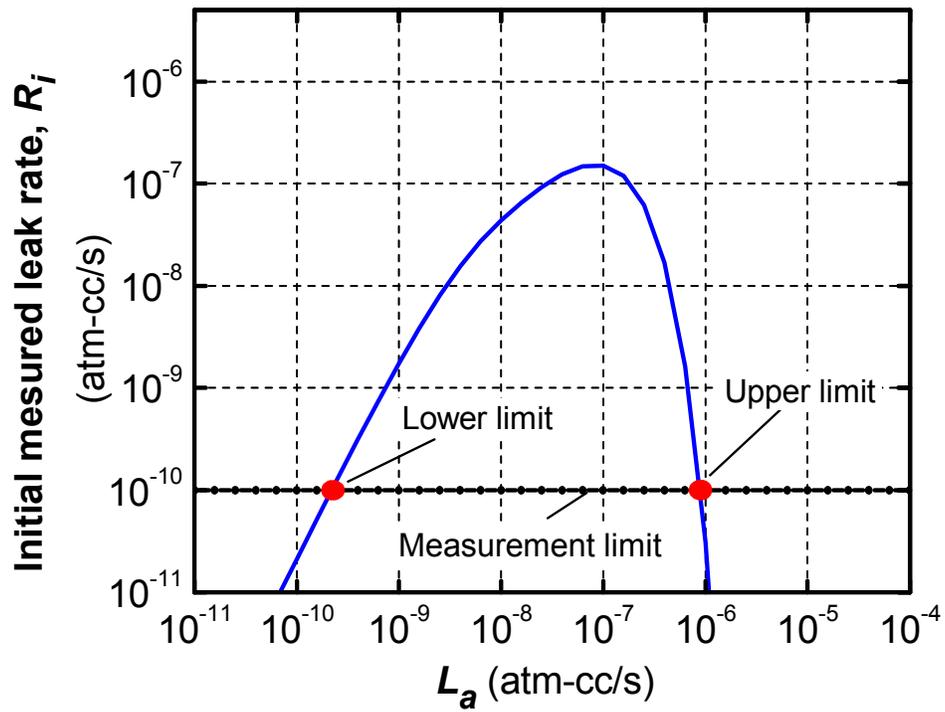
Figure 3-3 Initial apparent leak rate as a function of the true leak rate [16, 19].

In Ref. [16, 19], the practical upper and lower limits were determined as a function of cavity volume using the spectrometer measurement limit, R_{limit}, as 10^{-10} atm-cc/s. The results are shown in Figure 3-4.
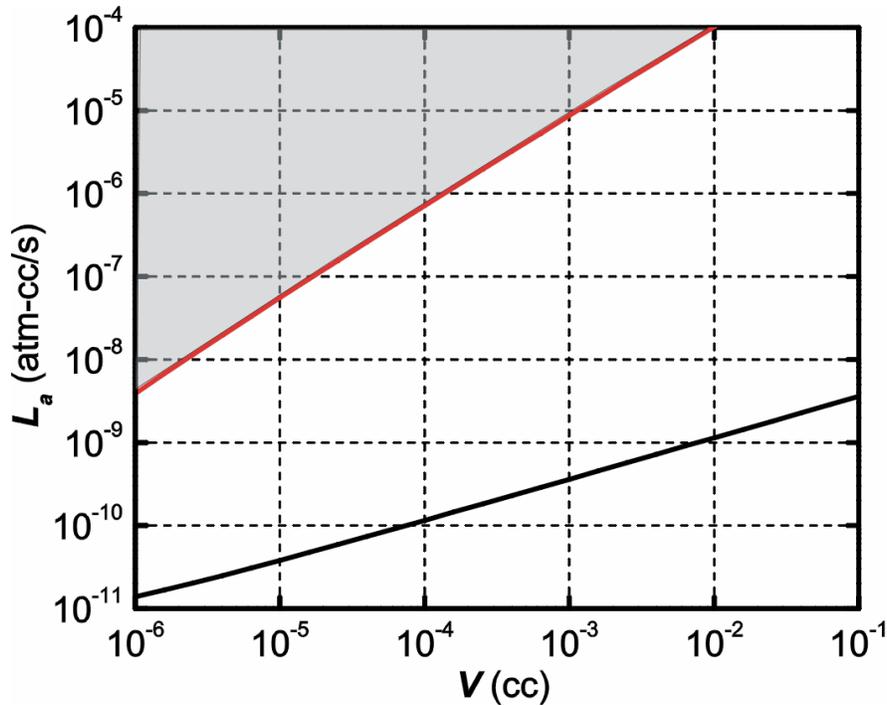
Figure 3-4 Range of leak rates that can be measured by the helium leak test [16, 19].

It is worth noting that the packages with true leak rates higher than the upper limit (region shaded in grey) can contain "*False Pass*" ones because the apparent leak rate produced by the packages (≈ 0) is always lower than the signal that the reject limit can produce regardless of the test conditions. This will be addressed for each test condition below.

3.3.2 Test Condition A₁

Consider a package with $V = 10^{-3}$ cc. The reject limit of Test condition A_1 is 5 x 10^{-8} atm-cc/s (Table 3-1). The R_i versus L_a plot and the specified reject limit are shown in Figure 3-5. For the specified reject limit, there are two corresponding true leak rates, L_{a1} and L_{a2}. For the current example, substituting $R_i = 5$ x 10^{-8} atm-cc/s in Equation 2 and solving for L_a yields two values: $L_{a1} = 4.32$ x 10^{-9} atm-cc/s, $L_{a2} = 1.03$ x 10^{-7} atm-

cc/s. The spectrum of true leak rates in the plot can be divided into the *three* regions, as shown in Figure 3-5.
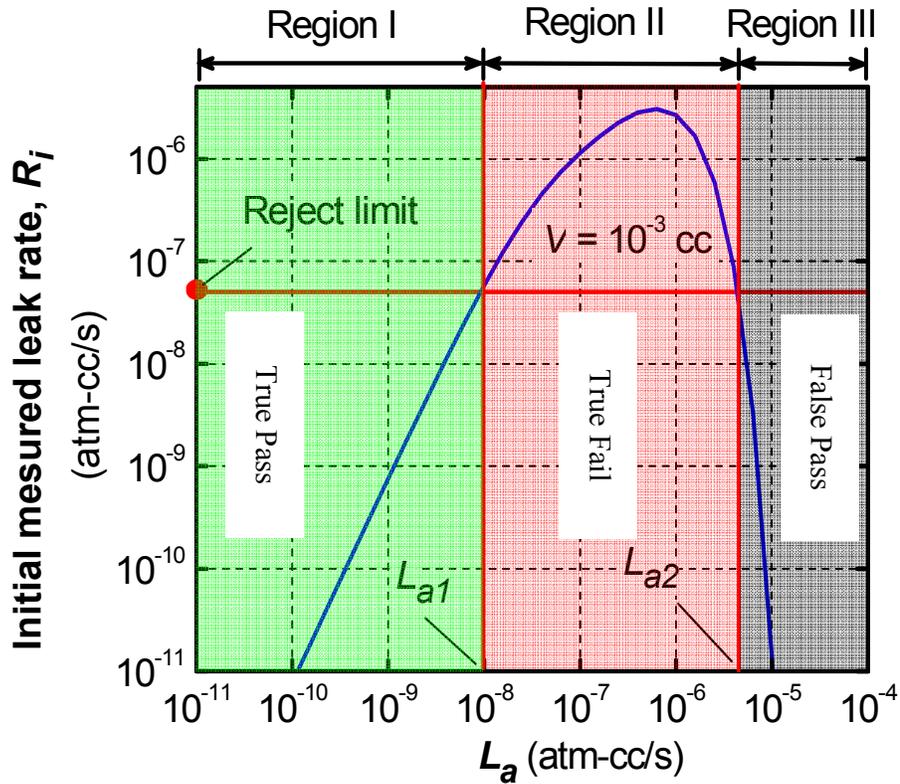
Figure 3-5 R_i as a function of L_a for a cavity volume of 10^{-3} cc, where the reject criterion of Test Condition A_1 ($R_i = 5 \times 10^{-8}$ atm-cc/s) divides the true leak domain into three regions.

Packages with leak rates in Region I ($L_a < L_{a1}$) and Region II ($L_{a1} < L_a < L_{a2}$) fall into the categories of *True Pass* and *True Fail*, respectively. Region III ($L_a > L_{a2}$) represents *False Pass*. The apparent leak rate of Region III is lower than the specified reject limit but the true leak rate of Region III is actually higher than that of *True Fail* packages (Region II). As mentioned earlier, the helium bombed into the specimen leaks out significantly during the dwell time due to the high true leak rate, and hence the apparent leak rate becomes lower than the specified reject limit.

Region II can be detected without any ambiguity since a true leak in Region II produces an apparent leak rate higher than the specified reject limit. However, true leak rates in both Regions I and III produce apparent leak rates lower than the specified reject limit and are not distinguishable from each other. For larger volumes that exhibit the one to one correspondence between R_i and L_a, only *two* regions (Regions I and II) exist, which can be easily distinguishable by comparing the apparent leak rate with the specified reject limit.

3.3.3 Test Condition A₂

Test condition A_2 uses the true leak rate as the rejection criterion. The package is *True Pass* if the true leak rate of the package is lower than the specified reject limit (L_r). Since the true leak rate is not directly measured, the value of R_i corresponding to the rejection criterion (will be referred to as R_r) is first determined using Eq. 2 and the condition for *True Pass* and *Fail* can be established if the measured apparent leak rate, R_i, is lower or higher than R_r.

The same problem seen in Test Condition A_1 exists due to the loss of the one-to-one correspondence. The value of R_i corresponding to the rejection criterion uniquely exists but one more value of true leak rate will exist if the one-to-one correspondence is lost; this true leak rate will be referred to as *conjugate true leak rate*, L_c. Two false signals are possible depending upon whether or not the rejection criterion is higher or lower than the conjugate rate. They are illustrated in Figure 3-6 and Figure 3-7, where the arrows indicate the sequence of calculations.
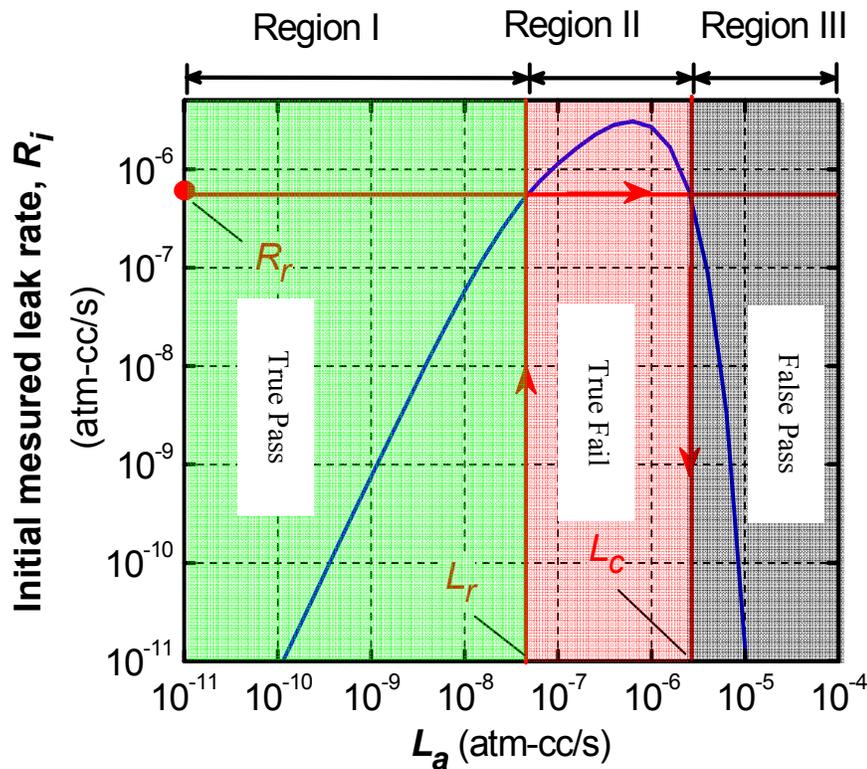
Figure 3-6 R_i as a function of L_a for a cavity volume of 10^{-3} cc; the reject criterion of Test Condition A₂ ($L_r = 5 \times 10^{-8}$ cc) produces $R_r = 5.84 \times 10^{-7}$ atm-cc/s and $L_c = 2.52 \times 10^{-6}$ atm-cc/s.

CASE 1 ($L_r < L_c$): Consider a package with $V = 10^{-3}$ cc. The specified reject limit for the package is $L_r = 5 \times 10^{-8}$ cc (Table 3-2). The Howl-Mann equation (Eq. 2) yields $R_r = 5.84 \times 10^{-7}$ atm-cc/s. Substituting $R_r = 5.84 \times 10^{-7}$ atm-cc/s in Eq. 2 and solving for L_a yields the conjugate true leak rate $L_c = 2.52 \times 10^{-6}$ atm-cc/s. The entire R_i versus L_a plot for Case 1 is shown in Figure 3-6, which is similar to Figure 3-5. Like Test condition A₁, packages with leak rates in Region I ($L_a < L_r$) and Region II ($L_r < L_a < L_c$) fall into the category of *True Pass* and *True Fail*, respectively. Region III ($L_a > L_c$) represents *False Pass* packages as the apparent leak rate of Region III is lower than R_r.

It should be noted that any further testing using a gross leak test, which can only measure leak rates of 10^{-4} atm-cc/s and higher [6], will not be able to detect these *False Pass* packages.
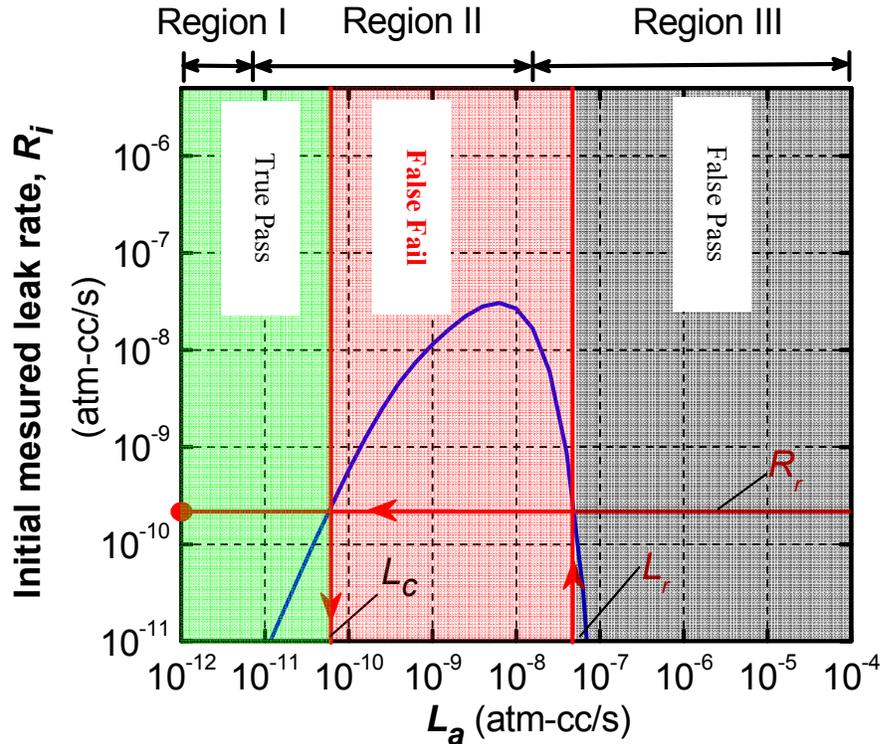
Figure 3-7 R_i as a function of L_a for a cavity volume of 10^{-3} cc; the reject criterion of Test Condition A$_2$ ($L_r = 5$ x 10^{-8} cc) produces $R_r = 2.16$ x 10^{-10} atm-cc/s and $L_c = 5.74$ x 10^{-11} atm-cc/s.

CASE 2 ($L_r > L_c$): Let's consider a package with $V = 10^{-5}$ cc. The specified reject limit for this volume is also $L_a = 5$ x 10^{-8} cc (Table 3-2). The Howl-Mann equation (Eq. 2) yields $R_r = 2.16$ x 10^{-10} atm-cc/s. Substituting $R_r = 2.16$ x 10^{-10} atm-cc/s in Eq. 2 and solving for L_a yields the conjugate true leak rate $L_c = 5.74$ x 10^{-11} atm-cc/s. The entire R_i versus L_a plot for Case 2 is shown in Figure 3-7. As in Case 1, Region I ($L_a < L_c$) includes the *True Pass* packages and Region III ($L_a < L_r$)

includes the *False Pass* ones. The packages with true leak rates within Region II (L_c

< L_a < L_r) also produce R_i larger than R_r. According to the test criterion, these parts

should be rejected. However, these packages are "*False Fail*" because their true leak

rates are lower than the reject limit.

3.4 Domain of Applicability

The theory discussed above was used to generate the applicable domain of

Test conditions A_1 and A_2 prescribed in Method 1014.11 of the MIL-STD-883F

document. The results are shown in Figure 3-8 and Figure 3-9 for Test conditions A_1

and A_2, respectively, where the domains of true leak rate, corresponding to the four

definitions (*True Pass*, *True Fail*, *False Pass* and *False Fail*), are plotted as a

function of the internal cavity volume.
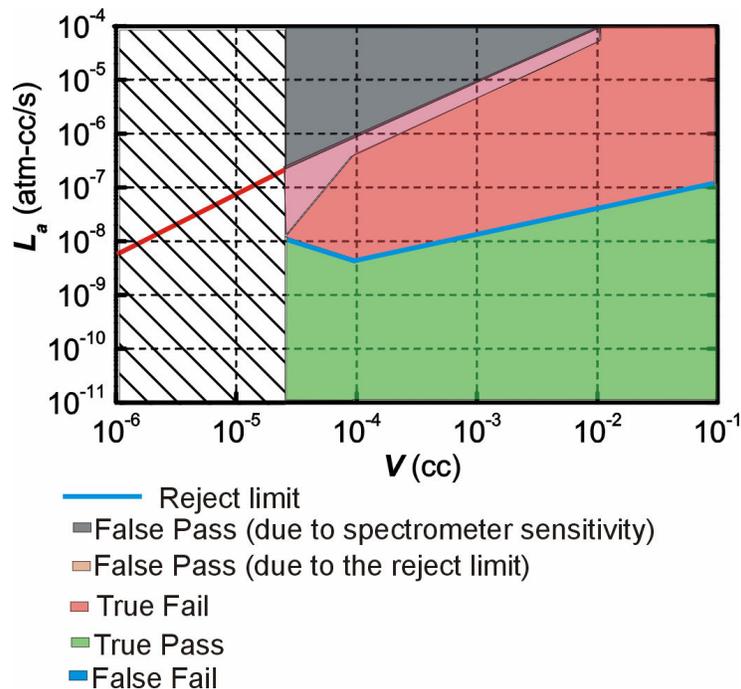
Figure 3-8 Domain of leak qualification of Test Condition A₁ for the test

parameters of P_b= 5 atm, t_b = 6 hours, t_{dwell} = 10 minutes.
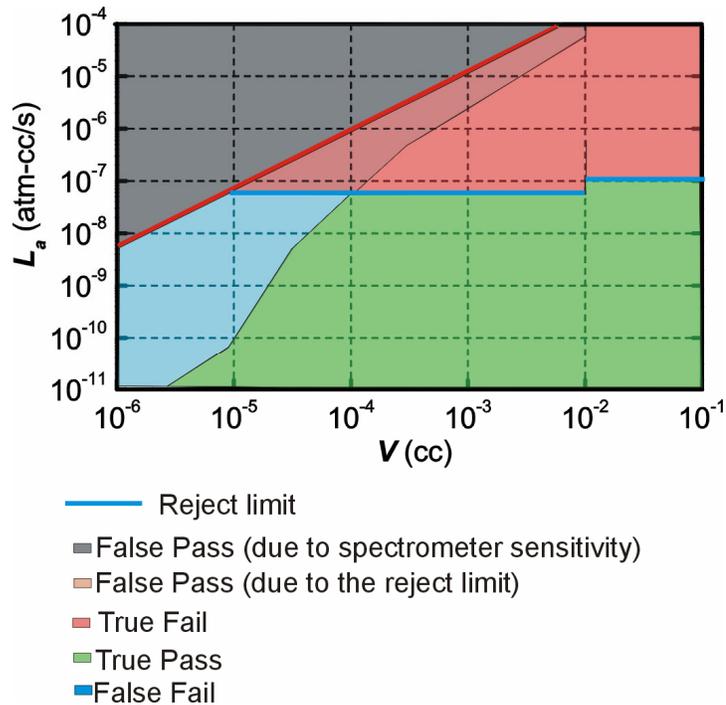
Figure 3-9 Domain of leak qualification of Test Condition A$_2$ for the test parameters of P_b= 5 atm, t_b = 6 hours, t_{dwell} = 10 minutes.

Since the reject limit (5 x 10^{-8} atm-cc/s for the given range of volumes) for Test condition A$_1$ is in terms of the measured leak rate (Table 3-1), this reject limit was converted into an equivalent true leak rate by using Eq. 2. It should be noted that solving Eq. 2 yields two roots, i.e., two true leak rate values corresponding to the specified reject limit[7].

In Figure 3-8, the lower one of these two values is plotted as the reject limit. The inflexion at $V = 10^{-4}$ cc in Figure 3-8 implies that the equivalent true leak rate based reject limit attains a minimum value at that point.

---

[7] Graphically, this is similar to plotting an R_i versus L_a plot for each of the considered volumes (similar to 0) and locating the points at which it intersects with the line $R_i = 5$ x 10^{-8} atm-cc/s.

The practical upper limit of the helium fine leak test is also shown in Figure 3-8 and Figure 3-9. Physically, these plots depict how the range of true leak rates is divided into different domains by (1) the measurement sensitivity of the spectrometer that imposes an upper and a lower limit on the measurement capability and (2) the reject limit imposed by the relevant MIL Spec guideline. In these plots, the *False Pass* due to the spectrometer sensitivity domain implies that for a very leaky package the measured signal will be below the measurement sensitivity of the spectrometer and hence undetectable.

For both test conditions, the cavity volumes larger than 10^{-2} cc do not produce any false signal. The domain for *False Pass* first takes place when the cavity volume becomes 10^{-2} cc and increases as the cavity volume decreases.
It should be noted that Test condition A_1 will not be valid for volumes less than 1.65 x 10^{-5} cc because the signal produced by the spectrometer will always be lower than the reject limit, $R = 5$ x 10^{-8} atm-cc/s, regardless of the true leak rate of the packages. The case of 1.65 x 10^{-5} cc is shown in Figure 3-10. It is also worth noting that *False Fail* signal occurs only with Test condition A_2 when the cavity volumes become smaller than 10^{-4} cc.
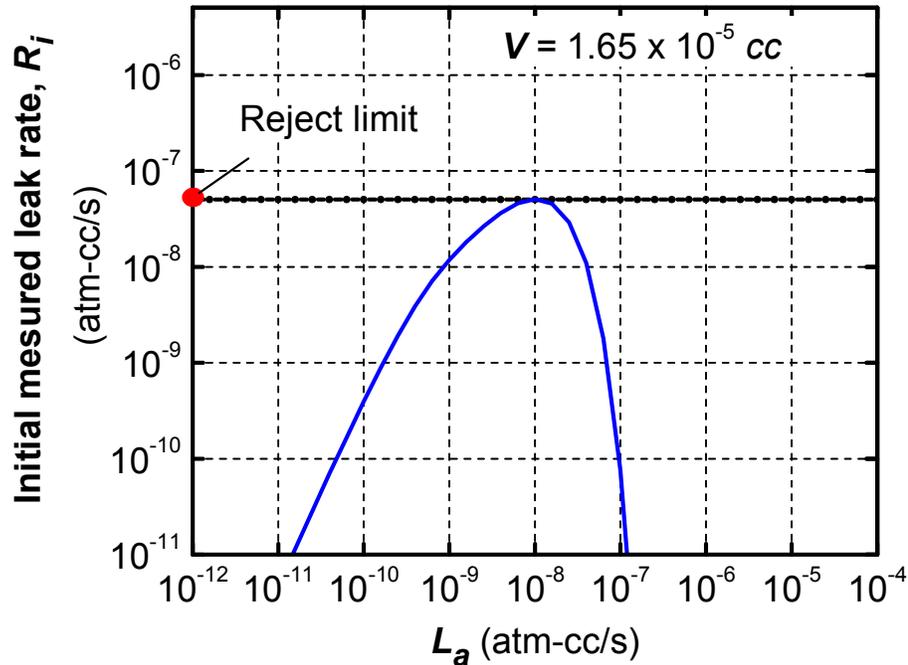
Figure 3-10 Illustration of inherent invalidity of Test condition A_1 for the volumes smaller than 1.65×10^{-5} cc; the plot shows that the spectrometer signal of the package with $V = 1.65 \times 10^{-5}$ cc is always be lower than the reject limit regardless of the true leak rate.

3.5 Discussion: Constant Reject Limit of Condition A_2

It is instructive to examine the validity of the constant reject limit of Test Condition A_2 for the internal cavity volume smaller than 10^{-2} cc. There is an inherent flaw in the constant reject limit in that as volumes get smaller, hermeticity requirement should become more stringent. The critical parameter in evaluating the effect of the ingress of a gas into the package is not the absolute amount of gas but the partial pressure (or concentration). The same amount of gas will produce a lower partial pressure in a larger package, and thus less detrimental.

If the package is initially at vacuum, the pressure inside the package at time t when it is exposed to an ambient pressure of P_b is:

$$p_t = P_b(1 - e^{-L_a t/VP_o})$$ (4)

It is evident from Eq. 4 that the pressure build-up over a fixed period of time[8] will be the *same* for different packages as long as the L_a/V ratio is constant. As mentioned earlier, the MIL-STD document states that Test Condition A_2 is flexible in that it allows the user to set a different reject limit. For the cavity volumes smaller than 10^{-2} cc, a variable reject limit that takes the constant partial pressure into account is proposed as a more realistic reject limit.

The reject limit of the existing criterion for $V = 0.01$ cc is $L_a = 5$ x 10^{-8} atm-cc/s (Table 3-2), which yields the L_a/V ratio of 5 x 10^{-6}. The reject limit (L_a) for each volume (V) can be adjusted to produce the constant value of L_a/V ratio. These values are summarized in Table 3-3.

Table 3-3 Variable reject limit suggested for Test Condition A_2

Volume (cc)	Reject limit (atm-cc/s)
10^{-5}	5 x 10^{-11}
10^{-4}	5 x 10^{-10}
10^{-3}	5 x 10^{-9}
10^{-2}	5 x 10^{-8}

These modified limits were used to recalculate the domain of leak qualification. The results are plotted in Figure 3-11 (a). A significant enhancement

---

[8] In a practical situation this would be the lifetime over which the package is designed to be reliable.

of the domain of leak qualification is evident. Yet a small region of *False Pass* due to

the reject limit exists.

   This *False Pass* region can be eliminated if the suggested variable reject limit

is further adjusted to make it equal to the lower limit of the measurable range for that

particular volume. These modified limits are tabulated in Table 3-4 and the

corresponding domain of leak qualification is depicted in Figure 3-11 (b).

Table 3-4 Modified variable reject limit suggested for Test Condition A_2

Volume (cc)	Reject limit (atm-cc/s)
10^{-5}	3.80×10^{-11}
10^{-4}	1.15×10^{-10}
10^{-3}	3.61×10^{-10}
10^{-2}	1.13×10^{-9}
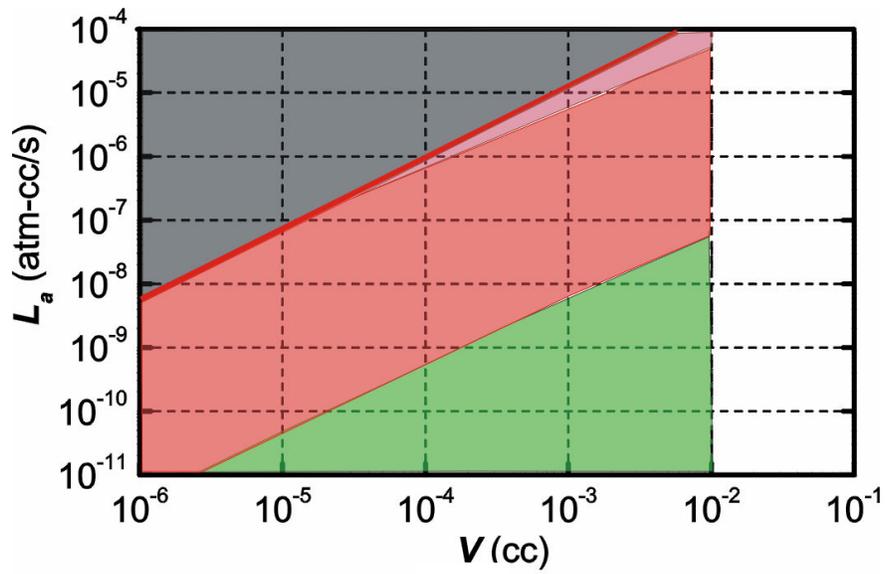
(a)
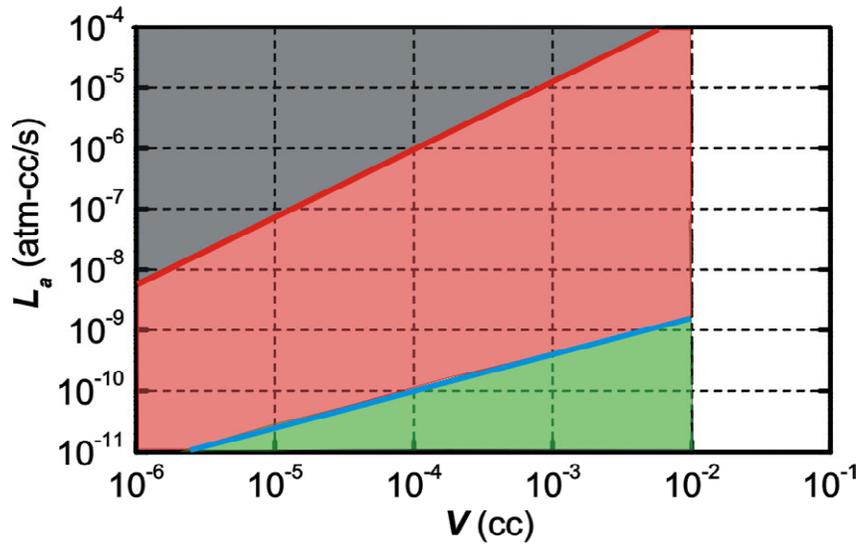
(b)

Figure 3-11 Domain of leak qualification of Test Condition A$_2$ using the variable reject limits.

It should be noted that these are only examples of how the limits for Test Condition A_2 can be modified. No matter how the reject limits are set, the inherent *False Pass* due to the spectrometer measurement sensitivity cannot be eliminated. In practice, it would be imperative to develop limits in tune with the performance requirements of the packages under consideration while increasing the measurement sensitivity of the spectrometer in order to increase the range of the measurable true leak rates for a given cavity volume.

3.6 Conclusion

The guidelines specified in Method 1014.11 of MIL-STD-883F for the optical interferometry and helium mass spectrometer based fine leak tests (Test conditions C_5 and A_1 and A_2) were reviewed. The existing gas conduction models were utilized to investigate the validity of the criteria defined in the test guidelines in term of true leak rates for their applicability to the packages with sub-micro liter cavity volumes. The results showed that only finite domain of true leak rates is valid when the volume is smaller than 10^{-2} cc and the invalid domain increases as the cavity volume decreases. The analytical framework was used to suggest the variable reject limits for Test Condition A_2 to extend its domain of applicability.

Chapter 4: Quantitative Characterization of True Leak Rate of Micro to Nanoliter Packages Using Helium Mass Spectrometer[9]

ABSTRACT

We propose a method to quantify the true leak rate of micro to nano-liter packages using the helium mass spectrometer. A new concept called "*pre-processing time*" is introduced to take into account (1) the instability of the helium mass spectrometer during the initial part of its operation and (2) the contribution of viscous conduction to the total conduction. The proposed method utilizes the complete profile of the apparent leak rate measured by the mass spectrometer and determines the true leak rate by performing a non-linear regression analysis. The method is implemented successfully to measure the true leak rate of MEMS packages. The validity of the proposed scheme is corroborated experimentally.

4.1 Introduction

Hermeticity is the ability of a seal to maintain an acceptable level of stable and sometimes inert ambience for packaged devices. Detection of fine leaks is critical for reliability assessment of Electronic/MEMS packages. Examples include a packaged cavity containing gyroscopes that require a near-vacuum ambient or a

---

[9] This chapter has been accepted for publication in the *IEEE Transactions on Advanced Packaging* under the title "Quantitative characterization of true leak rate of micro to nanoliter packages using a helium mass spectrometer", by A. Goswami, B. Han and S. J. Ham.

packaged cavity containing RF bulk acoustic resonators whose performance degrades significantly due to moisture ingress into the cavity.

A schematic of a typical MEMS package of interest is shown in Figure 4-1. As illustrated in the figure, the package comprises of a cap and a substrate bonded to each other such that they enclose a cavity between them which houses the MEMS device. Anodic bonding, fusion bonding and eutectic bonding are used widely for sealing MEMS packages. Cavity volumes are typically less than 10^{-3} cc.
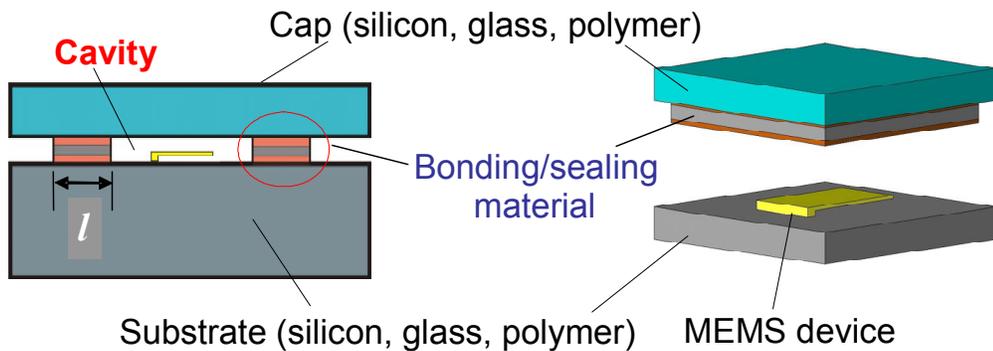
Figure 4-1 Schematic illustration of a MEMS package and the length of the leak channel, l.

The helium mass spectrometer based leak testing has been widely used in the industry for fine leak detection [21, 22]. In the helium fine leak test, the package is subjected to pressurized helium and then transferred to a helium mass spectrometer. The spectrometer measures the rate at which helium leaks out while the package is subjected to a vacuum.

The output of the spectrometer is the measured leak rate (R), which is defined as the leak rate of a given package as measured under specified test conditions [7]. The measured leak rate is also referred to as "*apparent leak rate*", which decreases as

a function of time. In practice only the *initial* apparent leak rate (R_i), i.e., the measured leak rate at the instant the spectrometer is switched on, is used as a measure of hermeticity [7].

The equivalent standard leak rate (L_a) of a package is defined as the leak rate when the high-pressure side is at 1 atmosphere (760 mm Hg absolute) and the low-pressure side is at a pressure of less than 1 mm Hg absolute (i.e., $\approx$ vacuum) [7]. The equivalent standard leak rate is also referred to as "*true leak rate*". The *true* leak rate (L_a) is the characteristic of the package and is only a function of leak opening geometries, while the *initial* apparent leak rate (R_i) is a function of the test parameters, the true leak rate and the specimen volume (V).

For relatively large packages, there exists one-to-one correspondence between the initial apparent leak rate and the true leak rate in the fine leak domain (less than 10^{-4} atm-cc/s). As the package volume becomes smaller (less than 10^{-3} cc), however, the one-to-one correspondence vanishes [16, 19]. This is illustrated in Figure 4-2, where the initial apparent leak rates are plotted for two different volumes (10 cc and 5 x 10^{-5} cc) as a function of the true leak rate. The approach established in Ref [16, 19] was used for the simulation, and the test conditions used for the simulation include the bombing pressure of 5 atm, the bombing time of 6 hours and the dwell time of 10 minutes. The loss of the one-to-one correspondence for the smaller volume (5 x 10^{-5} cc) is evident.
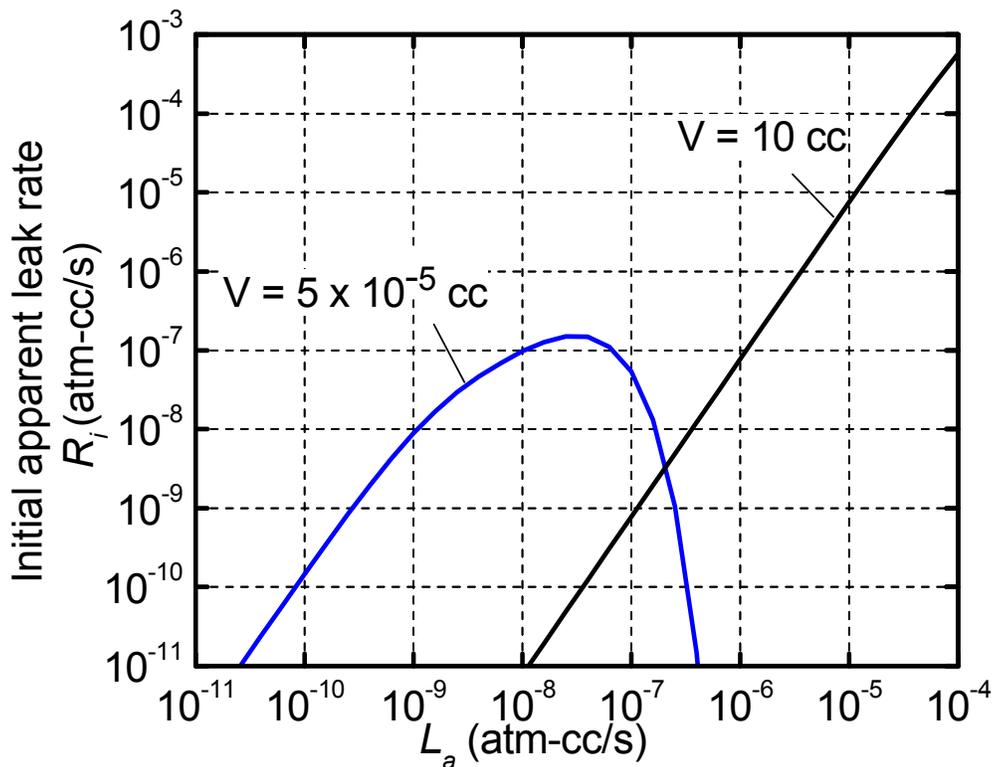
Figure 4-2 Initial apparent leak rate, R_i, as a function of the true leak rate, L_a, for two different cavity volumes (5 x 10^{-5} cc and 10 cc). The test conditions used for the simulation are: P_b = 5 atm, t_b = 6 hours and t_{dwell} = 10 minutes.

The consequence of this loss of one-to-one correspondence is that the initial apparent leak rate no longer carries quantitative meaning; for example, a package with a higher true leak rate (i.e. poor hermeticity) can produce a lower apparent leak rate signal than a package with a lower true leak rate (i.e., good hermeticity), thereby leading to erroneous interpretations of hermetic quality. This is illustrated in Figure 4-3, where the apparent leak rates of two packages with the same volume (5 x 10^{-5} cc) but with different true leak rates (5 x 10^{-7} and 5 x 10^{-8} atm-cc/s) are plotted as a

function of time. Under these test conditions, the package with the lower true leak rate (5×10^{-8} atm-cc/s) produces a higher apparent leak rate signal.
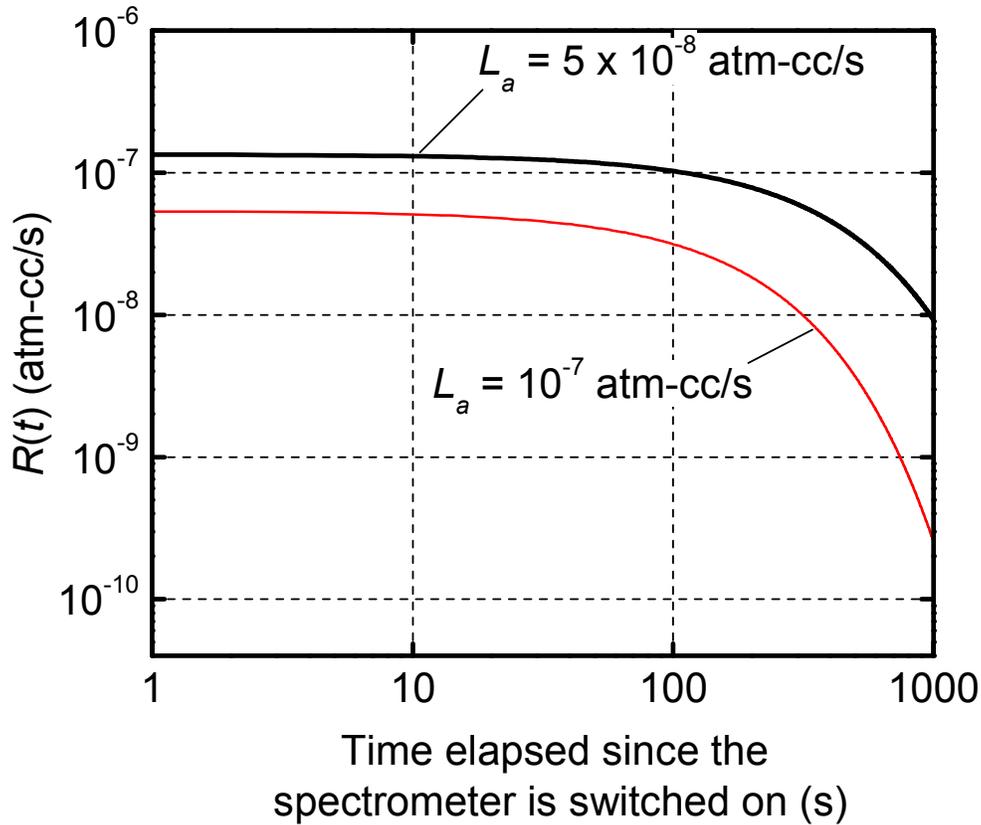
Figure 4-3 Apparent leak rates of a package ($V = 5 \times 10^{-5}$ cc) with two different true leak rates as a function of time. The test conditions used for the simulation are: $P_b = 5$ atm, $t_b = 6$ hours and $t_{dwell} = 10$ minutes.

The above illustrations confirm that the current approach based on the initial apparent leak rate has inherent limitations since it can only "indicate" what the true leak rate may be, and thus it can serve only as a qualitative benchmark. Furthermore, the current approach cannot be used to correlate the leak rate of two different gases or to predict the leak rate under a different set of ambient conditions. This is important in practice since many MEMS packages are subjected to accelerated testing

conditions in high temperature and high humidity environments. The use of the true leak rate as a measure of hermeticity facilitates a meaningful correlation between how the package performs under the accelerated test conditions as well as during actual operating conditions.

This paper proposes a method to extract the true leak rate using the He mass spectrometer. Unlike the current approach, the proposed method utilizes the complete profile of the apparent leak rate collected by the mass spectrometer and determines the true leak rate by performing a non-linear regression analysis. The theoretical limit of true leak rates that can be measured by the fine leak test was studied previously [16, 19]. The results are shown in Figure 4-4, where the upper and lower limits of the measurable true leak rates are plotted as a function of the package volume. The theory and the procedure to extract the true leak rates in this measurable range will be presented in the following sections.
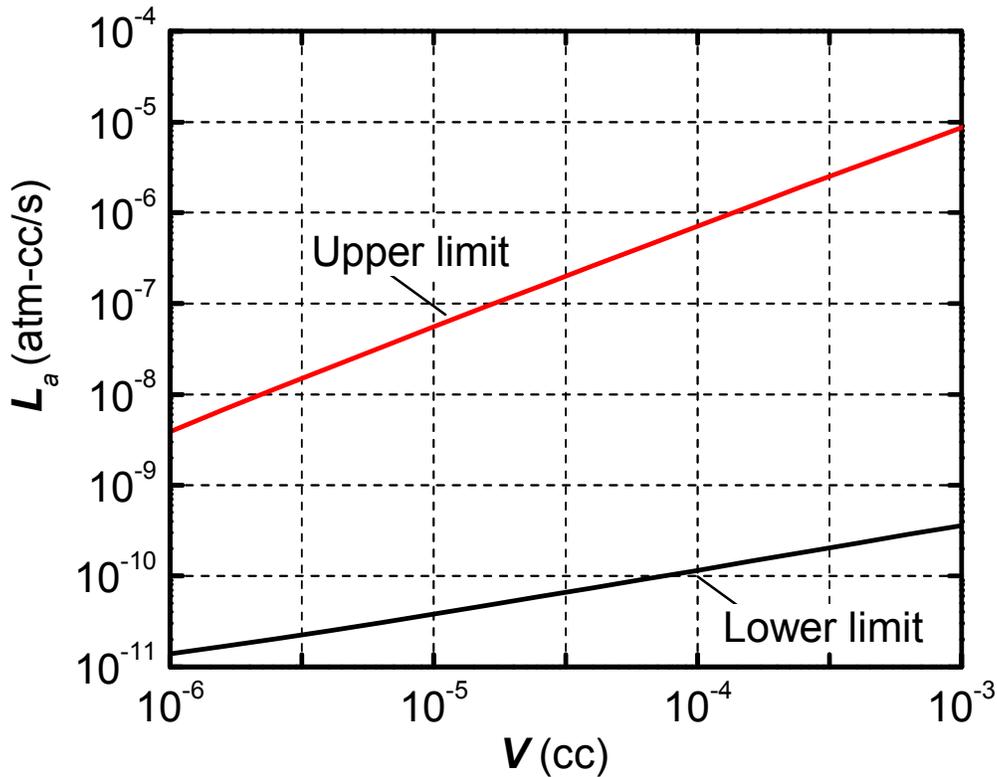
Figure 4-4 Theoretical upper and lower limits of true leak rates that can be measured by the helium leak test [16, 19].

4.2 Background: Conductance of Leak Channels [23]

The conductance of a leak channel is defined as the *apparent leak rate* (or the leak rate at any instant), R, per unit difference of pressure between the upstream (P_u) and the downstream (P_d) of the channel. Mathematically, it can be expressed as:

$$F = \frac{R}{P_u - P_d} \tag{1}$$

Conductance can be expressed in terms of the channel dimensions, fluid properties and ambient conditions. The exact expression depends on the nature of the flow regime. Gas flow is divided into three regimes based on the nature of the flow as

determined by the ratio of the characteristic dimension of the leak channel (the radius

of the circular cross section, a) and the mean free path, mfp, of the gas which is

defined as the average distance traveled by the molecules of the gas between

successive collisions. The mean free path is mathematically expressed in cgs units as:

$$mfp = \frac{kT}{\sqrt{2}\pi P \sigma^2} \qquad (2)$$

where K is the Boltzman constant, σ is the diameter of the molecule (Helium: 2.2 x

10^{-8} cm, Air: 3.7 x 10^{-8} cm [24]), T is the absolute temperature and P is the pressure

of the chamber in which the gas is enclosed. In determining the mfp of a gas flowing

through a leak channel, the average pressure, P_a $\left(= \frac{P_u + P_d}{2} \right)$, should be used in Eq.

2.

The three flow regimes are [23]:

a) Molecular flow regime: The mean free path of the gas molecules is large

compared to the characteristic dimension of the leak channel. The rate of flow is

limited, not by collisions between molecules, but by collisions of the molecules

with the walls of the leak channel. In the molecular flow regime, the molecules

move independently of each other.

b) Viscous flow regime: The mean free path of gas molecules is small compared to

the characteristic dimension of the leak channel. In the viscous flow regime, the

rate of flow is limited by intermolecular collisions.

c) Transition flow regime: The flow characteristics are determined by both intermolecular collisions as well as collisions between the molecules and the walls.

Analytical expressions for conductance in the molecular and viscous regimes are available in the literature [23]. For a cylindrical leak channel with radius a and length l, the conductance in the molecular regime, F_m, can be expressed in cgs units as:

$$F_m = \frac{2}{3}\pi \frac{a^3}{l}\left(\frac{8R_0T}{\pi M}\right)^{\frac{1}{2}} = \frac{30480a^3}{l}\sqrt{\frac{T}{M}} \qquad (3)$$

where R_0 is the gas constant and M is molecular weight of the gas.

The conductance in the viscous regime, F_v, can be expressed as:

$$F_v = \frac{\pi a^4 P_a}{8\eta l} \qquad (4)$$

where η is the viscosity of the gas (Helium: 194 micro-Poise, Air: 184 micro-Poise [24]). According to the kinetic theory of gases, the viscosity can be expressed as:

$$\eta = 0.499\rho v_a mfp = 0.499\rho\left(\frac{8R_0T}{\pi M}\right)^{\frac{1}{2}} mfp \qquad (5)$$

where ρ is the density of the gas and is equal to $P_a\left(\frac{M}{R_0T}\right)$.

In the transient flow regime, the total conductance is a sum of contributions from both molecular and viscous conduction mechanisms. Knudsen experimentally measured the conductance of a cylindrical leak channel and developed a semi-empirical equation for the total conductance, F, in the transient flow regime as [25]:

$$F_T = F_v + ZF_m = F_m\left(\dfrac{F_v}{F_m} + Z\right) \quad \text{where} \quad Z = \left(\dfrac{1 + 2.507\dfrac{a}{mfp}}{1 + 3.095\dfrac{a}{mfp}}\right) \tag{6}$$

It should be noted that as the $\dfrac{a}{mfp}$ ratio decreases, the conductance defined by Eq. 6

(F) will approach the pure molecular conductance (Eq. 3). Similarly, as the ratio

increases, the value of F will approach that of pure viscous conductance (Eq. 4).

Recalling the definition of the true leak rate as the leak rate at $P_u = 1$ atm and $P_d \approx$

vacuum, the true leak rate leak rate (L_a) of a package can be expressed as

$$L_a = |F|_{P_a=0.5}(1-0) = |F|_{P_a=0.5} P_o \tag{7}$$

where $P_o = 1$ atm and $|F|_{P_a=0.5}$ is the conductance for an average pressure of 0.5 atm.

It is worth noting that for given values of the true leak rate and length of the

conductance channel, the corresponding radius, a, can be calculated using Eqs. 6 and

7.

4.3 Mathematical Analysis of Helium Leak Test

4.3.1 Procedure of Modified Helium fine leak test

The steps that comprise the modified helium fine leak test are illustrated in

Figure 4-5.
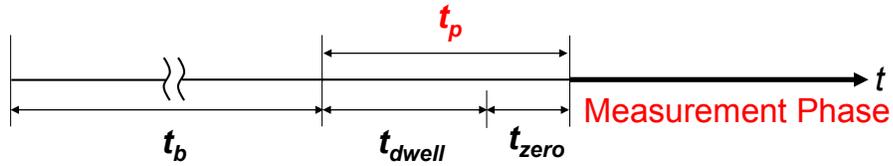
- Bombing time, t_b: The duration for which the specimen is exposed to pressurized helium (on the order of hours)

- Dwell time, t_{dwell}: Time elapsed between the end of bombing and the start of the spectrometer (on the order of about 10 minutes).

- Zero signal time, t_{zero}: Time taken by the zero signal to stabilize (on the order of a couple of minutes).

- Preprocessing time, t_p: Time elapsed between the end of bombing and the point at which the zero signal stabilizes; i.e., $t_p = t_{dwell} + t_{zero}$

Figure 4-5 Different stages of the modified helium fine leak test.

The first step comprises of "bombing" the specimen with helium, i.e., subjecting it to helium pressurized at the bombing pressure, P_b, for the bombing period, t_b, and then transferring it to a helium mass spectrometer where a vacuum is pulled to measure the rate at which He leaks out. It should be noted that in this measurement procedure there is "*dwell time*", t_{dwell}, between the instant the specimen is taken out of the bombing chamber and the instant the spectrometer is switched on, during which some of the helium escapes from the package.

Ideally the spectrometer should measure only the helium leaking out of the package, i.e. the *actual* signal. In practice, however, a small amount of helium present in ambient air contributes to the signal in the form of noise [16, 19]. This extra signal is called the "*zero signal*". The zero signal becomes negligible as soon as the air

present inside the test chamber of the mass spectrometer is drawn out. This short

duration will be referred to as "*zero signal time*", t_{zero}.

For quantitative characterization of the true leak rate, stable apparent leak rate

data must be utilized for consistency and accuracy. Therefore, the data to be used for

a subsequent regression analysis should be taken only after the zero signal becomes

negligible. We introduce a new parameter called *"preprocessing time"*, which is the

sum of the dwell time, t_{dwell}, and the zero signal time, t_{zero}. Physically, the

preprocessing time, t_p, is the time that elapses from the instant when the specimen is

taken out of the bombing chamber to the instant that collection of useful leak rate data

is started.

4.3.2 Mathematical Formulation

An approach similar to the one outlined in reference [13] is adopted to model

the modified helium leak test. In the analyses the initial pressure of the package

cavity is assumed to be zero (at vacuum). It is also assumed that the leak path is a

single cylindrical channel with radius, *a*, and length *l*.

The test is divided into three phases, viz. bombing, preprocessing, and

measurement phases. For the purpose of mathematical modeling, the preprocessing

phase is further divided into two sub-phases, the dwell phase and the zero signal

phase, since the downstream pressure of each sub-phase is different (1 atm and

vacuum for the dwell and zero signal phases, respectively). In each phase, the ratio

between *a* and *mfp* (*a/mfp*) is continuously calculated to update the value of

conductance using Eq. 6. The conductance is used to determine outflow/inflow of

gas and thereby calculate changes in the internal pressure.

Bombing:

During the bombing phase, the upstream pressure, P_u, is equal to the bombing pressure, P_b. The internal pressure of the cavity, $P_i(t)$, increases steadily and reaches a constant value of $P_i(t_b)$ at $t = t_b$, which can be expressed as:

$$P_i(t_b) = P_i(0) + \int_0^{t_b} \frac{R(t)}{V} dt \ ; \quad R(t) = F(t)\left(P_b - P_i(t)\right)$$

$$\text{for } 0 < t < t_b$$

(8)

where V is the cavity volume, and $R(t)$ and $F(t)$ are the apparent leak rate and the total conductance at any given instant during bombing.

Dwell:

In this phase the internal cavity pressure is the upstream pressure, P_u, and it decreases steadily as helium leaks out of the package. The initial value of P_u is equal to the final cavity pressure calculated at the end of the bombing phase, i.e., $P_i(t_b)$, and the downstream pressure, P_d, is equal to 1 atm. The final cavity pressure after the dwell time can be calculated using the following equation:

$$P_i(t_b + t_{dwell}) = P_i(t_b) - \int_{t_b}^{t_b + t_{dwell}} \frac{R(t)}{V} dt \ ; \quad R(t) = F(t)\left(P_i(t) - 1\right)$$

$$\text{for } t_b < t < t_b + t_{dwell}$$

(9)

Zero signal time:

The internal cavity pressure is still the upstream pressure, P_u. The initial value of P_u is equal to the final cavity pressure calculated at the end of the dwell phase, $P_i(t_b + t_{dwell})$ and the downstream pressure, P_d, is equal to 0 (vacuum). The

final cavity pressure after the zero signal time can be calculated using the following

equation:

$$P_i(t_b + t_p) = P_i(t_b + t_{dwell}) - \int_{t_b + t_{dwell}}^{t_b + t_p} \frac{R(t)}{V} dt \ \ ; \ R(t) = F(t)(P_i(t) - 0)$$ (10)

for $t_b + t_{dwell} < t < t_b + t_p$

Measurement phase:

The internal cavity pressure is the upstream pressure, P_u. The initial internal

cavity pressure in the measurement phase is equal to the final cavity pressure

calculated at the end of the preprocessing, $P_i(t_b + t_p)$. The internal cavity pressure at

any time, t, i.e., the instantaneous value of upstream pressure can be calculated using

the following equation:

$$P_i(t) = P_i(t_b + t_p) - \int_{t_b + t_{dwell}}^{t_b + t_p} \frac{R(t)}{V} dt \ \ ; \ R(t) = F(t)(P_i(t) - 0)$$ (11)

for $t > t_b + t_p$

The model outlined above was used to simulate the helium leak test for the

package illustrated in Figure 4-1. The package, initially at vacuum, has an internal

cavity volume, $V = 5$ x 10^{-5} cc, and contains a leak channel with $a = 150$ nm and $l =$

50 μm. The test parameters used in the routine practice of the fine leak test are

employed for the simulation: $P_b = 5$ atm, $t_b = 6$ hours, $t_{dwell} = 10$ minutes and $t_{zero} =$

2.5 minutes. It is to be noted that the zero signal time is an experimentally

determined value and the procedure to determine this value will be explained in the

later section. The preprocessing time, t_p, is 12.5 minutes.

The results from the simulation are plotted in Figs. 4-6, 4-7 and 4-8. The

internal cavity pressure during the bombing phase is shown in Figure 4-6.
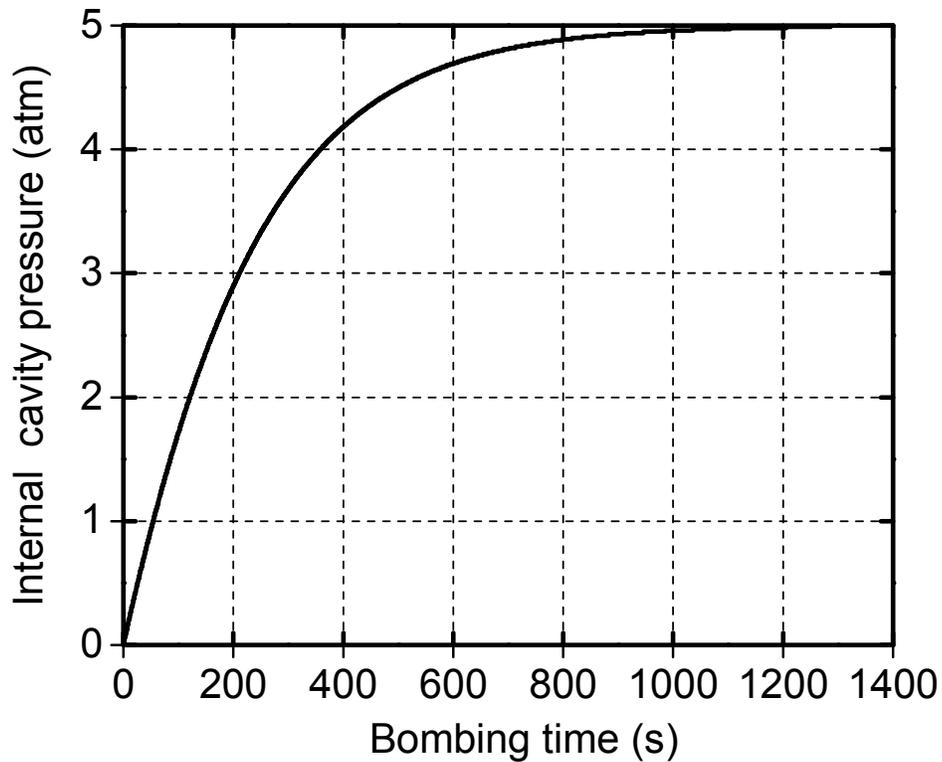
Figure 4-6 Internal cavity pressure during bombing (P_b = 5 atm), for a package (V = 5 x 10^{-5} cc) with a leak channel radius, a, of 150 nm and a leak channel length, l, of 50 μm.

The pressure increases exponentially as the bombing time increases. It should be noted that only a portion of the bombing phase has been plotted since the cavity attains the saturation pressure of 5 atm before the bombing is completed. The internal cavity pressure during the other phases is shown in Figure 4-7.
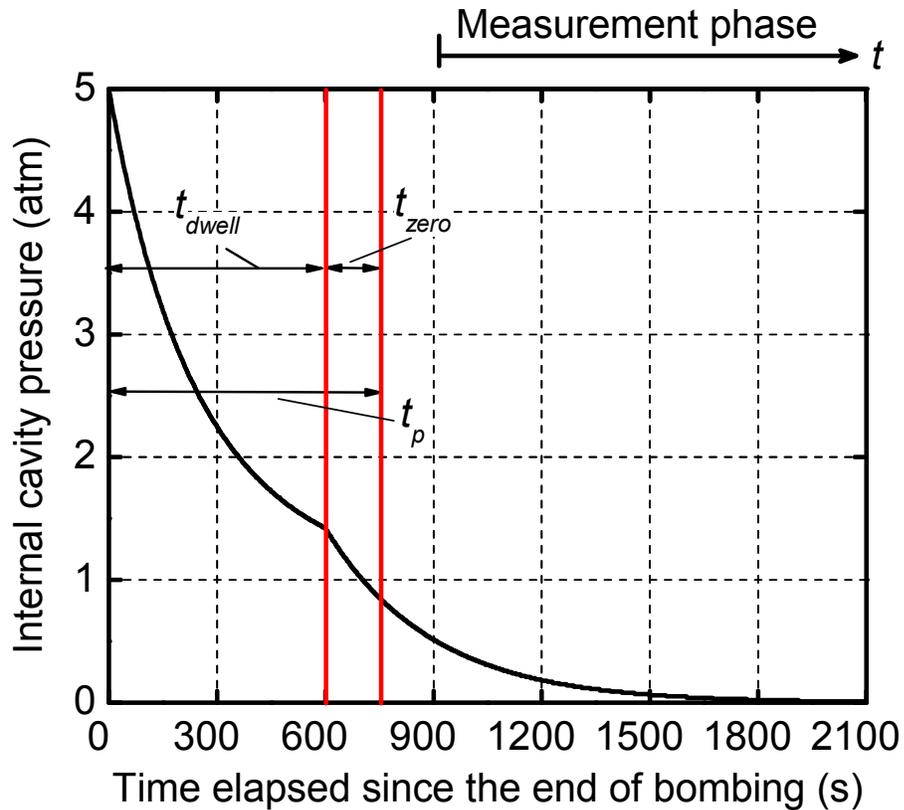
Figure 4-7 Internal cavity pressure of the package of Fig. 4-6 as a function of time elapsed since the end of bombing.

During the preprocessing, the cavity pressure decreases exponentially. It is worth noting that there is a sudden change in the slope of the cavity pressure at the end of the dwell time. It was attributed to the sudden change of the downstream pressure, P_d, from 1 atm to zero at the beginning of the zero signal time. The apparent leak rate during the measurement phase is shown in Figure 4-8. The exponential decrease of the apparent leak rate illustrates the expected output of the spectrometer for this theoretical case.
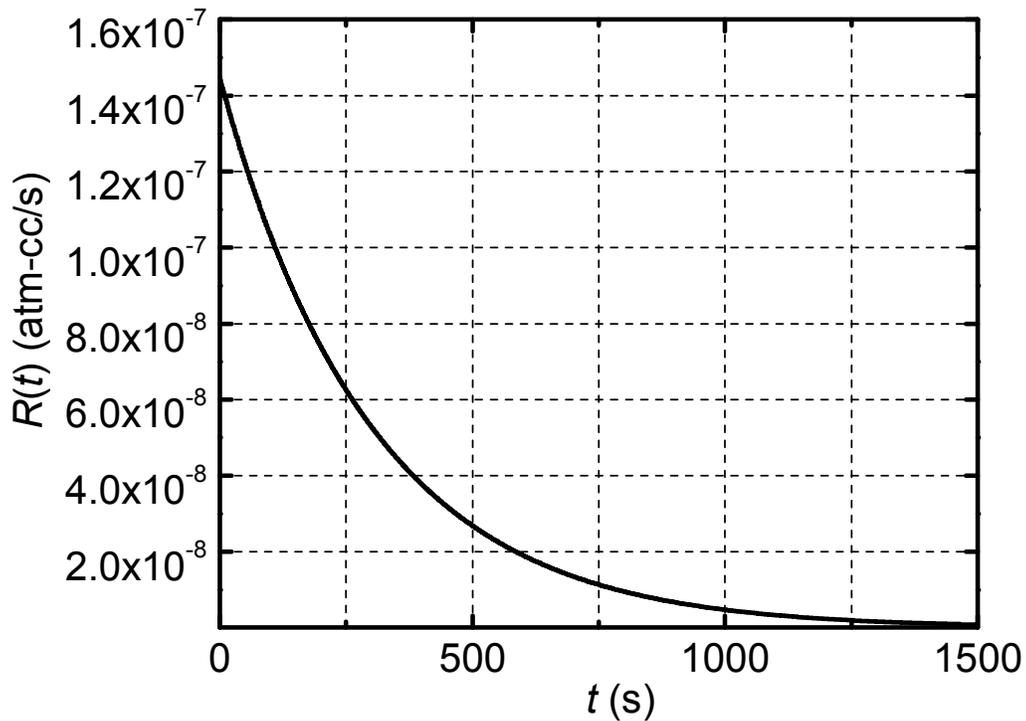
Figure 4-8 Apparent leak rate of the package of Fig. 4-6 as a function of time in the measurement phase.

It is instructive to know the true leak rate, L_a, of the channel used for the simulation. Using Eqs. 2 and 6 with an average pressure of 0.5 atm and a temperature of 298K, the true leak rate, L_a, can be calculated from Eq. 7 and it is 6.75 x 10^{-8} atm-cc/s.

4.4 Determination of the True Leak Rate from Apparent Leak Rate

The task of inferring L_a from $R(t)$ is to calculate the value of L_a inversely from the apparent leak rate profile after taking into account the test parameters and the cavity volume. A closed form analytical solution is always desired for the inverse problem since it allows an easy implementation of the over-deterministic approach [26]. Unlike the case of pure molecular flow, the conductance in the transition

regime is a function of the average pressure, which changes with time. As a result, a general simple closed form solution that defines the relationship between the apparent and true leak rates does not exist.

It is important to recall that viscous conduction dominates only when the leak channel opening (the true leak rate) is large and/or the average pressure is high. When the viscous contribution is high, helium leaks out fast during the preprocessing time. As a result, the internal pressure, and thus the pressure differential, drops so fast that the effect of the viscous conduction becomes insignificant after the preprocessing time. In other words, even when the viscous conduction is high after bombing, the contribution of viscous conduction decreases rapidly and the flow can be assumed molecular during the *measurement phase*. The following analysis is presented to support this argument.

4.4.1 Viscous Conductance during Preprocessing Time

The time dependent viscous contribution was calculated using the same test parameters in order to investigate the effect of viscous conduction in the cavity volumes of interest. A larger true leak rate implies a larger radius, and thus a larger viscous contribution. Consequently, the upper limits of the measurable leak rates shown in Figure 4-4 were used in the analysis as the upper limits produce the largest viscous contribution for the given cavity volume. The largest measurable true leak rates and the corresponding radius of the leak channel were calculated using Eqs. 2, 6 and 7 and are summarized in Table 4-1.

Table 4-1: Volume dependant largest measurable true leak rate and the corresponding radius of the leak channel.

V (cc)	L_{upper} (atm-cc/s)	a (cm)
10^{-6}	3.89 x 10^{-9}	5.93 x 10^{-6}
10^{-5}	5.54 x 10^{-8}	1.41 x 10^{-5}
10^{-4}	7.13 x 10^{-7}	3.14 x 10^{-5}
10^{-3}	8.69 x 10^{-6}	6.60 x 10^{-5}

The contribution of the viscous conduction is plotted in Figure 4-9 for the various volumes of interest (10^{-3} cc to 10^{-6} cc), where the percentage contribution of the viscous conductance, defined as $\dfrac{F_v}{F_T} \times 100$, is shown during the preprocessing time.
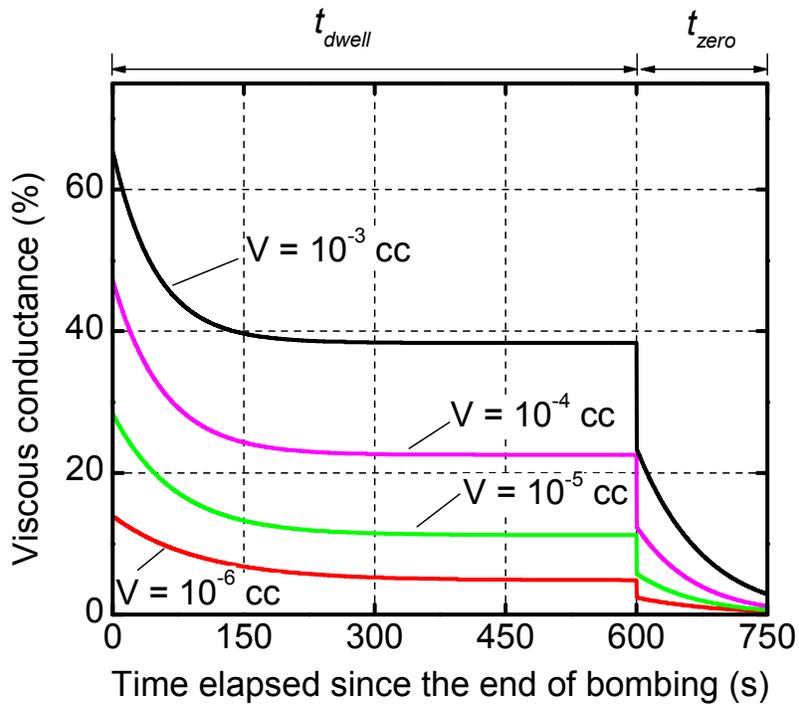
Figure 4-9 **Maximum contribution of the viscous conduction to the total conduction during the preprocessing time for various package volumes.**

It is evident that a viscous flow can contribute significantly to the apparent

leak rate during the preprocessing time, but for the *entire range* of volumes of the

current interest, the viscous contribution becomes negligible at the end of the

preprocessing time. The results imply that the flow becomes virtually molecular

during the *measurement phase*. It is worth noting that there is a sudden drop of the

viscous contribution at the end of the dwell time; this is caused by the change of the

downstream pressure, P_d, from 1 atm to zero at the beginning of the zero signal time

as mentioned before.

4.4.2 Governing Equation and Over-deterministic Approach

The previous analysis provides a technical rationale for using the governing

equations of molecular conduction to model the helium flow during the measurement

phase. The apparent leak rate can be modeled as:

$$R(t) = \Omega e^{-\frac{L_a t}{VP_0}\left(\frac{M_a}{M_{helium}}\right)^{\frac{1}{2}}} = \Omega e^{-\frac{2.68 L_a t}{VP_0}} \tag{12}$$

where M_a (28.7) and M_{helium} (4) are the molecular weight of air and helium (in grams),

respectively, and Ω is the apparent leak rate at the beginning of the measurement

phase. By taking logarithms, Eq. 12 can be written as:

$$\ln R(t) = \ln \Omega - \left(\frac{2.68 L_a}{VP_0}\right)t \tag{13}$$

Under idealized conditions, the two unknowns (Ω and L_a), can be obtained using two

arbitrary data points in the apparent leak rate profile. In practice, however, the errors

contained in the experimental data are not always negligible and this is the rationale

of the least-squares approach to fit the experimentally determined data to the theoretical solution [15, 26].

The least-squares method has been used in a regression analysis. The basic assumption that underlies this approach is that there are always differences between experimental results and theoretical values. Their relationship can be expressed using the error function, S, as:

$$S = \sum_{k=1}^{n} \left[\ln R_{t_k} - \left\{ \ln \Omega - \left(\frac{2.68 L_a}{V P_0} \right) t_k \right\} \right]^2 \tag{14}$$

where n is the number of data points, $R(t_k)$ and t_k are the corresponding data points of the apparent leak rate profile. The objective is to find the values of Ω and L_a that minimize the error function. This is achieved when the following conditions are satisfied:

$$\frac{\partial S}{\partial \Omega} = 0 \quad \text{and} \quad \frac{\partial S}{\partial L_a} = 0 \tag{15}$$

Eq. 15 can be solved numerically to determine R_i and L_a.

4.5 Implementation

The proposed method was implemented for a MEMS package. The package enclosed MEMS devices and comprised of a silicon cap bonded to a silicon substrate by means of a metallic seal (see Figure 4-1). The overall package dimensions are 2.5 mm x 2.5 mm x 0.7 mm. The internal cavity volume, V, of the tested packages is 2.156×10^{-4} cc.

4.5.1 Zero signal

The zero signal is a noise signal and should be excluded when the true leak rate is to be measured. Although it can vary slightly from an instrument to an instrument, the zero signal time can be measured experimentally simply by operating the mass spectrometer without any specimen inside the test chamber. Representative zero signals are shown in Figure 4-10. Although the initial signal strength varies, the signal stabilizes at a value of $\sim 10^{-10}$ atm-cc/s after $\sim$150 s.
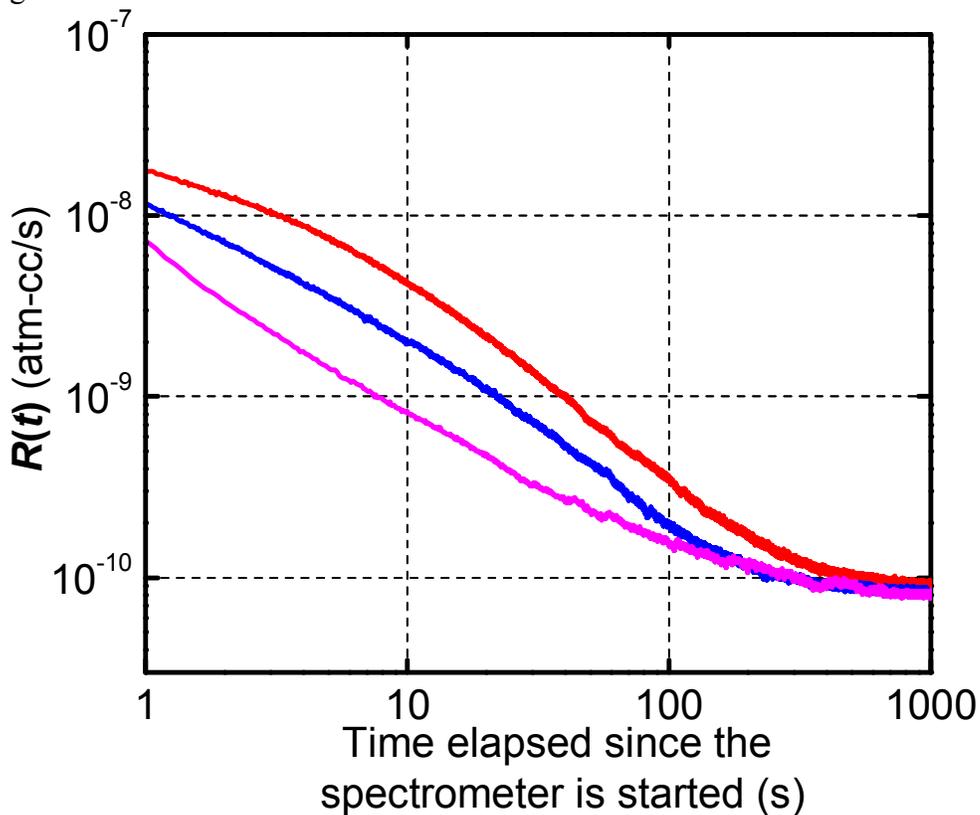
Figure 4-10 Representative zero signals

4.6 Test procedure

The following procedure was used in the experiment:

a) A single package was subjected to pressurized helium ($P_b = 5$ atm) for the duration of the bombing time, $t_b = 6$ hours.

b) It was transferred into the spectrometer in time, t_{dwell}, of 10 minutes, and the

spectrometer was switched on immediately after the dwell time.

c) Data recording started after the zero signal time t_{zero}, of 2.5 minutes.

4.6.1 Results

The apparent leak rate signal was measured using a commercial helium fine

leak tester (Model DGC 1001, Alcatel). The data was recorded at 5 Hz and the

results of Package 1 are shown in Figure 4-11(a), where the zero signal time and the

apparent leak rate at the beginning of the measurement phase (Ω) are also illustrated.

The data of the measurement phase was utilized to determine the true leak rate

through the regression analysis. The data was trimmed at a value of $R(t) = 2.5$ x 10^{-10}

atm-cc/s in order to negate the effect of the stabilized zero signal (10^{-10} atm-cc/s) on

the regression. The analysis was conducted using MATLAB, and yielded a true leak

rate value of 4.12 x 10^{-7} atm-cc/s with the goodness of fit, R^2, equal to 0.995. The

experimental data of the measurement phase are replotted in Figure 4-11(b) together

with the numerical result from the regressions analysis (i.e., a plot of Eq. 12 using the

values of Ω and L_a determined from the regression analysis). As expected from the

extremely high value of R^2, the regression results and the experimental data are nearly

identical. It is to be noted that only a few experimental data points are shown in

Figure 4-11(b) in order to distinguish them from the regression fit.
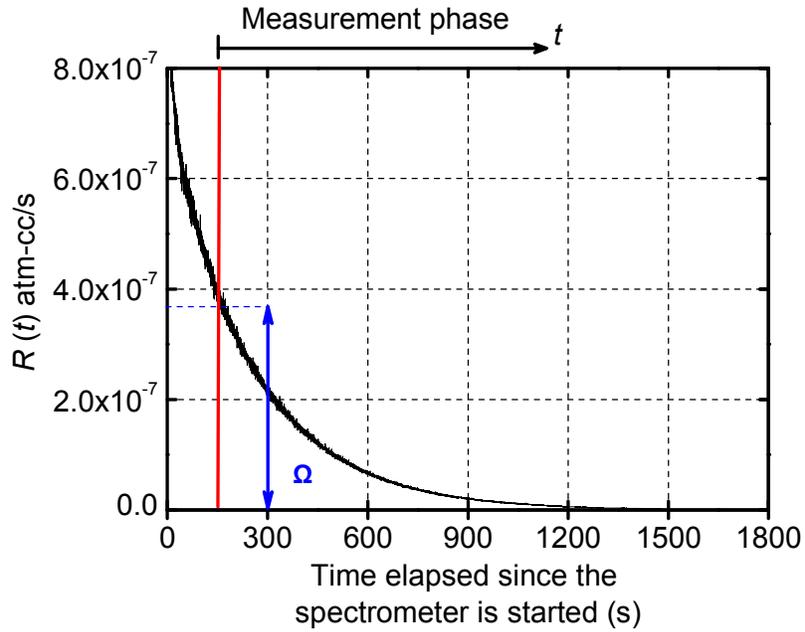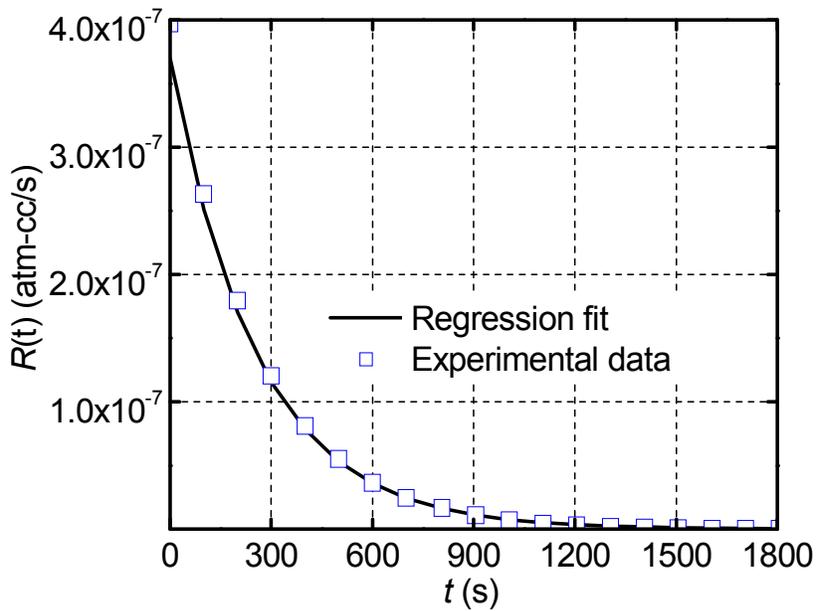
Figure 4- 11 (a) Apparent leak rates of Package 1 obtained from the mass

spectrometer; and (b) the data of the measurement phase are repotted with the

results from the regression analysis.
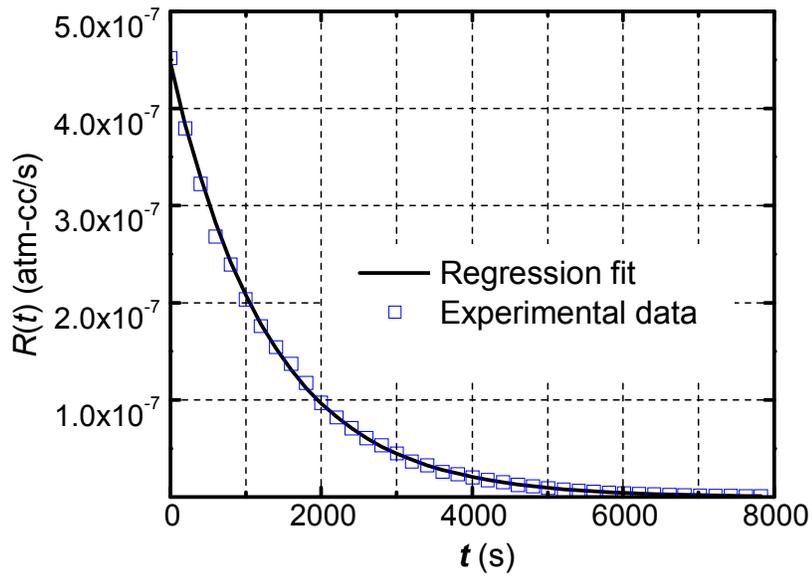
(a)
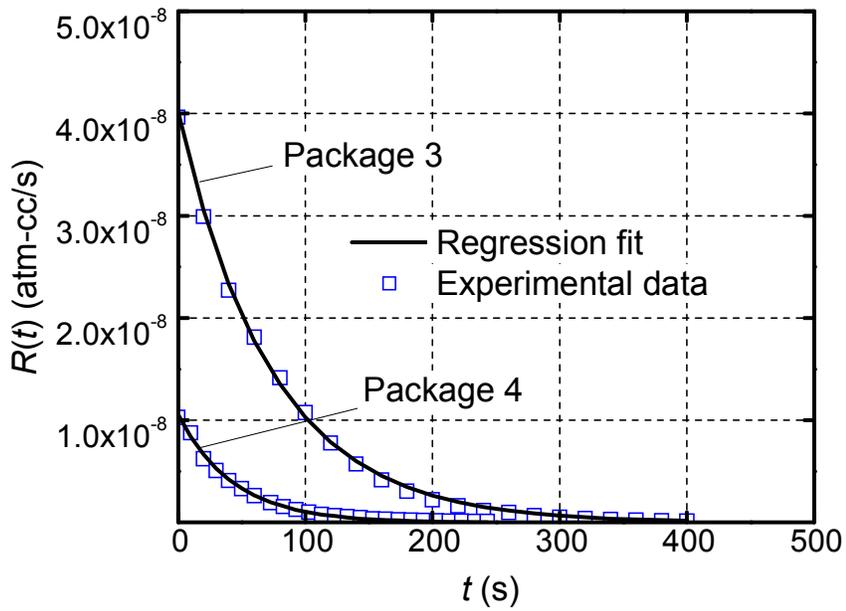
(b)

Figure 4-12 Apparent leak rates of (a) Package 2 and (b) Packages 3 and 4 over the measurement phase with the corresponding regression fits.

The method was used to test three more packages. The apparent leak rate signals of the packages and the corresponding regression fits are shown in Figure 4-12. The true leak rates of the packages obtained from the regression analysis are summarized in Table 4-2.

Table 4-2: Experimental results

	L_a (atm-cc/s)	Ω (atm-cc/s)	R^2 (Goodness of fit)
Package 1	3.12 x 10^{-7}	3.50 x 10^{-7}	0.9995
Package 2	6.17 x 10^{-8}	4.47 x 10^{-7}	0.9994
Package 3	1.10 x 10^{-6}	4.01 x 10^{-8}	0.9983
Package 4	1.84 x 10^{-6}	1.06 x 10^{-8}	0.9984

Despite the large range (the true leak rate of Package 4 is nearly 30 times larger than that of Package 2), the proposed method predicted all true leak rates accurately.

4.7 Discussion

The robustness of the technique was assessed by testing Package 1 again with different dwell times: 5 minutes (Case A) and 20 minutes (Case B). The apparent leak rate profile of each case and the corresponding regression fits are shown in Figure 4-13, where the reference case with a dwell time of 10 minutes is also shown for comparison.

The regression technique yields the true leak rate values of 2.99 x 10^{-7} atm-cc/s (Case A) and 3.20 x 10^{-7} atm-cc/s (Case B), which have less than 4% variation compared with the value of the reference case (3.12 x 10^{-7} atm-cc/s). These consistent values validate the efficacy of the proposed method.

The value of Ω was treated as an unknown in the regression analysis. It is tempting to utilize the experimentally measured value of Ω to reduce the number of unknowns in Eq. 13. A supplementary analysis was conducted to investigate the stability (convergence as well as accuracy) of the true leak rate solution with the experimentally measured value of Ω. The results revealed that the experimentally determined value of Ω did not alter the true leak rate significantly. This fact was attributed to the large number of data used in the *over-deterministic* approach in the current study.
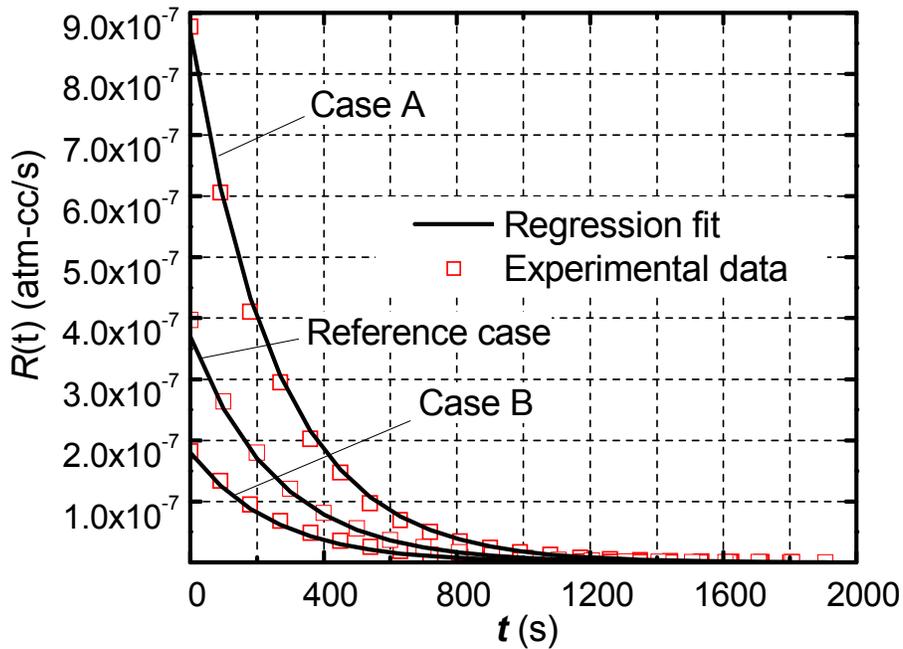
Figure 4-13 Apparent leak rates and the corresponding regression fits of Package 1 with various dwell times: Case A = 5 min; Case B = 20 min. The reference case has a dwell time of 10 min (Figure 4-11(b)).

In practice, the experimental value of Ω inherently contains uncertainties associated with the instrument, in particular, He mass spectrometer, and can be very

unstable. If large, the uncertainties in Ω can affect the true leak rate, and it is suggested that the value of Ω treated as an unknown as proposed in this study.

4.8 Conclusion

A procedure to extract the true leak rate from the apparent leak rate data generated by the helium mass spectrometer was proposed. A mathematical frame work was presented, and an over-deterministic approach was adopted to manipulate the experimental data. The technique was applied successfully to determine the true leak rate of a MEMS package with an internal cavity volume of 2.156 x 10-4 cc. The robustness of the proposed technique was confirmed by the consistent true leak rates obtained from the same package but subjected to different test parameters. The results clearly indicated that the proposed method can be applied to packages with a wide range of true leak rates. It should be noted, however, that only one type of MEMS package was used in this study. Further testing with different types of MEMS packages is suggested in order to establish the validity of the proposed method for all types of MEMS packages.

Chapter 5: Hermeticity Evaluation of Polymer-Sealed MEMS Packages Part I – Governing Equation and Numerical Implementation[10]

ABSTRACT

A gas transport mechanism is studied to characterize the hermetic behavior of polymer-sealed MEMS packages. The study is reported in two parts. In this first part, diffusion-based governing equations, which are fundamentally different from the conduction-based governing equations used for metallic seals, are proposed to predict a change in cavity pressure when a polymer-sealed MEMS package is exposed to a pressure differential. An effective numerical scheme to implement the governing equations is developed and its accuracy is verified by analytical solutions. The numerical scheme is used to investigate the effect of the diffusion properties and geometries of polymeric seals on gas leak behavior.

5.1 Introduction

MEMS devices are ubiquitous. They are found in various fields such as medical diagnostics, communications, automobiles, etc. The most critical role of MEMS packaging is to provide an internal cavity for moving parts and to maintain the initial condition of the cavity. The cavity is produced by sealing a gap between

---

[10] This chapter has been submitted for review to the *Journal of MEMS* under the title of "Hermeticity evaluation of polymer-sealed MEMS packages, Part I – Governing equations and numerical implementation" by C. Jang, A. Goswami, B. Han and S.J. Ham

cap and substrate wafers. The most commonly used sealing materials are low-melting point eutectics such as AuSn [27], AuSi [28] and other tin based alloys [29].

Polymers have recently gained widespread acceptance due to several advantages that they offer [30]; they include lower processing temperatures, compatibility with integrated circuit wafers and the ability to join practically any kind of wafer materials [31]. In addition, polymer wafer bonding does not require special wafer surface treatments such as planarization and excessive cleaning, and thus structures and particles on the wafer surfaces can be tolerated and compensated to some extent by the polymer adhesive [31]. Examples of polymeric seals include benzocyclobutene (BCB), parylene, polyimides and negative photoresists [6, 32].

Hermeticity of a MEMS package is a measure of the ability to maintain an acceptable level of stable and sometimes inert ambient for the packaged device. It impacts device reliability and hence lifetime expectation. Poor hermeticity can lead to ingress of contaminants, ambient gases and moisture thereby causing performance degradation. Good hermeticity is essential for compliance with performance and reliability standards.

Two methods are currently practiced in industry to characterize the hermeticity of MEMS packages: JEDEC based accelerated tests and helium fine leak test [19, 33]. In the accelerated tests the package is subjected to a high temperature and high humidity environment for an extended period of time [34]. Package failure is decided based on a package dependent reliability criterion. This may include degradation of the bond and performance metric change of the packaged device in a predetermined amount of time. It should be noted that these tests are basically

pass/fail tests and do not quantify hermeticity; they are not Physics of Failure (PoF) based tests. Therefore, it is extremely challenging to develop a universal accelerated test model, which offers a direct correlation between the test results and actual failures in the field.

On the other hand, the helium fine leak test [19, 35, 36] can be utilized to quantify hermeticity [35]. The conceptual idea of the helium fine leak test is to "bomb" the specimen with helium, i.e., subject it to pressurized helium for a period of time and then transfer it to a helium mass spectrometer to measure the rate at which the helium inside the package leaks out. Hermeticity is quantified by performing a regression analysis of the helium leak test data using the gas conduction based governing equation. This technique has been successfully implemented to determine the true leak rates of metal-sealed MEMS packages, where the following closed form equation was used for the regression analysis [35].

$$R(t) = \Omega \exp\left(-\frac{l_a t}{V p_0} \sqrt{\frac{M_{air}}{M_{He}}} \right) \qquad (1)$$

where R is the apparent leak rate, Ω is the initial apparent leak rate obtained at the He spectrometry test, l_a is the true leak rate, V is the volume of the cavity and , p_0 is a constant (1 atm) and M_{air} and M_{He} are the molar mass of air and He, respectively.
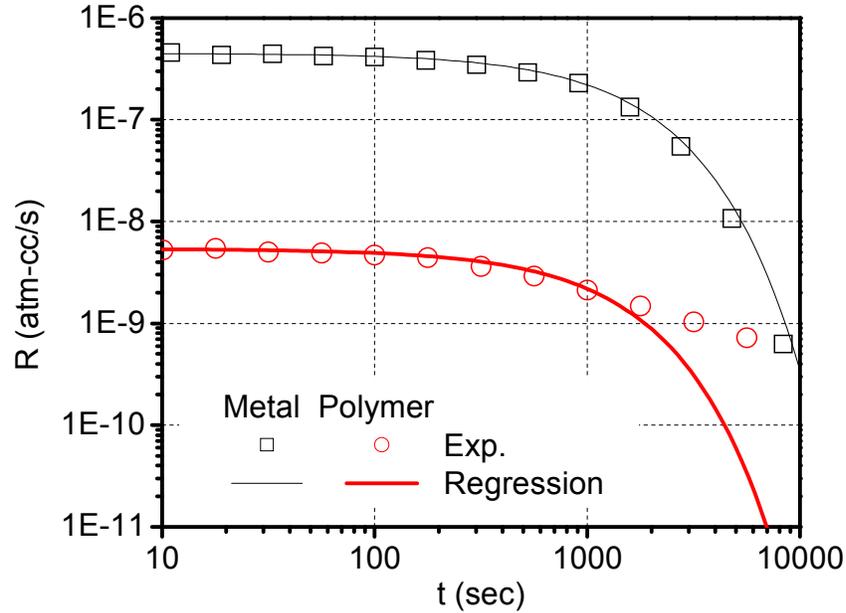
Figure 5-1 **Regression analysis using gas conduction equations to curve-fit helium leak test data of a metal-sealed packages ($V_{cavity} = 2.156 \times 10^{-4}$ cc) and a polymer-sealed package ($V_{cavity} = 3.1 \times 10^{-4}$ cc). For both packages, the bombing time was 6 hours at 4 atm and the dwell time was 10 minutes.**

Figure 5-1 shows He fine leak test results obtained from a metal-sealed packages ($V_{cavity} = 2.156 \times 10^{-4}$ cc) and a polymer-sealed package ($V_{cavity} = 3.1 \times 10^{-4}$ cc). The test conditions include a bombing time of 6 hours at 4 atm and a dwell time of 10 minutes. The results from the regression analysis using the gas conduction equations (Eq. (1)) are also plotted in Figure 5-1. Nearly perfect correlation exists for the metal-sealed package while for the polymer-sealed package correlation starts to fail after 1000 seconds. The regression was conducted in the linear scale for both data sets and the result was plotted in the log scale to highlight the discrepancy of the polymer-sealed package at the later stage of testing. The results clearly indicate that

the gas transport mechanism in the polymer seal is different from that in the metallic seal.

In metallic seals gas transport occurs through a few nanoscale leak channels (*gas conduction*), and thus the leak rate depends on the gas molar mass and the geometry of the channel (diameter and length). On the other hand, as indicated by the leak rate profiles obtained from the helium fine leak test of polymer-sealed packages [37], gas transport in polymeric seals occurs through a different mechanism, *gas diffusion*, and thus the leak rate depends on the gas diffusion properties (diffusivity and solubility) and the structure of polymer seals.

The objectives of this study are (1) to propose a gas diffusion mechanism based governing equation for hermeticity evaluation of polymer-sealed MEMS packages, (2) to develop a numerical scheme to implement the governing equation, (3) to verify the validity of the governing equation experimentally, and (4) to develop a procedure to measure gas diffusion properties. The study is reported in two parts. In this first part, the gas diffusion-based governing equations are described for polymer-sealed MEMS packages and a numerical scheme to implement the governing equations is presented. The numerical scheme is utilized to investigate the effect of the diffusion properties and geometries of polymeric seals on the gas leak behavior. Internal cavity pressure measurement, model validation and diffusion property measurement are addressed in the second part of this study [37].

5.2 Governing Equations

5.2.1 Gas diffusion equations

In both molecular gas conduction and gas diffusion, the gas flux can be described by the gas conductance equation in its general form as

$$J = F \Delta p \qquad (2)$$

where J is the gas mass flux (kg/m^{2}sec), F is the gas conductance (sec/m), Δp is the gas pressure differential (Pa). In the case of gas conduction, the expression for gas conductance is derived from the kinetic theory of gases while it is determined from Fick's first law in the case of gas diffusion. These expressions are

$$F = \frac{d_{tube}}{3L} \sqrt{\frac{8}{\pi M R_0 T}} \quad \text{for gas conduction} \qquad (3)$$

$$F = \frac{P}{L} \quad \text{for gas diffusion} \qquad (4)$$

where d_{tube} is the diameter of a nanoscale leak channel (m), L is the conduction or diffusion path length (m), M is the gas molar mass (kg/mol), R_0 is the universal gas constant (8.3145 J/molK), T is the temperature (K) and P is the permeability of the gas (sec). Although the two mechanisms are described by the same form of equations, there are two fundamental differences between them in terms of the geometry of gas transport paths and the time required for pressure gradient development inside the transport paths.

In gas conduction, gas molecules travel through a nanoscale channel and thus can be regarded as a Cartesian 1-D flow problem. The pressure gradient inside the flow channel is developed almost instantaneously, and transient effects are negligible.

Thus, the gas transport can be predicted by simply considering the conduction equation (Eq. (2)) with appropriate boundary conditions at both channel ends.

As opposed to gas conduction, gas diffusion takes place through the entire sealing area. Multi-dimensional modeling is necessary to account for the actual sealing layer structure. In addition, the gas pressure gradient inside the sealing material develops very slowly (usually on the order of hours to days). The conductance equation based on Fick's first law cannot model such a slow pressure gradient development and hence Fick's second law has to be considered.

Fick's second law is derived from the principle of mass continuity for an infinitesimal volume as

$$\frac{\partial C}{\partial t} = \nabla \cdot (D\nabla C) \tag{5}$$

where C is the gas concentration (kg/m^3), ∇ is the gradient operator and D is the gas diffusivity (m^2/sec). Introducing the linear Henry's law ($C = Sp$),

$$\frac{\partial (Sp)}{\partial t} = \nabla \cdot \left[D\nabla (Sp) \right] \tag{6}$$

where S is the solubility (sec^2/m^2) and p is the gas pressure (Pa). The permeability P is defined as the product of solubility and diffusivity ($P = DS$). In an isothermal problem, the above equation can be simplified as

$$\frac{\partial p}{\partial t} = D\nabla^2 p \tag{7}$$

5.2.2 Axisymmetric formulation

The transient boundary conditions are illustrated using an axisymmetric model. This will be used to verify a finite element method based numerical

implementation of the governing equation and its normalized form is utilized for an
extensive parametric study. A schematic diagram of the axisymmetric model is
illustrated in Figure 5-2. The axisymmetric form of Eq. (7) is

$$\frac{\partial p}{\partial t} = D\left(\frac{\partial^2 p}{\partial r^2} + \frac{1}{r}\frac{\partial p}{\partial r}\right) \tag{8}$$

and the boundary and initial conditions are

$$p(r_o,t) = p_a, \quad p(r_i,t) = p_c, \quad p(r,0) = 0 \tag{9}$$

The cavity pressure (p_c) change during each time step (Δt) can be calculated as

$$p_c(t + \Delta t) = p_c(t) - \frac{A_i R_0 T}{M V_c}\int_{\Delta t} J_{r=r_i}(t)dt \tag{10}$$

where A_i is the inner surface area ($= 2\pi r_i t$), M is the gas molar mass (kg/mol) and V_c
is the cavity volume ($= \pi r_i^2 t$).
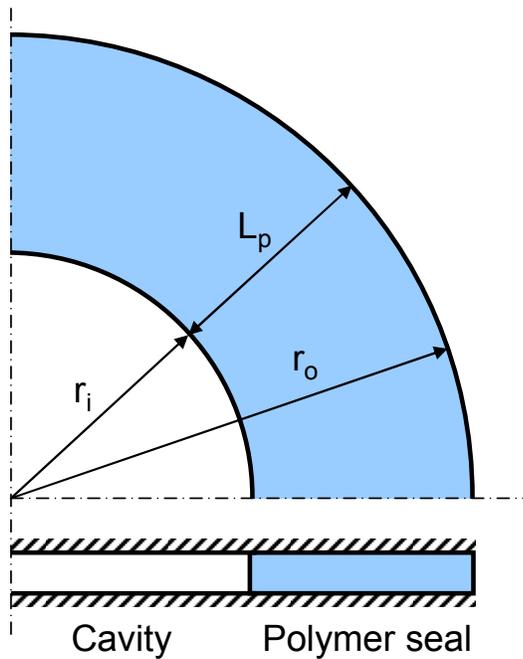
Figure 5-2 Schematic of geometry of 1-D axisymmetric case

95

5.3 Implementation of Gas Diffusion Model

5.3.1 Effective Volume Scheme

As illustrated in Figure 5-3, a 3-D package (Figure 5-3(a)) can be modeled as a 2-D structure Figure 5-3(b)) since the cavity and seal are in general sandwiched by an inorganic substrate or a silicon chip through which gas cannot penetrate and, if it does, the amount is negligible. The 2-D diffusion model can be solved numerically using commercially available finite element analysis (FEA) software packages using the initial and boundary conditions defined in Eq. (9). It is important to recall that the boundary condition at the polymer seal and cavity interface is transient; the cavity pressure increment at each time step should be calculated and used to update the boundary condition at the inner surface after each time step. This updating procedure requires a user-defined algorithm.

(a)

x = 0

x

p(L) = p$_c$(t)

D$_p$
S$_p$

p(W) = p$_a$

(b)

x = 0

x

D$_c$ >> D$_p$
S$_c$ = M/R$_0$T

D$_p$
S$_p$

p(W) = p$_a$

(c)
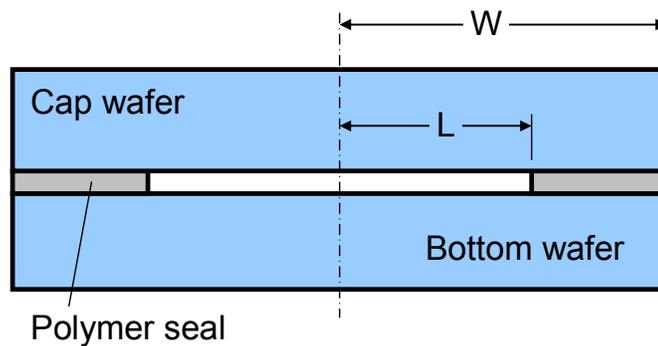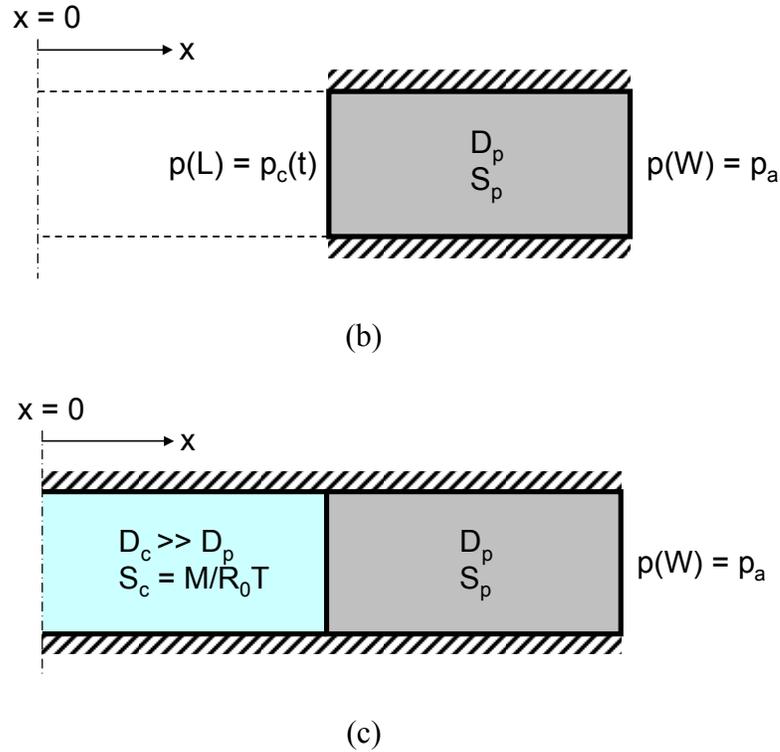
Figure 5-3 Schematic illustration of (a) package cross-section, (b) two-dimensional model and (c) "effective volume" model.

An effective modeling scheme is proposed to avoid the user-defined algorithm (this scheme will be referred to as the "effective volume" scheme). A schematic illustration of the effective volume scheme is shown in Figure 5-3(c). It models the package cavity as an imaginary polymer with an extremely large diffusivity and an equivalent solubility. The large diffusivity (several orders higher than that of the polymeric seals) ensures that the gas pressure is uniform within the cavity. It is important to note, however, that the solubility of the imaginary polymer cannot be chosen arbitrary. Instead the effective solubility should be derived from the gas law and Henry's law as:

$$S_c = \frac{C}{p} = \frac{\rho}{nR_0T/V} = \frac{M}{R_0T} \tag{11}$$

where ρ is the gas density, which has the same dimension as the gas concentration (kg/m^3; note that gas concentration can be interpreted as gas density inside the imaginary polymer), V is the gas volume (m^3) and n is the number of moles (mol).

The effective volume scheme transforms the original single material diffusion problem with transient boundary conditions into a bi-material gas diffusion problem with fixed boundary conditions. Consequently, the Nernst distribution law is applied at the cavity-polymer seal interface (the inner surface of the polymer seal, $x = L$ in Figure 5-3(c)), which can be expressed as [38]

$$p(L) = \frac{C_c(L-)}{S_c} = \frac{C_p(L+)}{S_p} \tag{12}$$

where C_c and C_p is the gas concentration (density) of the cavity and the polymer seal, respectively.

5.3.2 Validation of the Effective Volume Scheme

In the effective volume modeling scheme, the flux (and mass) continuity is automatically satisfied at the interface and the interface condition does not have to be updated manually. Thus, it can be readily implemented using commercial FEA software packages without a user-defined program. It is worth noting that not every commercial FEA software package offers a mass diffusion analysis function but the current problem – namely, a diffusion analysis of a multi-material system subjected to an isothermal condition – can be solved by the thermal diffusion (or heat transfer) function by adopting the well-established the thermal-moisture analogy [39, 40].
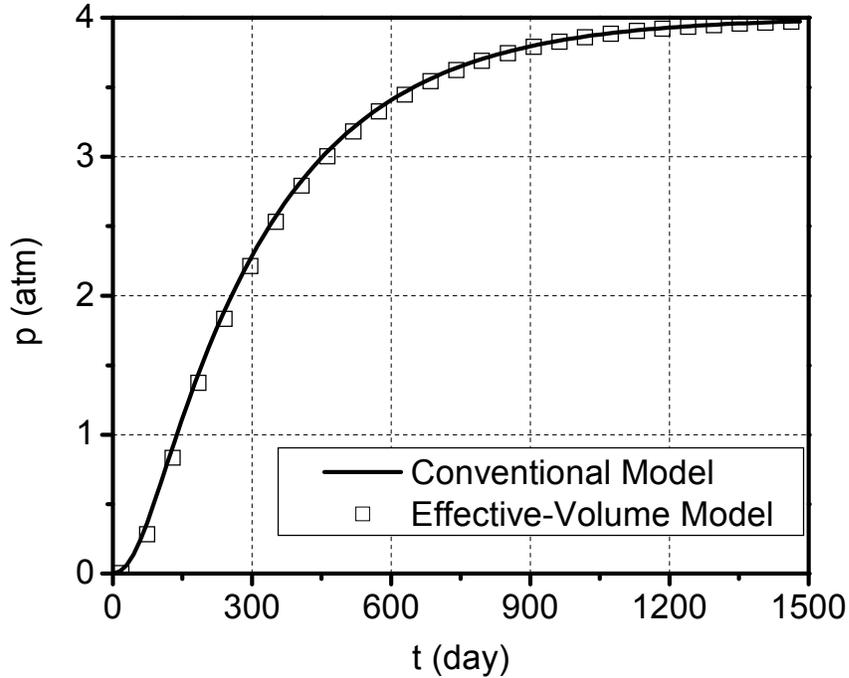
Figure 5-4 Cavity pressure evolutions obtained from two numerical schemes are compared.

The original single material diffusion problem with transient boundary conditions was solved directly by the finite difference method (FDM). The results were used to verify the validity of the effective volume scheme. The details of the FDM formulations for the axisymmetric problems can be found in Appendix. Cavity pressure evolutions calculated from the two schemes are plotted in Figure 5-4. The parameters used in the calculation include: $r_o = 4$ mm, $r_i = 2$ mm, $D = 1 \times 10^{-7}$ mm^2/sec, $S = S_c = 1 \times 10^{-12}$ sec^2/mm^2 and $p_a = 4$ atm. The two schemes produced identical results, confirming the validity of the effective volume scheme.

The validity of the diffusion based governing equations for polymer-sealed packages was also confirmed from the experimental data obtained from an optical gas

leak test. The details of the experimental setup, procedures and results are described in the second part of this paper [37].

5.4 Fundamentals of Gas Leak Behavior

The axisymmetric model used to verify the FEA solution of the effective volume scheme is further utilized to investigate the fundamental behavior of gas leak in polymer-sealed packages.

5.4.1 Diffusion regimes: extreme cases and their practical implications

For a cavity enclosed by a polymeric seal the diffusion equation can provide an approximate mass continuity relationship over the entire axisymmetric sealing structure as [41]

$$D_p S_p \frac{p_a - p_c}{L_p} A_p \delta t \approx \delta p \left(S_p V_p + S_c V_c \right) \tag{13}$$

where A_p is the area of the polymer seal at the center ($= \pi(r_i + r_o)t$; t is the seal thickness), δt is the time duration, δp is the pressure rise during δt, L_p is the width of the sealing layer ($= r_o - r_i$), V_c is the cavity volume ($= \pi r_i^2 t$), V_p is the polymer seal volume ($= \pi(r_o^2 - r_i^2)t$), D_p and S_p are the diffusivity and solubility of the polymer seal, respectively, and S_c is the effective solubility of the cavity. The left hand side of Eq. (13) is the gas amount transferred through the polymeric seal and the right hand side is the amount of gas accumulated in both the polymer and cavity. Rearranging Eq. (13) yields:

$$\frac{\delta p}{\delta t} \approx \frac{D_p S_p \left(p_a - p_c \right)}{L_p \left[S_p (r_o - r_i) + S_c r_i^2 / (r_o + r_i) \right]} = \frac{D_p S_p \left(p_a - p_c \right)(r_o + r_i)}{L_p \left[S_p \left(r_o^2 - r_i^2 \right) + S_c r_i^2 \right]} \tag{14}$$

When $S_p\left(r_o^2 - r_i^2\right) \gg S_c r_i^2$, Eq. (14) is simplified as

$$\frac{\delta p}{\delta t} \propto \frac{D_p}{L_p^2} \tag{15}$$

In this regime (referred to as *diffusivity-dominant regime*), the gas leak into the cavity is proportional to the diffusivity of the sealing polymer and is inversely proportional to the square of seal width. It is worth noting that the gas leak is independent of the size of the cavity.

On the other hand, when $S_p\left(r_o^2 - r_i^2\right) \ll S_c r_i^2$, Eq. (14) is simplified as

$$\frac{\delta p}{\delta t} \propto \frac{P_p}{L_p L_c S_c} \cdot \frac{r_o + r_i}{r_i^2} \tag{16}$$

In this regime, the gas leak is proportional to the permeability of the sealing polymer (will be referred to as *permeability-dominant regime*). It is also governed by the size of both seal and cavity.

For a more effective parametric study, Eqns. (8) through (10) are converted into non-dimensional forms by normalizing independent variables with the outer radius (r_o) and the ambient pressure (p_a) as:

$$\frac{\partial \tilde{p}}{\partial \tilde{t}} = \left(\frac{\partial^2 \tilde{p}}{\partial \tilde{r}^2} + \frac{1}{\tilde{r}} \frac{\partial \tilde{p}}{\partial \tilde{r}} \right) \tag{17}$$

$$\tilde{p}(1,\tilde{t}) = 1, \ p(\tilde{r}_i, \tilde{t}) = \tilde{p}_c, \ p(\tilde{r}, 0) = 0 \tag{18}$$

$$\tilde{p}_c(\tilde{t} + \Delta \tilde{t}) = \tilde{p}_c(\tilde{t}) - \frac{2 r_o}{r_i} \frac{S_p}{S_c} \int_{\Delta t^*} \tilde{J}_{r=r_i}(\tilde{t}) d\tilde{t} \tag{19}$$

$$\text{where } \tilde{p} = \frac{p}{p_a}, \ \tilde{r} = \frac{r}{r_o}, \ \tilde{t} = \frac{D_p t}{r_o^2} \text{ and } \tilde{J} = \frac{J r_o}{D_p S_p p_a} \tag{20}$$

The normalized form of the Nernst distribution law can be written as

101

$$\tilde{p}(\tilde{r}_i) = \frac{S_p}{S_c} \tilde{C}_c(\tilde{r}_i-) = \tilde{C}_p(\tilde{r}_i+) \quad \text{where} \quad \tilde{C} = \frac{C}{S_p p_a} \tag{21}$$
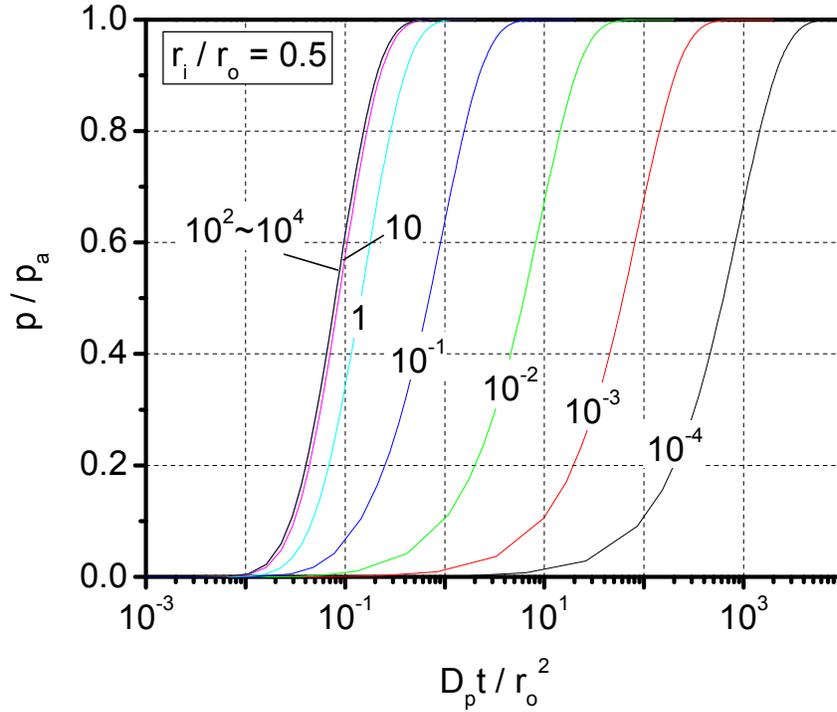
Figure 5-5 Normalized cavity pressure evolution with respect to solubility ratio (S_p / S_c). Radius ratio (r_i / r_o) is 0.5 for all cases and numbers in the plot indicate solubility ratio.

Figure 5-5 shows the normalized cavity pressure evolution obtained with various solubility ratios when the radius ratio is 0.5 ($r_i = L_p$). Interestingly, all curves with the solubility ratios above 100 overlie each other. On the other hand, for solubility ratios below 0.01, all curves shift along the log time axis while maintaining the same shape. They represent the two extreme cases discussed above.

The wide range of solubility ratios considered in the study appears to cover both extreme regimes. In the diffusivity-dominant regime (high solubility ratios), gas

leak is not affected by the solubility of the sealing polymer (Eq. (15)), resulting in the identical pressure rise as shown in Figure 5-5. In the permeability-dominant regime (low solubility ratios), the time required to reach a certain cavity pressure is inversely proportional to the permeability of the sealing polymer (Eq. (16)), which results in a shift along the log time axis. It should be noted that the diffusivity is constant for all plots in Figure 5-5 and thus solubility change is equivalent to permeability change.
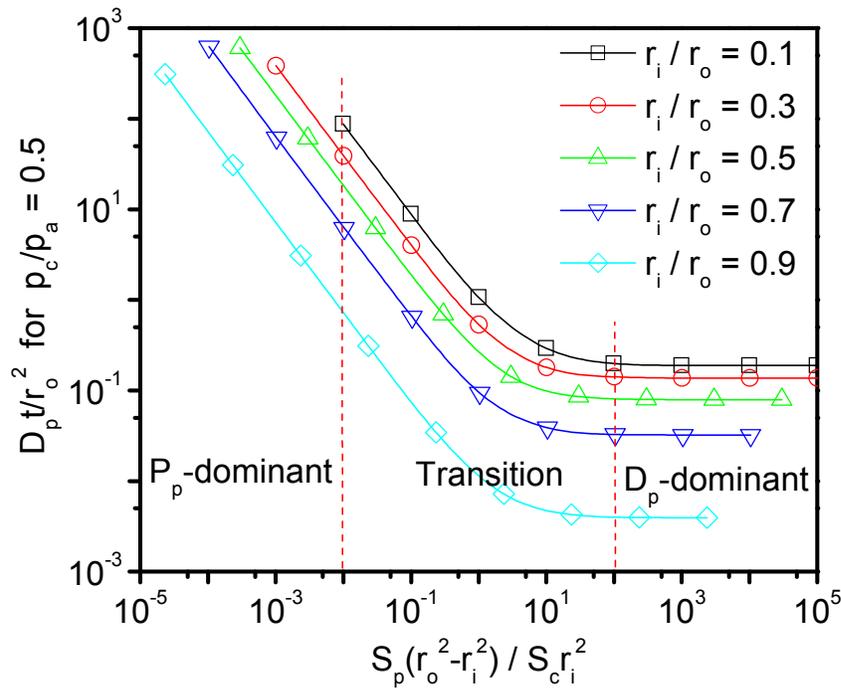
Figure 5-6 Normalized time to reach a half normalized pressure with respect to radius ratio and $S_p(r_o^2 - r_i^2)/S_c r_i^2$ showing D- and P-dominant regimes

This is seen in Figure 5-6, where the time to reach half the ambient pressure as a function of R_S is plotted for various radius ratios; $R_S \equiv S_p(r_o^2 - r_i^2)/S_c r_i^2$. Based on these results, the permeability-dominant regime can be defined approximately as $R_S \leq 0.01$, the diffusivity-dominant regime as $R_S \geq 100$, and the transition regime as in-

between these two. The magnitude of R_S can now be used as the metric of diffusion regimes.

The extreme cases discussed above have two important practical implications. If a package is in the diffusivity-dominant regime, the solubility (or permeability) does not have to be measured since the diffusivity itself is sufficient to describe the gas leak behavior. Similarly, for a package in the permeability regime, only the permeability is required to predict gas ingress into the cavity.

A correct determination of the regime can also help make a decision about which sealing material should be used for a given package design. A sealing material with the lowest permeability will provide the best sealing performance if the gas leak falls into the permeability-dominant regime. Similarly, if the gas leak is in the diffusivity-dominant regime, a sealing material with the lowest diffusivity will offer the best hermetic performance.

The cavity of a typical MEMS package has a rectangular (or square) shape. The metric of diffusion regimes, R_S, was derived originally from the axisymmetric model. A concept of "effective" radius is proposed to link the two different shape parameters. The effective radii can be defined simply by using the equivalent area as

$$r_{i,e} = \sqrt{A_i / \pi} \text{ and } r_{o,e} = \sqrt{A_o / \pi} \tag{22}$$

where $r_{i,e}$ and A_i are the effective radius and the area of the rectangle of the cavity, and $r_{o,e}$ and A_o are the effective radius and the area of the rectangle of the package.

A supplementary numerical analysis confirmed that the internal cavity pressure change of packages with a rectangular seal can be predicted accurately by an equivalent circular seal with radii equal to the effective radii, provided the width of

104

polymer seals is the same in both cases. Accordingly, the diffusion regimes can be determined accurately by the effective radii. However, when the width of polymer seals varies significantly in the horizontal and vertical directions, the gas permeation may not be uniform; the permeation is likely to happen through a thinner seal area. For these cases, the accuracy of the effective radii concept should be reconfirmed numerically.

5.4.2 Lag Time

When a package is exposed to a gas, a certain amount of time (will be referred to as lag time) is required for gas molecules to travel from an ambient to a cavity. Actual gas leakage into the cavity begins after this lag time. Since it happens inside the polymer, it depends only on the width and diffusivity of the polymer seal. More specifically, the lag time is proportional to the square of the seal width and inversely proportional to the diffusivity (Eq. (20)).

Theoretically the lag time can be defined as the time for the fastest gas molecule to travel through the shortest diffusion path in a polymeric sealing, which is extremely difficult to measure. From a practical point of view, the lag time can be defined as the time to accumulate a threshold value of gas amount that has an impact on the device performance or reliability.
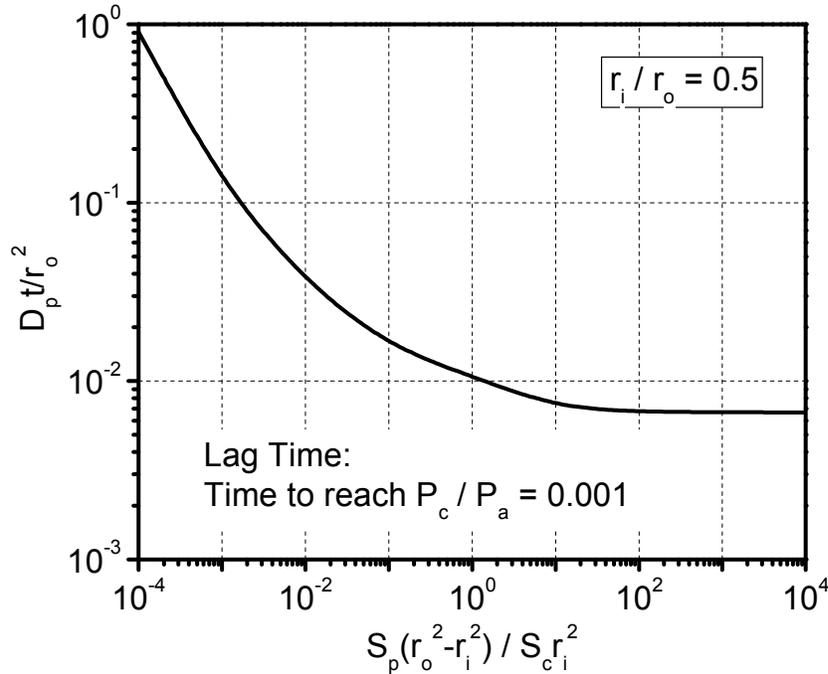
Figure 5-7 Normalized lag time versus R_S for $r_i / r_o = 0.5$

Considering a normalized threshold value of 0.001 $(\tilde{p} = 0.001)$, the normalized lag time $\tilde{t}$ as a function of R_S is illustrated in Figure 5-7 for the radius ratio of 0.5. The order of normalized lag time ranges from 10^{-3} to 10^{-1}. If the diffusivity is 1×10^{-7} mm^2/sec and the package radius is 4 mm, the actual lag time ranges from 297 hours for $R_S = 10^4$ to 40400 hours $R_S = 10^{-4}$.

This has important practical consequences. In the traditional helium fine leak test the package is bombed for a few hours before being transferred to the spectrometer. Due to the lag time which is usually much longer than the bombing time, the helium may not even enter the cavity of polymer-sealed packages during the bombing period. In fact, the test may only measure helium that has been absorbed in the polymer seal. The analysis of such data can lead to erroneous inferences about the hermeticity of the package.

5.5 Application: Leakage Characteristic of Water vapor

Water vapor is known to be one of the most detrimental gases to MEMS device reliability. Its leakage characteristic is investigated by the proposed modeling scheme. It is reasonable to assume that water vapor obeys the gas law within the range of temperature considered in the implementation (below 100°C). With this assumption, the effective water solubility of a cavity required for the numerical calculation can be calculated as $2.165/T$ (in Kelvin)$\times 10^{-9}$ sec^2/mm^2 from Eq. (11).

A diffusion analysis was implemented with actual temperature-dependent diffusion properties, which are known to follow the Arrhenius relationship as [38]

$$D = D_0 \exp\left(-\frac{E_D}{R_0 T}\right), \quad S = S_0 \exp\left(-\frac{E_S}{R_0 T}\right) \text{ and } P = DS = P_0 \exp\left(-\frac{E_P}{R_0 T}\right) \quad (23)$$

where D_0, S_0 and P_0 are diffusivity, solubility and permeability constants, respectively, and E_D, E_S and E_P are the corresponding activation energy. Arrhenius coefficients of diffusion properties for generic polyimide and liquid crystal epoxy found in the literature [1, 42] are listed in Table 5-1.

Table 5-1. Arrhenius coefficients for diffusion properties of generic polyimide and liquid crystalline epoxy estimated from the plots in Ref. [42] and [1], respectively.

	Polyimide	*LP Epoxy*
D_0 (mm^2/sec)	3.16	3.8×10^{-5}
E_D (J/mol)	41990	14200
S_0 (sec^2/mm^2)	5.15×10^{-16}	5.30×10^{-15}
E_S (J/mol)	-43240	-40600
P_0 (sec)	1.63×10^{-15}	2.01×10^{-21}
E_P (J/mol)	-1250	-26400
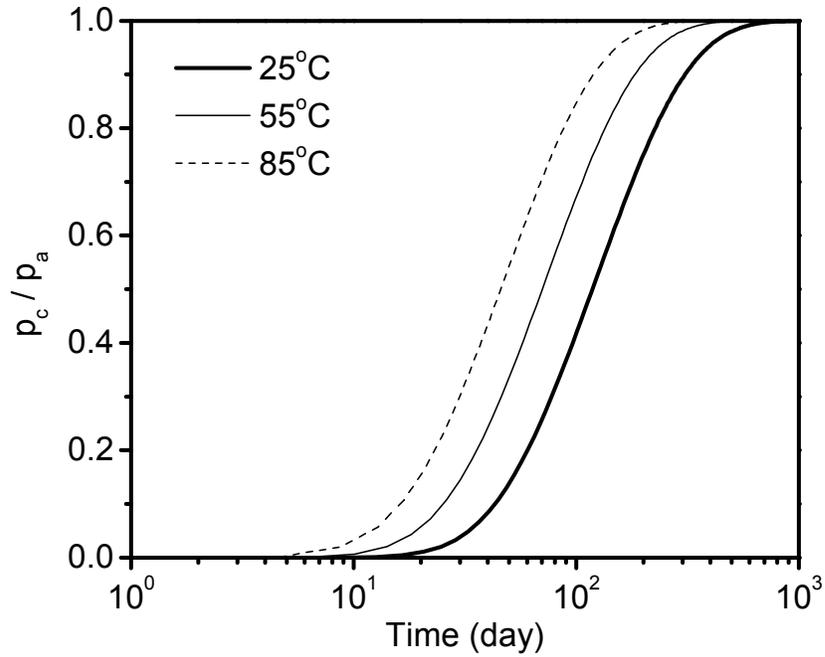
Figure 5-8 Relative humidity evolution inside cavity at three different environmental conditions (25°C/100%RH, 55°C/100%RH and 85°C/100%RH). Properties of liquid crystal epoxy [1] were used and r_o = 4mm, r_i = 2mm.
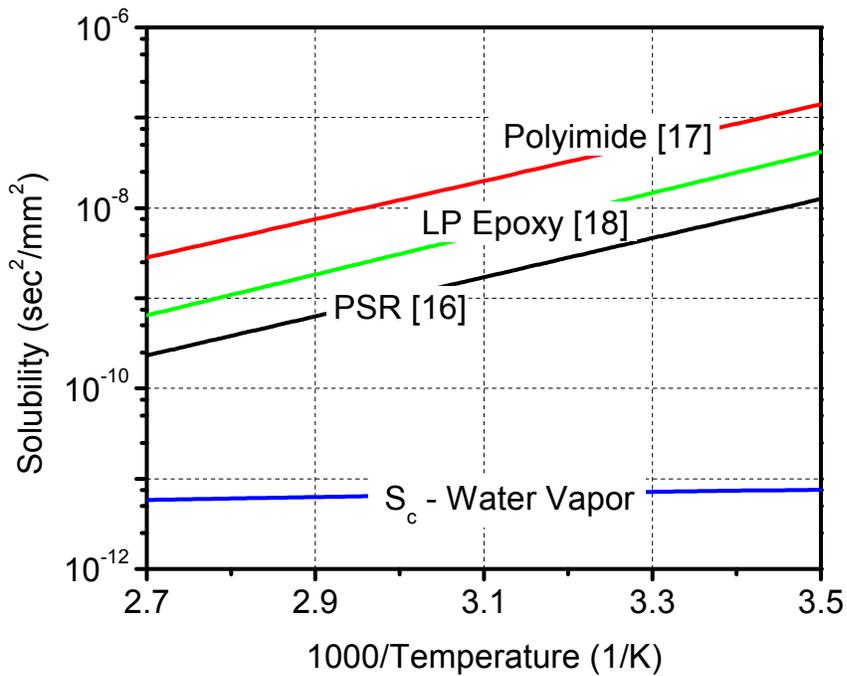
Figure 5-9 Solubility versus temperature for various polymers and cavity

An axisymmetric structure (r_o = 4 mm and r_i = 2 mm) was used for the analysis. The package was subjected to three environmental conditions (25°C/100%RH, 55°C/100%RH and 85°C/100%RH). The normalized pressures for two polymers are plotted in Figure 5-8. It is to be noted that the normalized pressure is identical to the relative humidity in the plot.

The R_S values of the three cases range from 28620 (25°C) to 2205 (85°C) due to the large solubility ratio between the seal and the cavity (Figure 5-9). All three cases belong to the diffusivity-dominant regime, in which the gas leak behavior is dependent only on diffusivity and is independent of solubility. Figure 5-8 confirms this; cavity pressure evolution curves having an identical shape are shifted along the log time axis by diffusivity changes (similar to the curve shift by permeability changes in the permeability-dominant regime observed in Figure 5-5). Other polymers shown in Figure 5-9 have solubility more than two orders higher than the cavity effective solubility over almost the entire temperature range. Thus, they will tend to exhibit behavior in the diffusivity-dominant regime for the same package geometry.

The above illustration shows that water vapor leakage is accelerated at elevated temperatures, as intended by the accelerated test standard (e.g., JEDEC standard [43], which is frequently adopted in MEMS device testing). However, it is worth mentioning that leakage may not always be accelerated at elevated temperatures as desired. Some liquid crystal polymers for hermetic sealing applications are known to have extremely low solubility (two orders lower than generic polymers for electronics applications) [44]. Polymer solubility comparable to

the cavity solubility may result in a shift of diffusion regimes from the diffusivity-dominant regime to the transition or even to the permeability-dominant regime. In the permeability-dominant regime, the water vapor leakage can be delayed at elevated temperature if the sealing polymer has a negative value of the activation energy of permeation (e.g., see Table 1). This warrants an extensive experimental and numerical study to establish a proper accelerated test guideline for diverse sealing polymer materials.

5.6 Conclusions

A gas diffusion based mechanism was proposed to describe the hermeticity of polymer-sealed packages. An effective numerical scheme was developed and implemented to solve the governing equations. The scheme was utilized to characterize the gas leak behavior in polymeric seals. The characterization revealed two important fundamental characteristics of gas transport in polymer-sealed packages: gas diffusion regimes and lag time. Three distinctive gas diffusion regimes were identified depending on package structure and sealing polymer properties and their practical implications on material property measurement and package design were described. The lag time, which is the duration for gas molecules to travel from an ambient to a cavity, is a unique characteristic of diffusion-based gas transport mechanism in polymer-sealed packages. The analysis showed that it ranges from several hours to hundreds of days depending on the polymer seal property and structure. The developed model was applied to predict the water vapor leak behavior of packages. Accelerated water vapor leakage was observed at elevated temperatures due to increased diffusivity, as intended by the accelerated test standard.

Appendix: Finite Difference Formulations for 1-D Axisymmetric Case

Equation (8) can be re-written in an implicit finite difference form as

$$\frac{p_n^{t+\Delta t} - p_n^t}{\Delta t} = D \left[\frac{p_{n+1}^{t+\Delta t} - p_n^{t+\Delta t} + p_{n-1}^{t+\Delta t}}{(\Delta r)^2} + \frac{1}{r_n} \frac{p_{n+1}^{t+\Delta t} - p_{n-1}^{t+\Delta t}}{2\Delta r} \right] \tag{A.1}$$

where Δt is the time step, Δr is the mesh size and p_n^t is the gas pressure at node n at time t. The change of cavity pressure at each time step is calculated as

$$
\begin{aligned}
p_c(t + \Delta t) &= p_c(t) + \frac{1}{S_c \pi r_1^2 t} \cdot DS \frac{p_2^t - p_1^t}{\Delta r} \cdot \pi (r_1 + r_2) t \cdot \Delta t \\
&= p_c(t) + \frac{DS(p_2^t - p_1^t)(r_1 + r_2)\Delta t}{S_c r_1^2 \Delta r}
\end{aligned}
\tag{A.2}
$$

Note that the first node ($n = 1$) is located at the inner surface of the polymer seal in the original scheme.

Chapter 6: Hermeticity Evaluation of Polymer-Sealed MEMS Packages

Part II: Optical Leak Test for Validation of Diffusion Model and Measurement of Diffusion Properties[11]

ABSTRACT

A novel optical leak test is developed and implemented to document the internal cavity pressure change of a polymer-sealed package subjected to a pressure differential. The experimental data is used to validate the gas diffusion based governing equation proposed in the first part of the paper. An inverse approach is subsequently implemented to determine the diffusion properties (diffusivity and solubility). The method can be used to characterize the leak behavior of various gas species that are difficult to evaluate using the existing equipment.

6.1 Introduction

The first part of the paper [45] reported that gas conduction based equations do not predict the helium fine leak test data of polymer-sealed packages properly. The reported observation prompted an investigation of the helium fine leak test data for packages with polymeric seals and those with metallic ones.

---

[11] This chapter has been submitted for review to the *Journal of MEMS* under the title of "Hermeticity evaluation of polymer-sealed MEMS packages, Part II – Optical leak test for validation of the diffusion model and measurement of diffusion properties" by A. Goswami, C. Jang, B. Han and S.J. Ham

A set of helium fine leak tests was conducted to elucidate the different

physical behavior of the two packages. In the experiment, individual packages as

well as batches containing multiple identical packages were tested; in the batch tests

54 metal-sealed and 20 polymer-sealed packages were used. The metal-sealed and

polymer-sealed packages had a volume of 2.156 x 10^{-4} cc and 3.1 x 10^{-4} cc,

respectively. The test parameters remained the same for all tests [19, 35]: bombing

time = 6 hours, bombing pressure = 4 atm (gage) and dwell time = 10 minutes. The

signals obtained from the batch tests and single package tests are shown in Figure 6-

1(a) and (b) for polymer sealed and metal sealed packages, respectively. The batch

test signals normalized by the number of packages in the batches are also plotted for

comparison.

The normalized signal of the polymer-sealed packages is similar to that of the

single package signal (Figure 6-1(a)). Additional tests of packages used in the batch

test revealed that the polymer-sealed packages produced virtually the same signal

when tested individually. On the other hand, the normalized signal of the metal-

sealed packages is much lower than that of the single package signal (Figure 6-1(b)),

which indicates that the average signal of the batch does not represent the leak

behavior of a single package. Additional tests confirmed that only five out of the 54

packages used in the batch test were leaky and these packages produce unique

apparent leak rate profiles [35].
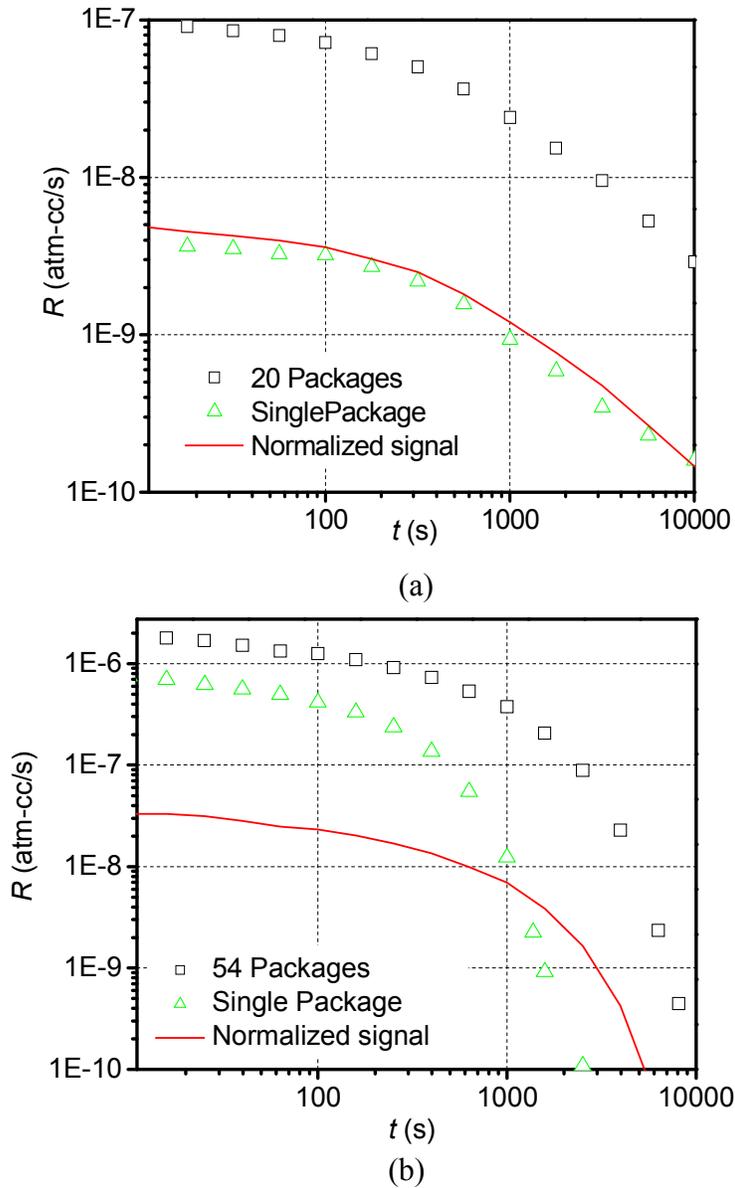
Figure 6-1 Helium leak test signals for (a) Polymer-sealed packages (b) Metal-sealed packages Note: The packages have a volume of 3.1 x 10^{-4} cc (polymer-sealed packages) and 2.156 x 10^{-4} cc (metal-sealed packages). Test parameters: Bombing Pressure = 4 atm (gage), Bombing Time = 6 hours and Dwell time = 10 minutes.

In the case of metal-sealed packages, gas transport occurs through nano-scale leak channels (i.e., gas conduction) that are randomly present. Even when multiple nano-scale leak paths exist, they can be modeled as an effective single leak channel and thus a regression analysis based on gas conduction equations can be employed to characterize the leak rate [35]. On the other hand, in polymer-sealed packages, gas transport occurs through the bulk material (i.e., gas diffusion). Consequently the effective single leak channel approach cannot be used for polymer-sealed packages.

The first part of the paper [45] described in detail a diffusion based governing equation to model the hermetic behavior of polymer-sealed MEMS packages. This second part presents a novel optical leak test to document the internal cavity pressure change of a polymer-sealed package subjected to a pressure differential. The experimental data are used (1) to validate the gas diffusion based governing equation, and (2) to subsequently determine the diffusion properties of the polymeric seal.

6.2 Optical Leak Test

6.2.1 Basic Principle

The basic principle of the optical leak test [8, 9, 19] is depicted in Figure 6-2.
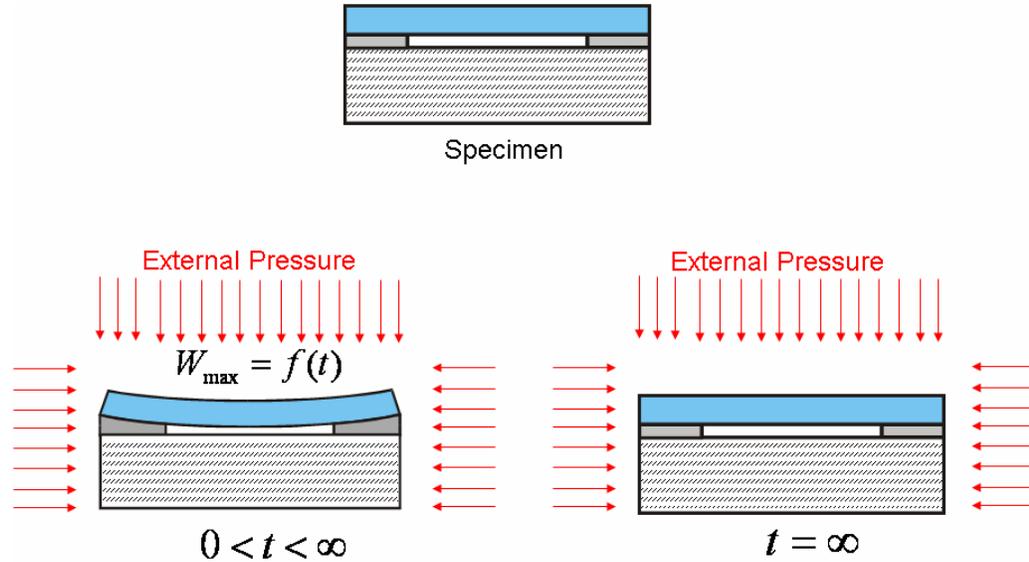
Figure 6-2 Schematic illustration of the Optical leak test.

A MEMS package is first subjected to a pressurized gas (i.e., constant external pressure). As gas leaks into the package, the pressure differential (i.e., the difference between the external pressure and the cavity internal pressure) changes over a period of time. This change in pressure differential induces a change in specimen deformation that is recorded experimentally as a function of time. The experimental data is converted to the pressure differential using the pre-determined relationship between pressure differential and the specimen deformation (calibration curve). Since the external pressure is known, the time-dependant cavity internal pressure can be obtained by subtracting the pressure differential from this value.

6.2.2 Experimental Setup

There are two major parts in the experimental setup: (a) an optical technique for deformation measurement and (b) a pressure chamber with a high-precision pressure regulation system. These are discussed in detail below.

A classical laser interferometry called Twyman/Green interferometry was employed as an optical technique to capture the surface topology of the package [46]. The technique is simple and is ideally suited for MEMS packages since the package surface is specular, which is a critical requirement for the method. The principle of Twyman/Green interferometry is illustrated in Figure 6-3(a). Briefly, an expanded laser light is collimated by a collimating lens. The collimated light is split into two – one directed towards the specimen and the other towards the reference mirror (an optical flat). The reflected wave fronts recombine and interfere to form an interferogram (or fringe pattern). The interferogram provides a contour map of the surface topography. An example of a fringe pattern captured by a camera is shown in Figure 6-3(b).

(a)

(b)
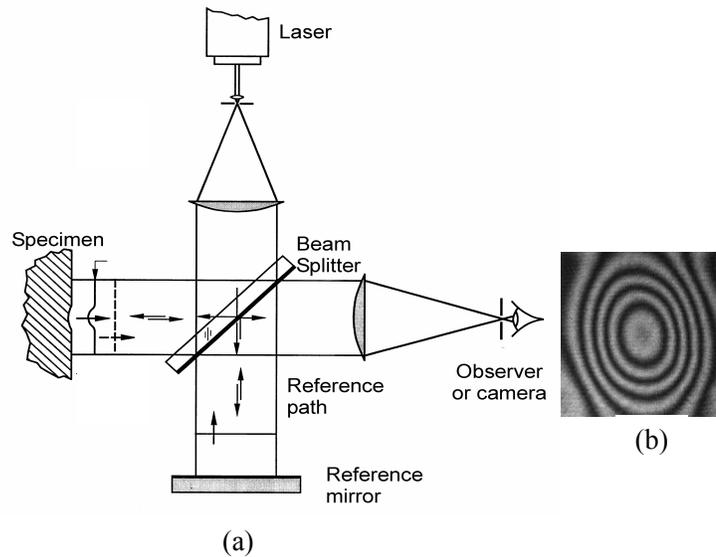
Figure 6-3 (a) Schematic illustration of Twyman Green interferometry (b) An interferogram or fringe "pattern"

The deformation, W, at any point on the specimen is given by

$$W = \frac{\lambda}{2} N \qquad \qquad (1)$$

where N is the fringe order at that point and λ is the wavelength of the laser. The basic contour interval of this arrangement is defined as $\lambda/2$. For a helium neon laser ($\lambda = 632.9$ nm) this provides 316.5 nm/fringe order.

The optical/mechanical configuration is shown schematically in Figure 6-4(a). The specimen is held inside a cylindrical stainless steel pressure vessel which is provided with a window for direct viewing. Both the vessel and the window are designed to withstand pressures up to 50 atm. The pressure vessel is mounted on a heavy duty stage in order to prevent vibrations on account of forces exerted by the pressure tubing that supplies gas into the vessel. This stage offers x-y translation and rotational adjustment of the vessel, and hence the specimen inside it as desired. The fringe pattern is captured by a high resolution camera (Pulnix TM-1040) through an imaging lens.

Any high pressure gas tank can be used as the source of gas. A mechanical regulator located on the tank reduces the gas pressure from the tank pressure value (~ 1000 psi) to 100 psig. This reduced pressure gas is then supplied to a PID controller (TESCOM ER3000). The PID controller has an internal sensor which is used in conjunction with PID logic and user defined PID parameters to reduce gas pressure to the desired pressurization value. An additional pressure sensor (TESCOM 200-1000-2527) with a range of 0 - 1000 psig is screwed into the pressure vessel in order to read the pressure inside the chamber, which enables detection of any large leakage of gas due to an accidental failure/rupture of the chamber gaskets and seals. The uncertainty of measurement using this pressure regulation setup is ±0.3 psi (±0.02 atm)

It should be noted that light reflected from the front and back surfaces of the window can interfere with each other and also with light reflected by the specimen, and thereby contributes to noise in the recorded interferogram. As shown in Figure 6-4(b), the specimen surface was positioned with an angle (approximately by 8º) with respect to the window. In this way, only the light reflected from the specimen surface was collected by the camera. This arrangement ensures that the light beams reflected from the window surfaces are not collected by the camera.

(a)

(b)
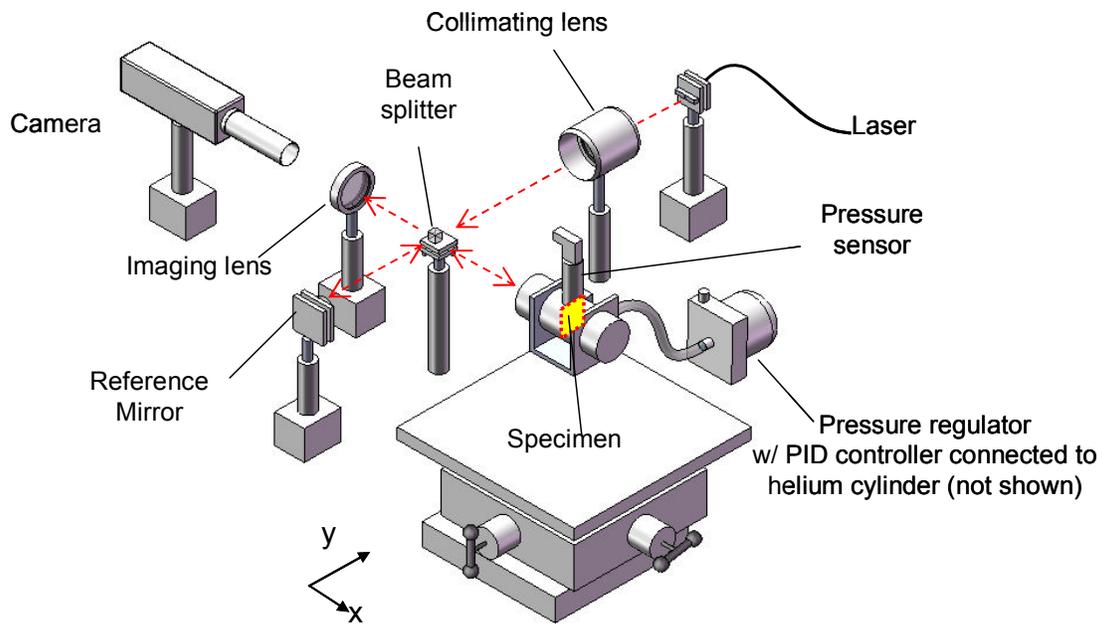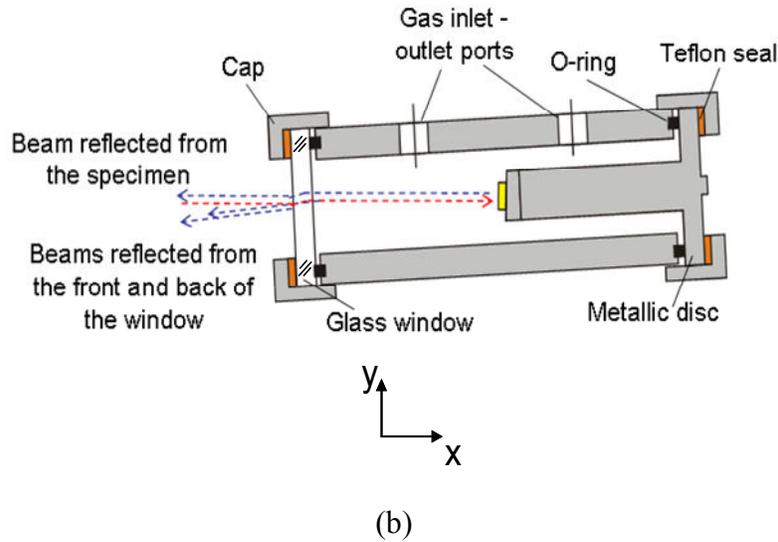
Figure 6-4 (a) Schematic of the experimental setup (b) Arrangement for mitigation of optical noise

6.3 Image analysis to obtain surface deformation

6.3.1 Package description

The package used in this study is shown in Figure 6-5. It consists of a glass cap bonded to a silicon substrate with a photo-definable adhesive polymer. It was fabricated in a controlled nitrogen environment (0.9 bar). The height of the silicon substrate, the glass cap and the polymer seal are 120 μm, 500 μm and 46 μm, respectively. The overall package dimensions are 4.6 mm × 4.5 mm. The cavity dimensions are 2.22 mm × 2.86 mm, which yields an internal cavity volume of ~ 3 × 10^{-4} cc.

6.3.2 Automatic fringe analysis using FFT

The goal of the automatic fringe analysis is to enhance displacement measurement resolution by determining the phase information at every pixel, and thus

the fractional fringe order at every point in the fringe pattern. In the present study the Fast Fourier Transform (FFT) method is employed for automatic fringe analysis [18] since the region of interest does not contain any boundaries and the deformation of the package surface is supposed to vary smoothly. An added benefit of the FFT method is that the inherent frequency due to random noise can be eliminated effectively during the inverse FFT process. The FFT method is illustrated using the actual package below. A more detailed mathematical description of the method can be found in [18] .
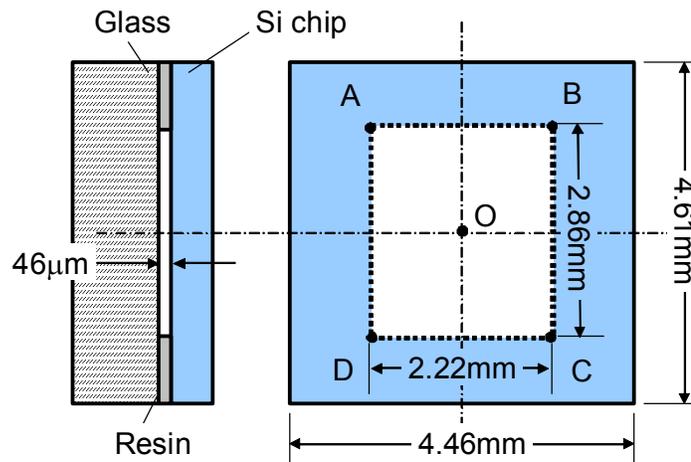
Figure 6-5 Schematic illustration of test specimen

The original fringe pattern of the specimen in an unpressurized state is shown in Figure 6-6(a). A carrier pattern of constant displacement gradient is added to the original pattern by a small rigid body rotation of the specimen. The modulated pattern is shown in Figure 6-6(b). After the two-dimensional FFT, the real harmonic is isolated in the frequency domain (Figure 6-6(c)). The center of the spectrum is moved to the origin of the frequency axis to remove the carrier frequency in the frequency domain. Then, the inverse Fourier transform is performed to restore the original phase map (Figure 6-6(d)). Unwrapping of this phase map yields a fractional

fringe orders with high fidelity at every point. This information is used to generate a 3D deformation map shown in Figure 6-6(e).

The desired deformation value is the relative deformation between the center of the cavity O, and any one of the corners: A, B, C and D (Figure 6-5). The relative deformations at these corner points should be virtually the same due to symmetry. In order to account for any rigid body rotation, the desired deformation value was determined by averaging the four relative deformations at the corners.

(a)   (b)   (c)   (d)

(e)
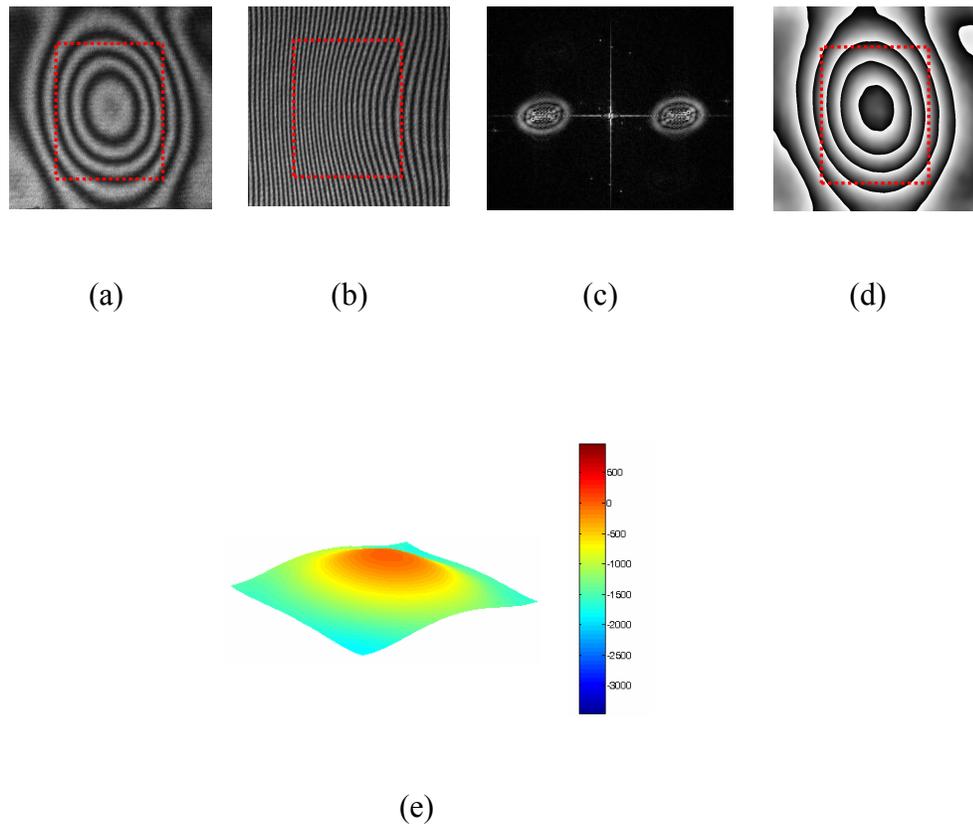
Figure 6-6 Illustration of FFT analysis: (a) Original fringe pattern, (b) Modulated pattern with carriers, (c) Fourier spectra, (d) Phase map after

inverse Fourier transform and (e) 3-D plot. (Dotted red line indicates the cavity

location)

The repeatability of deformation measurement was estimated by repeating measurements in an unpressurized state. In between the measurements the specimen was taken off the fixture and then remounted again. The results of 10 independent measurements are shown in Figure 6-7.
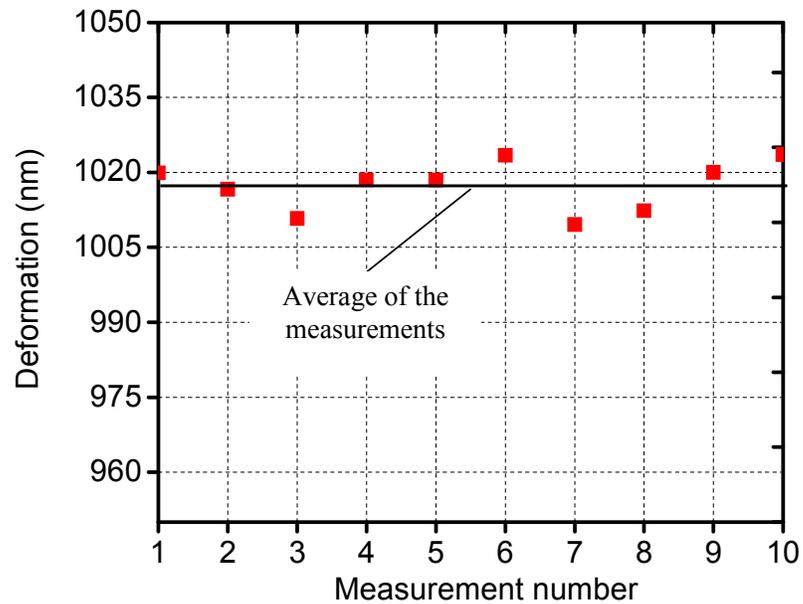
Figure 6-7 Repeatability of the measurement. The data points are scattered around the average value which is indicated by the solid black line.

The standard deviation, σ, of the measurements was 5 nm. For a 99.7 % confidence interval, the uncertainty in deformation is given by the $\pm 3\sigma$ range and is equal to ± 15 nm. [47].

6.3 Experimental Result Using Helium

In the optical leak test, cavity pressure evolution is measured indirectly. A calibration curve that provides the relationship between pressure differential and surface deflection is obtained experimentally first. Then the surface deflection measured during the leak testing is converted to the corresponding pressure differential value using the calibration curve. This pressure differential is used together with the known value of external pressure to determine cavity pressure.

6.3.1 Calibration curve

The applied pressure in the chamber was increased to 4 atm gauge in steps of 0.25 atm and the surface deformation was recorded at each step. Representative fringe patterns and the corresponding 3-D maps are shown in Figure 6-8. The maximum deflections were determined from these 3-D plots. They were subtracted from the reference deflection (1017 nm), obtained from the deformation map shown in Figure 6-6(e), to calculate the deformation-induced deflection corresponding to each pressure value.

$t = 20$ s, $\Delta p = 0.25$

$t = 160$ s, $\Delta p = 2$ atm

$t = 320$ s, $\Delta p = 4$ atm
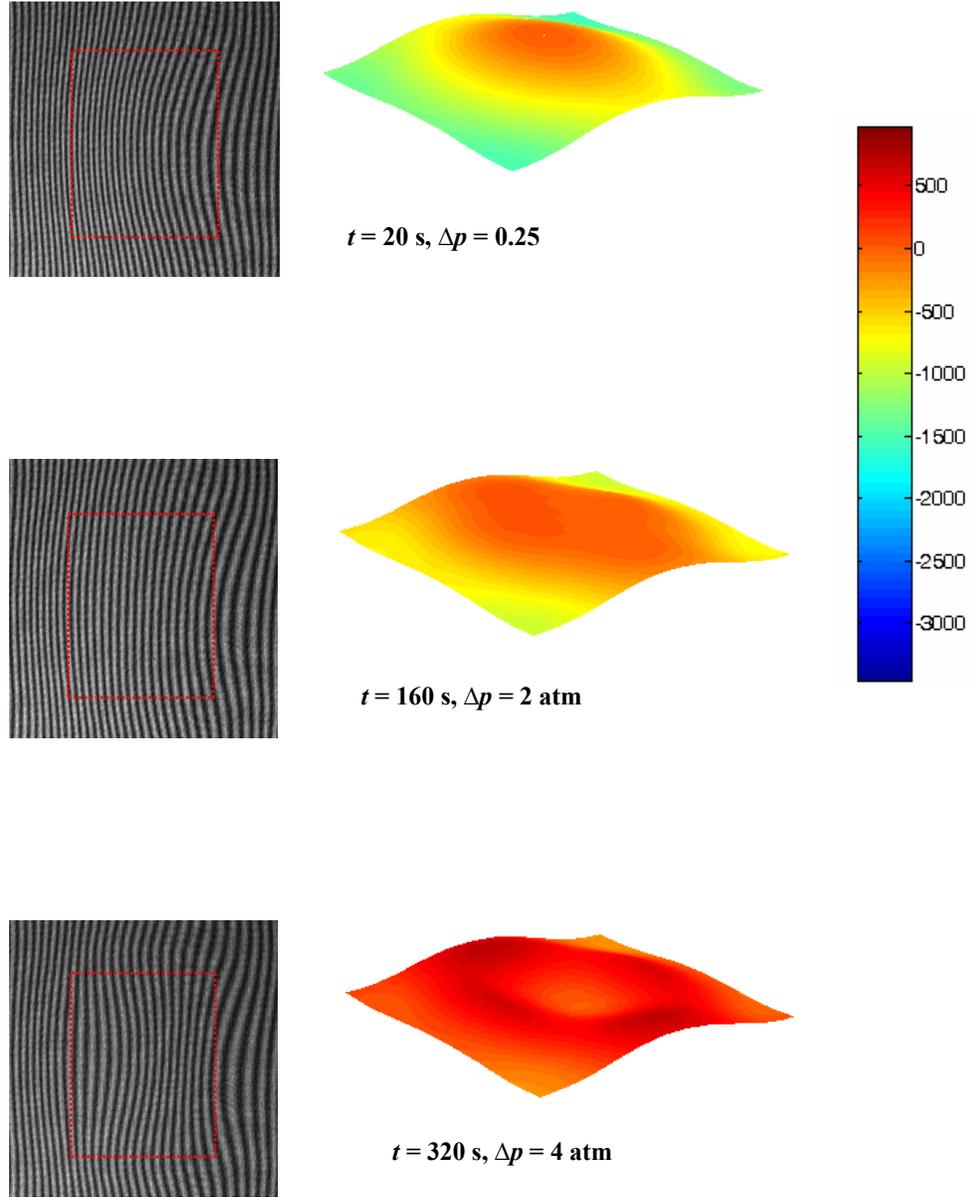
Figure 6-8 Representative fringe patterns and 3D deformation maps obtained during the calibration process. The units for the scale are nm. (Dotted red line indicates the cavity location)
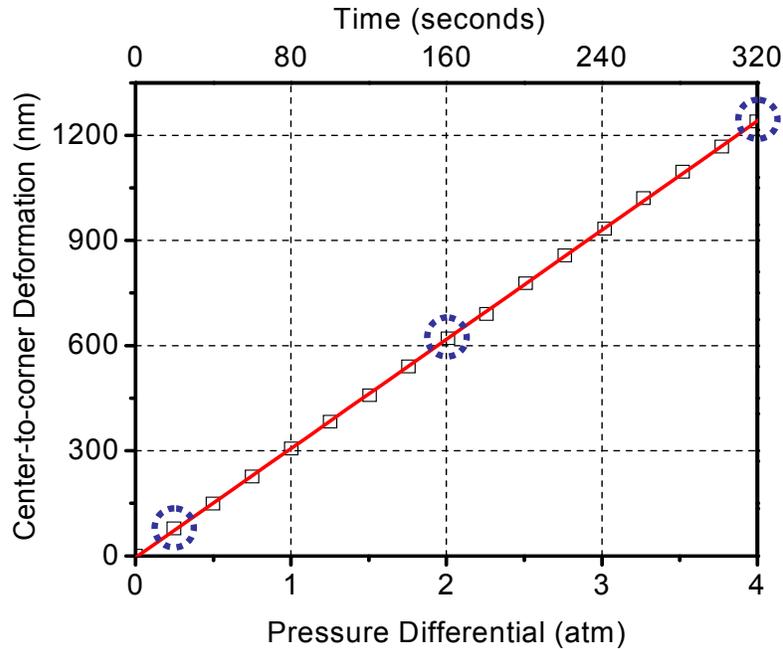
Figure 6-9 Calibration curve: The encircled values correspond to the fringes depicted in Figure 6-8.

The deformation-induced deflections are plotted as a function of the applied external pressure and bombing time in Figure 6-9, where three data points marked by a dotted circle were obtained from the results shown in Figure 6-8. From this plot the following linear relationship between pressure differential, Δp, and the maximum deflection, W_{max}, of the specimen was obtained

$$W_{max} = 309.58(\Delta p) \tag{2}$$

where the units for pressure and deformation are atm and nm, respectively.

The total measurement time for obtaining the calibration curve was 320 seconds and based on the subsequent experimental observation it is safe to assume that the effect of diffusion of helium into the cavity during the calibration experiment is negligible.

6.3.2 Cavity pressure evolution

After the calibration curve was obtained, the package was subjected to a constant bombing pressure of 4 atm (gage) and the deflections were measured as a function of time. The bombing pressure was maintained for 600 hours after which there was no noticeable deflection change indicating that the cavity pressure at that stage was equal to the bombing pressure. At this point, the "release" stage was started by closing the helium gas valve and opening the chamber to the atmospheric environment (0 atm of helium). The surface deflection was also documented regularly during the release stage. Representative fringe patterns and the corresponding 3D plots are shown in Figure 6-10(a) and (b) for the bombing and release stages, respectively.
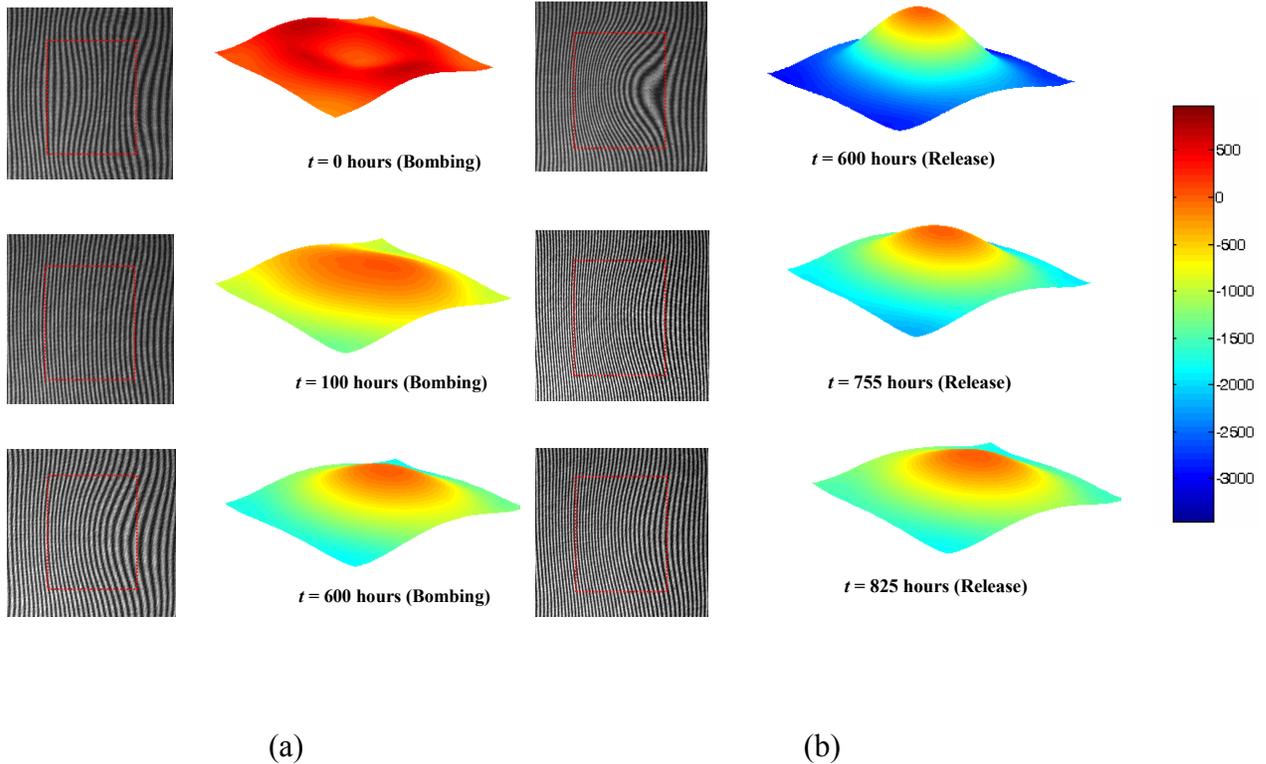
Figure 6-10 Representative fringe patterns and 3D deformation maps obtained during the (a) bombing and (b) release stages. The units for the scale are nm. (Dotted red line indicates the cavity location)

The effective deflections obtained from the 3-D maps are plotted in Figure 6-11, where the data points marked by a dotted circle were obtained from the results shown in Figure 6-10. Using the calibration curve (Eq. 2), the deflection values during the bombing and release stages were converted into pressure differential values. The internal cavity pressure was then calculated by subtracting these values from the known external pressure (4 atm while bombing and 0 atm during release) and is plotted in Figure 6-12.
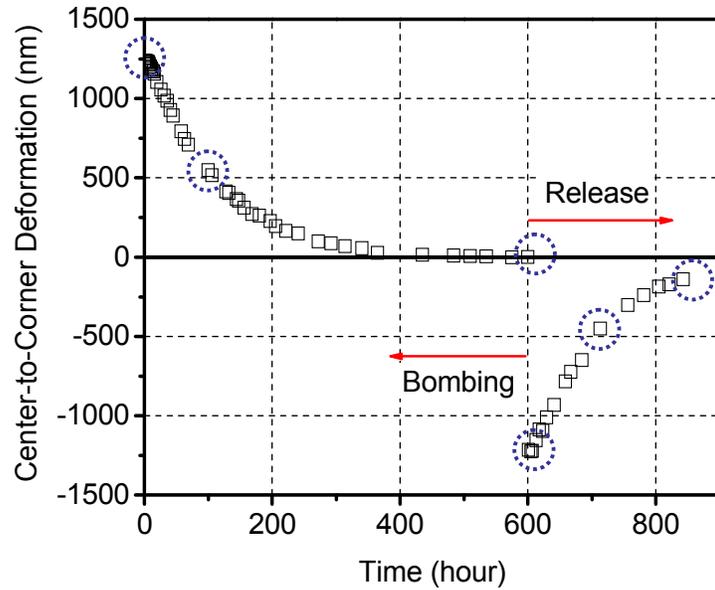
Figure 6-11 Effective chip surface deflections during the bombing and release stages. The encircled values correspond to the fringes depicted in Figure 6-10.
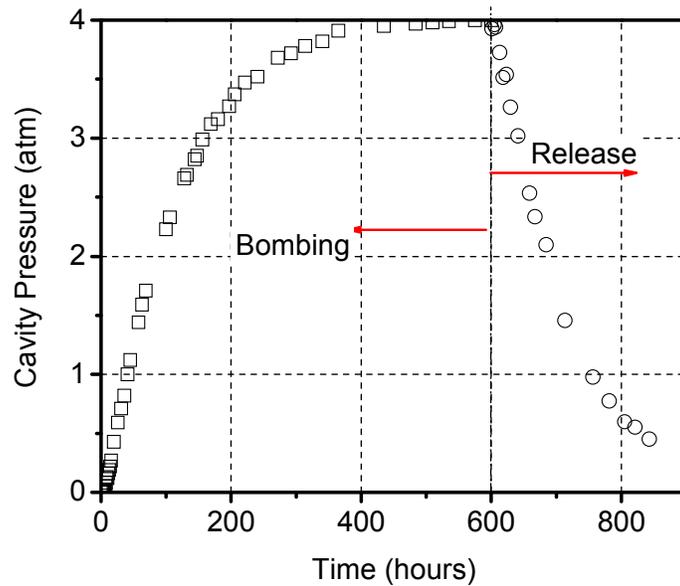
Figure 6-12 Internal cavity pressure during the bombing and release stages.

It is evident from Eq. (2), that the ±15 nm uncertainty in deformation measurement corresponds to an uncertainty of ±0.048 atm in the calculation of the corresponding pressure value. In addition, the accuracy of pressure control is ±0.02

atm as mentioned above. The uncertainty in pressure measurement depends on the

accuracy of both of these parameters. Considering sequential perturbation, the

uncertainty estimate at 95% confidence level, u_e, can be given by [48]

$$U_e \ (atm) = \pm \sqrt{\left(U_{dm}\right)^2 + \left(U_{pc}\right)^2} \qquad\qquad (3)$$

where U_{dm} (= ±0.048 atm), and U_{pc} (±0.02 atm) are the uncertainty associated with

error in deformation measurement and pressure control, respectively. From Eq. 3 the

uncertainty in the measurement of cavity pressure is ±0.052 atm.

6.4 Diffusion Model Validation and Measurement of Diffusion Properties

The experimental data for cavity pressure evolution was used to validate the

diffusion based gas transport model for polymer-sealed packages and subsequently

utilized for an inverse approach to determine the diffusion properties.

6.4.1 Validating the gas diffusion model

A Fickian diffusion model to simulate the hermetic behavior of polymer-

sealed packages was described in Ref [45]. The model was used to simulate the

internal cavity pressure change in the test specimen for the bombing stage of the

experiment. The modeling prediction is compared with the experimental data in

Figure 6-13. It is evident that the diffusion model follows the experimentally

observed cavity pressure change during bombing extremely accurately. This

confirms the diffusion based hermetic behavior of polymer-sealed packages and also

validates the assumptions used in the boundary conditions for model proposed in the

first part of this paper. The two diffusion properties (diffusivity and solubility)

required for the modeling were varied continuously until the prediction shown in

Figure 6-13 was obtained. This process is basically an inverse approach to obtain the unknown material constants. The following section details the approach.

6.4.2 Measurement of diffusion properties

The diffusion properties of polymeric seals can be determined from the optical leak test by an inverse approach. The procedure is described below using the experimental data obtained during the bombing stage.

1. A two dimensional 2 x 11 matrix was populated with diffusivity and solubility values with one row dedicated to each of these properties. The values are chosen uniformly (in the logarithmic scale) from a range of two orders of magnitude encompassing all potential values for these properties. The range of values included in this matrix is: $D = 10^{-7} \sim 10^{-5}$ mm^2/sec and $S = 10^{-14} \sim 10^{-12}$ sec^2/mm^2.

2. The 121 D-S combinations obtained from the matrix in the previous step are used as inputs to the 2-D finite element model to generate 121 sets of simulated data.

3. For each set of simulated data obtained in the previous step, the conventional coefficient of determination (R^2) is utilized to assess the degree of coincidence between experimental and simulated data. This metric is expressed as

$$R^2 = 1 - \frac{\sum_n \left(p_{exp,n} - p_{sim,n} \right)^2}{\sum_n \left(p_{exp,n} - \bar{p}_{exp} \right)^2} \qquad (4)$$

where $p_{exp,n}$ is the nth experimental data point, $p_{sim,n}$ is the nth simulation data point and $\bar{p}_{exp}$ is the average value of all the experimental data points.

4. The diffusivity-solubility combination, say $[D_1, S_1]$, which yields the largest R^2 metric in the previous step is used to create a new 2×11 "zoomed-in" matrix. This matrix has a narrower range of diffusivity and solubility with this range being based around D_1 and S_1.

5. Steps 2-4 are repeated until there is no further increase in the R^2 value. The $[D, S]$ combination which produces this best R^2 value is the output of the analysis.

The diffusivity and solubility determined from the matrix analyses are $4.57{\times}10^{-6}$ mm^2/sec and $5.50{\times}10^{-13}$ sec^2/mm^2, respectively[12] and this combination yields an R^2 value of 0.9998. The fit is plotted in Figure 6-13.
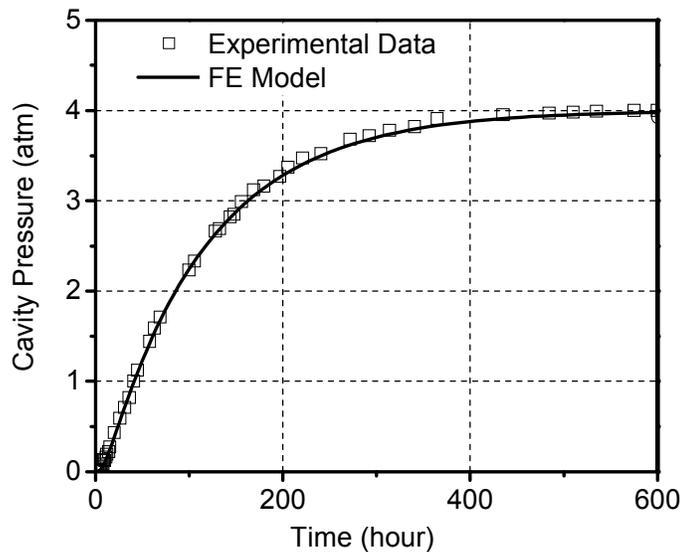
Figure 6-13 The best fit yielded an R^2 value of 0.9998 and the diffusion properties corresponding to this fit are $D = 4.57{\times}10^{-6}$ mm^2/sec and $S = 5.50{\times}10^{-13}$ sec^2/mm^2

---

[12] These values were used for model validation in the preceding section.

6.5 Discussion

Fick's second law implies that the time for the fastest gas molecule to travel from the outer surface of a package seal to the inner surface (lag time) is dominated only by the diffusivity of the sealing material. Therefore, in theory, the diffusivity can be determined from the measurement of lag time followed by the determination of the solubility from cavity pressure evolution data. However, in practice, the accurate measurement of lag time will require a technique which is sensitive enough to measure an infinitesimal increase in cavity pressure. Since no existing measurement technique can achieve that required high level of accuracy, the diffusivity and solubility are instead determined together as opposed to sequentially. This is achieved by the curve-fitting process explained above.

It should also be noted that beyond a certain point it is meaningless to continue refining the matrix in order to zero in on the "very best" D-S combination, because all such refinements will result in the same R^2 value. Physically this implies that discrepancies among curves obtained by different D-S combinations – albeit within a limited range – are smaller than the resolution of the experimental technique.

Plots of R^2 obtained for the different D-S combinations of the *last two* matrices in the procedure outlined above are shown in Figure 6-14. Figure 6-14(a) clearly demonstrates that there is a *finite* range of D-S combinations which yields a high R^2 value (0.9998), indicated by the yellow region. The last matrix is obtained by zooming into this yellow region. Plots of R^2 obtained for the different D-S combinations in the last matrix are shown in Figure 6-14(b).
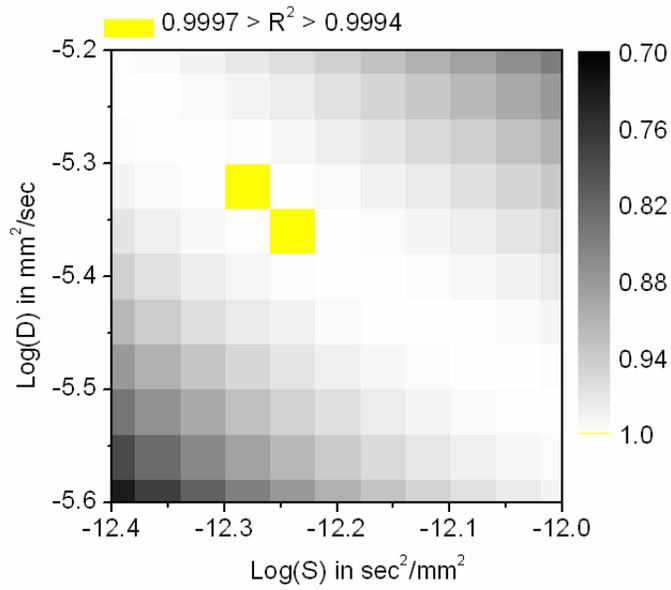
(a)
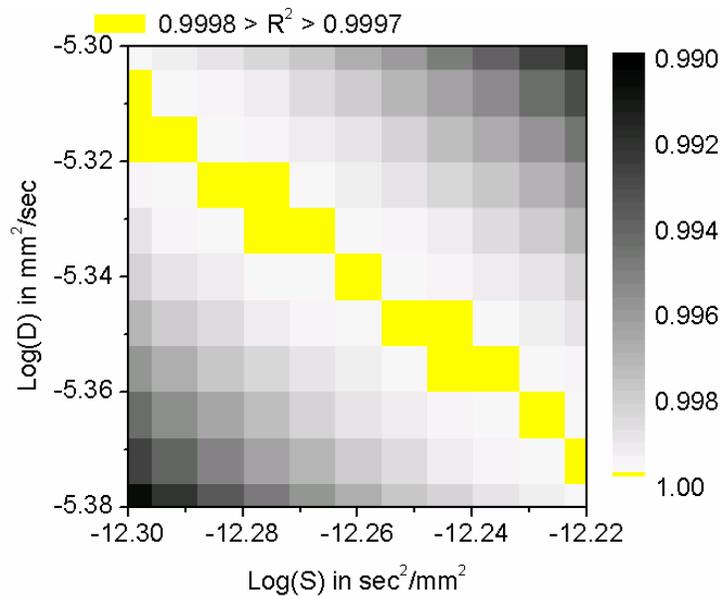
(b)

Figure 6-14 Plot of R^2 (i.e. the metric showing degree of agreement between experimental and simulated data) for different *D* and *S* combinations used in the simulations. (a) Penultimate matrix. (b) Last matrix.

It is evident that in this last matrix, for every value of diffusivity, there is one value of solubility such that the resulting R^2 value will be 0.9998. It can be seen that the size of this range is $\pm 10\%$ relative to the central values ($D = 4.57 \times 10^{-6}$ mm^2/sec and $S = 5.50 \times 10^{-13}$ sec^2/mm^2, - it should be noted that these values are the output of measurement procedure described above). The $\pm 10\%$ range of feasible diffusivity and solubility values arises due to uncertainty in measurement using the optical technique. Physically this implies that the different sets of data corresponding to the different D-S combinations belonging to this finite set of optimum combinations will be too close to be distinguished with the current resolution of the optical technique.

It is instructive to compare the experimentally obtained cavity pressure evolution data for the release stage with that simulated with the model using the D and S values obtained above. The comparison is shown in Figure 6-15. Excellent agreement between the experiment and the model implies that while the optical technique does not provide a unique D-S combination, it does yield a finite set of optimum D-S combinations. More importantly, any combination of diffusivity and solubility values belonging to this finite range can be used to predict gas leakage dependant cavity pressure evolution of polymer-sealed MEMS package with high accuracy.
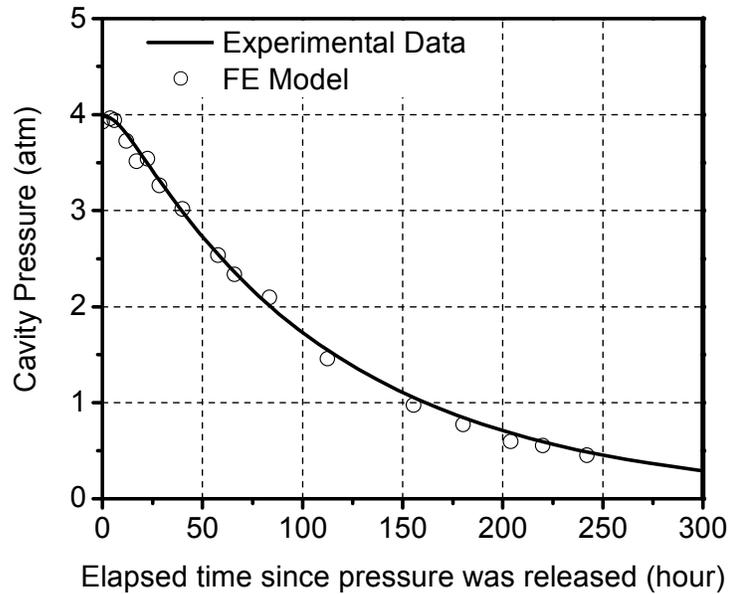
Figure 6-15 Experimental and numerical data for cavity pressure evolution during the release stage.

This implies that from a practical standpoint the optical leak test is an effective method to characterize the diffusivity and solubility of polymer-sealed packages and can potentially address the limitations of other techniques. For water vapor, the measurement of these properties has been routinely practiced through the simple water weight gain monitoring method [33, 49]. However, in the case of other gases such as oxygen, it is challenging to measure these properties since it requires dedicated instruments (e.g., MOCON equipment [50-52]) and/or sophisticated instrumentation, experimental techniques, facilities and procedures (e.g., the FTIR technique [53] for oxygen solubility). Compared with the existing techniques for gases other than water vapor, the optical leak test method has potential advantages. These include measurement of diffusion properties with a wide range of gases and the capability of high temperature testing and in-situ (i.e., in-package) measurement.

6.6 Conclusions

An optical leak test was developed and it was implemented by employing classical interferometry for deformation measurement together with a pressure chamber and a high-precision pressure regulation system. The classical interferometry with the automatic fringe analysis provided a displacement resolution of ±15 nm. Considering the pressure uncertainty of ±0.02 atm, the total measurement uncertainty in the internal cavity pressure was 0.052 atm. The method was utilized to characterize the leak behavior of the actual polymer-sealed package. In spite the small cavity volume (3 x 10^{-4} cc), the interval cavity pressure change was documented accurately during the bombing and release time. The experimental data was compared with the modeling prediction using a set of gas properties. The excellent agreement confirmed the diffusion based hermetic behavior of polymer-sealed packages and also validated the assumptions used in the boundary conditions for model proposed in the first part of this paper. The inverse approach to determine gas properties was also developed and implemented. The method has potential advantages in measuring the gas diffusion property of polymeric seals; measurements with a wide range of gas specifies and capability of high temperature and in-situ (i.e., in-package) measurement.

Chapter 7: Contributions and Future Work

7.1 Thesis contributions

Hermeticity of packages with sub-microliter volumes has been examined with both a theoretical and an experimental approach. The most significant contributions made in this dissertation are summarized below.

a) Gas conduction and gas diffusion based models available in the literature have been adapted to model leakage induced cavity pressure change in metal and polymer sealed packages. To the best of my knowledge, experimental validation of gas diffusion as a leakage mechanism in MEMS packages has never been done before and represents a very significant contribution to the hermeticity community.

   A physics based approach as outlined in this dissertation offers a better understanding of the hermeticity phenomenon and potentially will aid in the development of better hermeticity tests. For example, polymer sealed packages have been widely tested with the helium fine leak test. However, it is evident – as demonstrated in this dissertation – that this will produce erroneous results. A more fundamental understanding also reveals the role played by different parameters and will thereby aid in more optimum package design/material selection.

b) An effective method to measure diffusion properties has been developed. For gases other than water vapor, the existing techniques to measure diffusion properties have limitations, especially for high temperature measurements.

The optical leak test and the experimental method discussed in Chapter 6 provides a simpler alternative to measure the diffusivity and solubility of gases through polymeric materials and in fact versatile enough to address the temperature limitation.

c) A method to quantitatively assess hermeticity of metal sealed packages using the helium leak test has been developed. Quantitative hermeticity assessment takes away the ambiguity involved in testing packages that have different geometries (volumes) or have been tested with different test parameters. The accurate true leak rates provided by this method will also enable evaluation of new bonding materials/processes and package designs fast and effectively.

d) Establishing the domain of application of the MIL spec guidelines is another significant contribution made by this dissertation. These guidelines are used widely in both industry and research to measure hermeticity. As package volumes have scaled down, however, there was only a limited understanding of how this affects the validity of these guidelines. The present work clearly reveals that these guidelines can pass bad packages and fail good ones. This provides a framework for a revision/more judicious use of these guidelines.

7.2 Future work

As package volumes shrink and as new packaging materials/designs emerge, hermeticity will continue to be a critical concern. To that end, the contributions made by this thesis can be extended in many possible directions. Some of them are mentioned below:

a) Using the optical leak test with other gases/ambient conditions: The optical leak test is a very versatile technique to measure cavity pressure change. Unlike the helium fine leak test, it is not limited to any one gas or a certain fixed ambient temperature. It can be used with many different gases (N_2, O_2, CO_2 etc.) or combinations thereof and potentially coupled with a thermoelectric cooler in order to simulate different and more realistic operating conditions. This arrangement can also be used in conjunction with the insights provided by the gas diffusion model discussed in Chapter 5 to tailor appropriate accelerated tests for polymer sealed MEMS packages or to determine diffusion properties at elevated temperatures.

b) Using a higher resolution optical measurement technique: For packages with very small leak rates, the surface deformation changes very slowly. This necessitates either long test times so that there is measurable deformation change or a very high resolution so that even small changes can be measured. One way to increase the resolution of the test is to use a different optical measurement technique. One such technique is white light interferometry [8].

It is envisaged that by building up the physics based understanding of hermeticity developed in this dissertation and exploring further in the directions outlined above, a suite of tests will be available to compare the hermeticity of new package designs/materials and also to develop accelerated test protocols for hermetic qualification.

Bibliography

1. Feng, J., *Interaction and Permeability of Water with Liquid Crystalline Thermoset*. 2001, University of Florida.
2. Tummala, R. and E. Rymaszewski, *Microelectronics Packaging Handbook*. 1989: Van Nostrand Reinhold, New York.
3. Cai, X., et al., *A study of moisture diffusion in plastic packaging*. Journal of Electronic Materials, 2002. **31**(5): p. 449-455.
4. Tong, W. and A. Teng. *Moisture diffusion monitoring in globtop encapsulant with microdielectric sensors*. in *Electronic Materials and Packaging, 2000. (EMAP 2000). International Symposium on*. 2000.
5. Margomenos, A. and L.P.B. Katehi, *Fabrication and accelerated hermeticity testing of an on-wafer package for RF MEMS*. IEEE Transactions on Microwave Theory and Techniques, 2004. **52**(6): p. 1626-1636.
6. Jourdain, A., et al., *Investigation of the Hermeticity of BCB-sealed Cavities for Housing (RF-) MEMS Devices*, in *Proc. of the 15th IEEE Int. Conf. on Micro Electro Mechanical Systems*. 2002: Las Vagas. p. 677-680.
7. *MIL-STD-883F, Method 1014.11, Test method standard microcircuits*, U.D.o. Defense, Editor. 2004.
8. Elger, G., et al., *Optical Leak Detection for Wafer Level Hermeticity Testing*, in *Proc. 2004 IEEE/SEMI Int. Electron. Manuf. Technol. Symp.* 2004.
9. Goswami, A. and B. Han. *Hermeticity detection of wafer level MEMS packages using an optical technique* in *6th International Symposium on MEMS and Nanotechnology*. 2005.
10. Ruby, R.C., et al. *Thin film bulk wave acoustic resonators (FBAR) for wireless applications*. in *Ultrasonics Symposium, 2001 IEEE*. 2001.
11. Howl, D.A. and C.A. Mann, *The back-pressurizing technique of leak testing*. Vacuum, 1965. **15**(7): p. 347-352.
12. Greenhouse, H., *Hermeticity of electronic packages*. 2000, Noyes Publications: New Jersey. p. 85.
13. Tao, Y. and A.P. Malshe, *Theoretical investigation on hermeticity testing of MEMS packages based on MIL-STD-883E*. Microelectron. Reliab., 2005. **45**: p. 559-566.
14. Greenhouse, H., *Hermeticity of electronic packages*. 2000, Noyes Publications: New Jersey. p. 251.
15. Wang, Z., J.F. Cardenas-Garcia, and B. Han, *Inverse method to determine elastic constants using a circular disk and moire interferometry*. Experimental Mechanics, 2005. **45**(1): p. 27-34.
16. Goswami, A. and B. Han. *On Ultra-Fine Leak Detection of Hermitic Wafer-Level Packages*. in *Electronic Components and Technology Conference, 2006. Proceedings. 56th*. 2006.
17. Han, B., *Thermal stresses in microelectronics subassemblies: Quantitative characterization using photomechanics methods*. Journal of Thermal Stresses, 2003. **26**(6): p. 583.

18. Wang, Z., *Development and application of computer-aided fringe analysis*. 2003, University of Maryland at College Park.
19. Goswami, A. and B. Han, *On Ultra-Fine Leak Detection of Hermetic Wafer Level Packages*. IEEE Trans. Adv. Packag., 2008. 31(1): p. 14-21.
20. Greenhouse, H., Hermeticity of electronic packages. 2000, Noyes Publications: New Jersey. p. 198.
21. Hablanian, M., High-vacuum Technology a Practical Guide. 1997: CRC Press, Inc.
22. Knarr, O., Industrial Gaseous Leak Detection Manual. 1998: McGraw Hill.
23. Dushman, S., Scientific Foundations of Vacuum Technique. 2 ed. 1962, New York: John Wiley & Sons, Inc. .
24. Greenhouse, H., Hermeticity of electronic packages. 2000, Noyes Publications: New Jersey. p. 20.
25. Knudsen, M., The Law of the Molecular Flow and Viscosity of Gases Moving through Tubes Annalen der Physik, 1909. 28: p. 75-130.
26. Dally, J. and W. Riley, Experimental Stress Analysis, . 3 ed. 1991, New York: McGraw-Hill.
27. Dohle, G.R., et al., Low Temperature Bonding of Epitaxial Lift off Devices with AuSn. IEEE Trans. Comp. Pack. Manuf. Technol. - Part B, 1996. 19(3): p. 575-580.
28. Mitchell, J., G.R. Lahiji, and K. Najafi, Encapsulation of Vacuum Sensors in a Wafer Level Package Using a Gold-Silicon Eutectic, in Proc. 13th Int. Conf. TRANSDUCERS '05. 2005. p. 928-931.
29. Li, L., et al., Cu/Sn Isothermal Solidification Technology for Hermetic Packaging of MEMS, in Proc. 1st IEEE Int. Conf. Nano/Micro Engineered and Molecular Systems. 2006. p. 1133-1137.
30. Sarvar, F., D.A. Hutt, and D.C. Whalley, Application of Adhesives in MEMS and MOEMS Assembly: A Review, in Proc. IEEE Polytronic 2002 Conf. 2002. p. 22-28.
31. Niklaus, F., et al., Adhesive wafer bonding. Journal of Applied Physics, 2006. 99(3): p. 031101.
32. Noh, H., et al., Wafer bonding using microwave heating of parylene for MEMS packaging, in Proc. IEEE Electronic Components and Technology Conference. 2004. p. 924-930.
33. JESD22-A120A, Test Method for the Measurement of Moisture Diffusivity and Water Solubility in Organic Materials Used in Electronic Devices. JEDEC Standards, 2001.
34. Ruby, R.C., et al. High-Q FBAR filters in a wafer-level chip-scale package. in Solid-State Circuits Conference, 2002. Digest of Technical Papers. ISSCC. 2002 IEEE International. 2002.
35. Goswami, A., et al., Quantitative Characterization of True Leak Rate of Micro to Nanoliter Packages Using a Helium Mass Spectrometer. IEEE Trans. Adv. Packag., 2008. in press.
36. Goswami, A. and B. Han, On Applicability of MIL-Spec-Based Helium Fine Leak Test to Packages with Sub-micro liter Cavity Volumes. Microelectron. Reliab., 2008. in press.

37. Goswami, A., et al., Hermeticity Evaluation of Polymer-sealed MEMS Packages Part II - Optical Leak Test for Validation of the Diffusion Model and Measurement of Diffusion Properties. J. Microelectromech. Sys., 2008. submitted.

38. Jost, W., Diffusion in Solids, Liquids, Gases. 3rd ed. 1960, New York: Academic Press.

39. Yoon, S., B. Han, and Z. Wang, On Moisture Diffusion Modeling Using Thermal Diffusion Analogy. J. Electron. Packaging, 2007. 129(4): p. 421-426.

40. Jang, C., et al., Advanced Thermal-Moisture Analogy Scheme for Anisothermal Moisture Diffusion Problem. J. Electron. Packaging, 2008. 130(1): p. 011004.

41. Jang, C., Y.-R. Cho, and B. Han, Ideal Laminate Theory for Water Transport Analysis of Metal-coated Polymer Films. Appl. Phys. Lett., 2008. 93(14).

42. Sacher, E. and J.R. Susko, Water Permeation of Polymer Films. I. Polyimide. J. Appl. Polym. Sci., 1978. 23(8): p. 2355-2364.

43. J-STD-020D, I.J., Moisture/Reflow Sensitivity Classification for Nonhermetic Solid State Surface Mount Devices. JEDEC Standards, 2004.

44. Romhild, S., G. Bergman, and M.S. Hedenqvist, Transport and Adhesion Properties of an Unlined and a Liquid-Crystalline Polymer - Lined Vinyl Ester Thermoset Exposed to Severe Environement. J. Appl. Polym. Sci., 2005. 95: p. 797-805.

45. Jang, C., et al., Hermeticity Evaluation of Polymer-Sealed MEMS Packages Part I – Governing Equations and Numerical Implementation. J. Microelectromech. Sys., 2008. submitted.

46. Post, D., B. Han, and P. Ifju, Ch. 2. Elements of Optics, in High Sensitivity Moiré: Experimental Analysis for Mechanics and Materials. 1994, Springer-Verlag: New York.

47. Giri, D., M. Jouaneh, and B. Stucker, Error sources in a 3-D reverse engineering process. Precision Engineering, 2004. 28(3): p. 242-251.

48. Figliola, R.S. and D.E. Beasley, Uncertainty Analysis in Theory and Design for Mechanical Measurement. 4 ed. 2006, New York: John Wiley & Sons, Inc.

49. Galloway, J.E. and B.M. Miles, Moisture Absorption and Desorption Predictions for Plastic Ball Grid Array Packages. IEEE Trans. Comp. Pack. Manuf. Technol. - Part A, 1997. 20(3): p. 274-279.

50. Sekelik, D.J., et al., Oxygen Barrier Properties of Crystallized and Talc-Filled Poly(ethylene terephthalate). J. Polym. Sci. Pol. Phys., 1999. 37: p. 847-857.

51. Lin, J., S. Shenogin, and S. Nazarenko, Oxygen Solubility and Specific Volume of Rigid Amorphous Fraction in Semicrystalline Poly(ethylene terephthalate). Polymer, 2002. 43: p. 4733-4743.

52. Hu, Y.S., et al., Structural Model for Oxygen Permeability of a Liquid Crystalline Polymer. Macromolecules, 2003. 36: p. 3606-3615.

53. Scherzer, T. and H. Lagguth, Temperature Dependence of the Oxygen Solubility in Acrylates and its Effect on the Induction Period in UV Photopolymerization. Macromol. Chem. Phys., 2005. 206: p. 240-255.